THIOXANTHONE BASED PHOTOINITIATORS FOR TWO-PHOTON NANOLITHOGRAPHIC PRINTING

by

Teng Chi

A Dissertation

Submitted to the Faculty of Purdue University

In Partial Fulfillment of the Requirements for the degree of

Doctor of Philosophy

Department of Chemistry

West Lafayette, Indiana

December 2020

THE PURDUE UNIVERSITY GRADUATE SCHOOL
STATEMENT OF COMMITTEE APPROVAL

Dr. Bryan W Boudouris, Chair

Department of Chemistry and Davidson School of Chemical Engineering

Dr. Christina W Li

Department of Chemistry

Dr. Jianguo Mei

Department of Chemistry

Dr. Liang Pan

School of Mechanical Engineering

Approved by:

Dr. Christine Hrycyna

献给我亲爱的妻子，父亲和母亲

For my dear wife, father, and mother

ACKNOWLEDGMENTS

There are many people who I am going to express my deepest gratitude and appreciation to. First, I would like to thank my wife Yanjing Wang for supporting me in my whole life especially my PhD career. During this unforgettable 5 years, I have faced so much difficulty and uncertainty, but she is always on my side and comfort me by sweet love and encouragement all the time. I would like to thank my parents for their concrete support and countless love. They suggested me to pursue my PhD degree in chemistry and they unswervingly believe me that I can make it through and become Dr. Chi in the future.

I would also like to thank my advisor, Dr. Bryan Boudouris. Without his helpful support, none of my research can be achieved. As I have talked about with many people before, he is the best supervisor I have ever seen and I am so glad and excited that I can spend most of the PhD career working with him. Actually, I am a big fan of him though "fan" is not always used in science field. He has been an outstanding advisor and helped me out from the terrible confusion about future when I finished my second year in Purdue. He showed me what the real scientific research looks like and how to do research as a PhD student. Without his guidance and high standard, there was absolutely no way I could be an eligible PhD student and moved to the correct direction to my PhD degree. I desperately owe an overwhelming thank you to him.

Next, I would like to thank my committee members, Professor Jianguo Mei, Professor Christina Li and Professor Liang Pan for contributing time and kind support throughout my years at Purdue. I also would like to thank Professor Mingji Dai for training me on the organic synthesis and all the related skills in my first two years. He is a great professor and I have recommended many students to his group since they are interested in hardcore synthesis. Although I had many

confusions during the second year, it had no relationship with him, and I really appreciate his selfless teaching.

Next, I want to thank two of my best friends in Purdue: Dr. Duanchen Ding and Dr. Xikang Zhao. When I was a green hand in Purdue or even in America, Duanchen Ding helped me to set up almost everything. Dr. Xikang Zhao helped me a lot in terms of research. I owe a big thank you to both of them. Next, I would like to thank Prof. Xianfan Xu, Prof. Liang Pan, Dr. Daniel Wilcox, Paul Somers and Shih-hsin Hsu for the great collaboration we have together. And I want to thank Ying Tan, Zihao Liang and Kangying Liu who are partly supervised by myself for their great passion and engagement of our sharing projects.

Finally, I want to thank all brothers and sisters in our lab for your great support. Dr. Daniel Wilcox, Dr. Martha Hay, Dr. Jennifer Laster, John Hodul, Sheng-Ning Hsu, Siddhartha Akkiraju, Noelia Almodovar, Jaeyub Chung, Carsten Flores-Hansen, Ho Joong Kim, Oluwafemi Ogunlalu, Aaron Woppel, Kuluni Perera and Dr.Wenchao Zhao. They gave fruitful advice to me and help me out when I faced issues in my research. Especially I want to thank Dr. Jennifer Laster for introducing me to the group, which was the time when everything started; Dr. Daniel Wilcox for almost half of the equipment trainings; John Hodul and Siddhartha Akkiraju for the other half training; Carsten Flores-Hansen for being my final seminar's host and Noelia Almodovar as well as Jaeyub Chung for plenty of suggestions of the future career.

TABLE OF CONTENTS

LIST OF TABLES

LIST OF FIGURES

LIST OF ABBREVIATIONS

ITX	isopropyl thioxanthone
DFT	density functional theory
DLW	direct laser writing
BDAPT	2,7-bis[(4-(dimethylamino)phenyl ethynyl)-9H-thioxanthen-9-one]
DANT	2-bromo-7-[(6-(dimethylamino)naphthalen-2-yl)ethynyl]-9H-thioxanthen-9-one
DAPT	2-bromo-7-[(4-(dimethylamino) phenyl)ethynyl]-9H-thioxanthen-9-one
ITX-Br	2-bromo-7-isopropyl-9H-thioxanthen-9-one
ITX-pyridine	2-isopropyl-7-(pyridin-4-yl)-9H-thioxanthen-9-one
ITX-phenyl-CN	4-(7-isopropyl-9-oxo-9H-thioxanthen-2-yl)benzonitrile
ITX-phenyl	2-isopropyl-7-phenyl-9H-thioxanthen-9-one
ITX-phenyl-F	2-(4-fluorophenyl)-7-isopropyl-9H-thioxanthen-9-one
ITX-phenyl-OCH_3	2-isopropyl-7-(4-methoxyphenyl)-9H-thioxanthen-9-one
ITX-thiophene	2-isopropyl-7-(thiophen-2-yl)-9H-thioxanthen-9-one
DETC	7-diethylamino-3-thenoylcoumarin
MeO-DETC	7-methoxy-3-(thiophene-2-carbonyl)-2H-chromen-2-one
DETC-N-chain	1-(2-ethylhexyl)-3-(thiophene-2-carbonyl)quinolin-2(1H)-one
Br-DETC-N-chain	6-bromo-1-(2-ethylhexyl)-3-(thiophene-2-carbonyl)quinolin-2(1H)-one
MeO-DETC-N-branch	1-(2-ethylhexyl)-6-methoxy-3-(thiophene-2-carbonyl)quinolin-2(1H)-one

ABSTRACT

Printing of 3-dimensional nanostructures with high-resolution by two-photon polymerization has gained significant attention recently. Isopropyl thioxanthone (ITX) has been studied and used as a photoinitiator because of its unique property in initiating and depleting polymerization, but to further improve the resolution of 3D structures, new photoinitiating materials are necessary to decrease the power requirements especially in industrial world. In this dissertation, different new types of thioxanthone-based photoinitiators were synthesized and our new initiators possessed a clear enhancement in terms of excitation over ITX. To clearly reveal the writing mechanism behind it, the behavior of the initiators was evaluated by several methods such as low temperature phosphorescence spectroscopy and density functional theory (DFT) calculations. The first type of new molecules with alkyne bridge will be discussed in chapter 2 and the further developed initiators with electron donating and withdrawing groups will be discussed in chapter 3. By modifying the structure of ITX, we have revealed and proposed an important pathway to guide future development of photoinitiators in direct laser writing.

CHAPTER 1. INTRODUCTION

1.1 Introduction to Two-photon Lithographic Printing

Two-photon polymerization was first reported in 1997,[1] and it has caused fast growth in the field of nanolithographic printing and it has become an essential and important process in 3D nanofabrication. A type of direct laser writing (DLW), takes advantage of the nonlinearity of multi-photon absorption to build up the spatial confinement of the printed voxel in a significant manner with a polymeric photoresist. In turn, this allows for the polymerization to happen inside the monomeric photoresist, and the fabrication of arbitrary 3D structures is achieved with sub-micron resolution.[1,2] DLW has been highlighted recently as a low-cost and high-speed tool to create high-fidelity 3D nanoscale structures in specific fields such as photonics[3,4] and tissue engineering.[5,6] Although there was a huge development in the spatial resolution of DLW relative to analogous single-photon polymerization systems, it still remains a diffraction-limited process. This large barrier can be overcome by adding a polymerization-inhibiting depletion laser.[7] Specifically, in a concept first applied to microscopy,[8] the resolution of DLW was enhanced by spatially-overlapping a shaped depletion laser beam so that the DLW beam is directly placed in a minimum

of the depletion laser beam.[9] In this type of configuration, the photoinitiated polymerization can be inhibited everywhere outside of the depletion laser minimum.

1.2 Photoinitiators in Nanolithographic Printing

Critical to the success of the inhibition-based polymerization technique with 2 lasers is the optical response of the photoinitiating species in the DLW process. The photoinitiator must allow for efficient initiation (and subsequent propagation) of the polymerization by the excitation beam while the inhibition beam must stop the polymerization reaction in an effective manner.[10,11] That is, although there are so many organic molecules which can serve as super-efficient photo absorber with high extinction coefficient in one-photon test and great Z-scan results in two photon test, they fail to possess the ability to stop the polymerization by any possible depletion mechanism and can not be used in this DLW printing process, which shows that a proper way to modify the molecules and balance the two aspects of nanoprinting (excitation and depletion) is the key point towards qualified initiators.

1.2.1 Isopropyl Thioxanthone (ITX) and its Depletion Mechanism

Generally, photoinitiators can be classified into two different types: Norish type I initiators are molecules which can generate radicals directly by photo-cleavage; Norish type II initiators can absorb light to form excited states that remove electrons or hydrogens from a co-initiator to generate radicals. In DLW the widely-used commercially-available photoinitiator 2-isopropylthioxanthone (ITX) is a special type II initiator as ITX can perform without co-initiators. This has made it an established photoinitiator in two-photon nanolithographic processes.[12] Electrons in the ground (S_0) state of the ITX can be promoted to an excited (S_1) state through a two-photon optical transition using an 800 nm wavelength laser (Figure 1.1.). Then, the excited

state can undergo intersystem crossing to generate the triplet (T_1) state, which allows for initiation of the polymerization. As revealed by pump-probe spectroscopy, the ITX molecule can undergo depletion through both (1) stimulated emission depletion (STED) and (2) non-radiative decay from exciting long-lived species to terminate the polymerization. In most instances, it has been established that the latter of these two mechanisms dominates in two-photon nanolithographic properties. Thus, ITX is a useful material by which to manipulate the optical properties of high-performance photoinitiators.

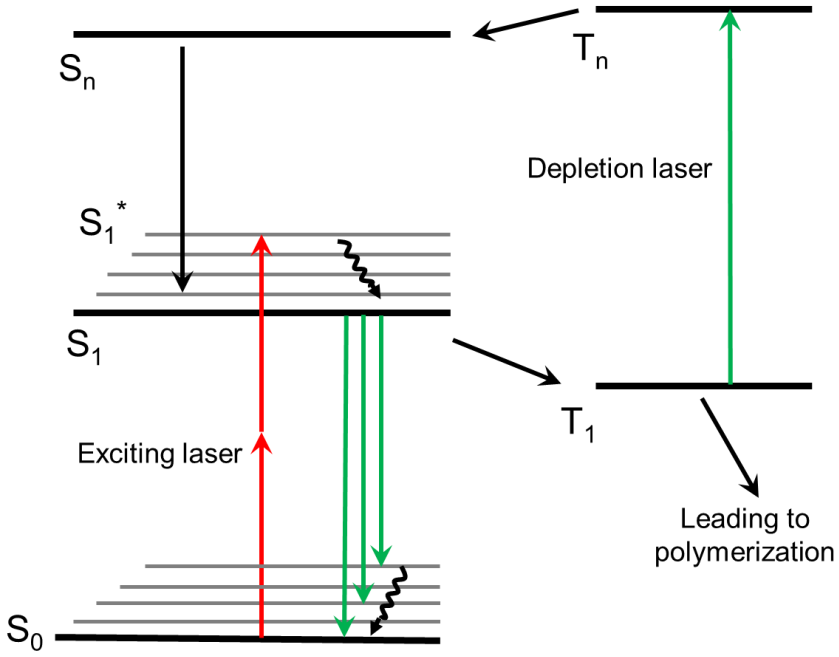

Figure 1.1. The energy diagram depicts the two possible pathways for ITX depletion.

1.3 The New Designed Derivatives of ITX with Alkyne Bridge

Printing of high-resolution 3-dimensional nanostructures utilizing two-photon polymerization has gained significant attention. In particular, isopropyl thioxanthone (ITX) has been implemented as a photoinitiator due to its capability of initiating and depleting

polymerization on demand, but new photoinitiating materials are still needed in order to reduce the power requirements for the high-throughput creation of 3D structures. To address this point, a suite of new thioxanthone-based photoinitiators were synthesized and characterized (Figure 1.2). Then two-photon polymerization was performed using the most promising photoinitiating molecule. Importantly, one of the initiators, 2,7-bis[(4-(dimethylamino)phenyl ethynyl)-9H-thioxanthen-9-one] (BDAPT), showed a 5-fold improvement in the writing threshold over the commonly-used ITX molecule. In chapter 2, to elucidate the fundamental mechanism, the excitation and inhibition behavior of the BDAPT molecule were evaluated using density functional theory (DFT) calculations, low temperature phosphorescence spectroscopy, ultra-fast transient absorption spectroscopy, and the two-photon Z-scan spectroscopic technique. The improved polymerization threshold of this new photoinitiator presents a clear pathway for the modification of photoinitiators in 3D nanoprinting.

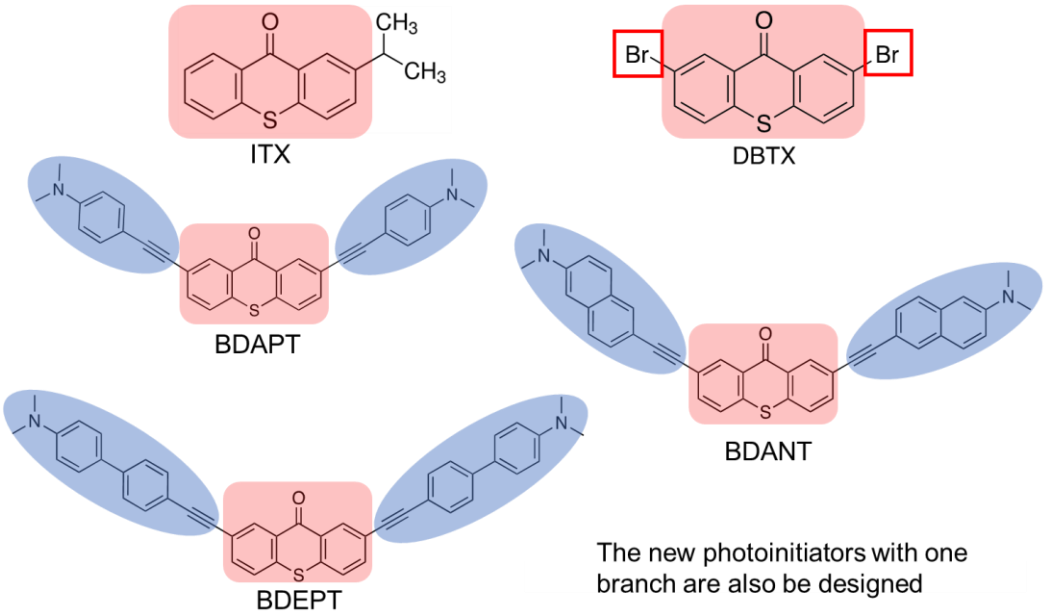

Figure 1.2. The new designed ITX derivatives as two-photon photoinitiators.

1.4 The New Derivatives of ITX with Electron Withdrawing and Donating Substrates

After isopropyl thioxanthone (ITX) has been widely used as a photoinitiator for its initiating and depleting polymerization, Complicated branches designed to attach to the ITX core in last paragraph have been introduced, but they suffered some problems like low yields, poor solubility and poor stability. Therefore, we are overcoming these barriers using a new chemical design and synthetic strategy without significantly influence the effectiveness of photoinitiators. To address this point, a series of new photoinitiators were synthesized and characterized (Figure 1.3) Specifically, new branches were classified into 3 groups based upon their chemical construct. Specifically, these substituents were: (1) electron-withdrawing groups (2) electron-donating groups and (3) groups that were neither strongly electron-accepting nor electron-donating. All of new initiators showed an improvement in the writing threshold over ITX and most of the disadvantages of BDAPT, DANT and DAPT were overcome by these new compounds. To reveal the mechanism, the optical and printing behavior of these molecules were evaluated using density functional theory (DFT) calculations, the two-photon Z-scan spectroscopic technique and low temperature phosphorescence spectroscopy in chapter 3. The improved results of these new photoinitiators undergo the pathway we discussed and march further for the modification of photoinitiators in 3D nanoprinting.

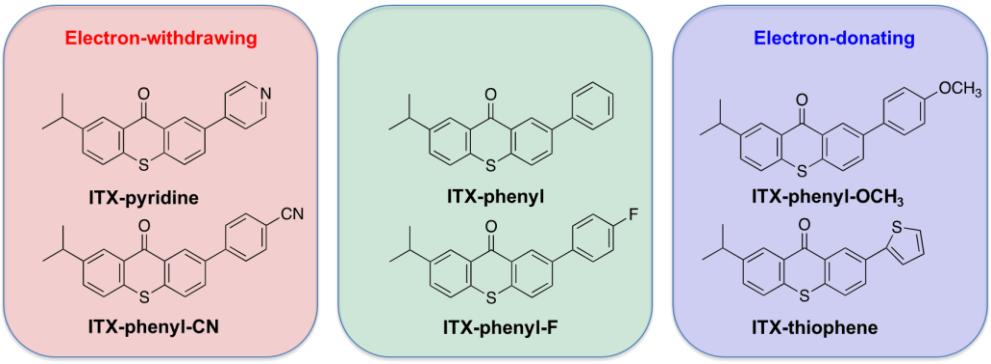

Figure 1.3. The new designed ITX derivatives with electron withdrawing/donating group.

1.5 Summary

In the first chapter, we introduce the basic concept of two-photon nanoprinting and the importance of its corresponding photoinitiators. The well-studied molecule ITX was introduced and new photoinitiating species were designed and developed based on a thiophene-9-one core for DLW photopolymerization. DFT calculations, ultra-fast spectroscopic experiments and low temperature phosphorescence spectroscopy were used in the following chapters to explain the mechanism of both excitation and depletion. Afterall, we have proposed a practical direction to modify and improve existing photoinitiators for two-photon DLW photopolymerization. In turn, this should allow for the ready modification of existing photoinitiators in the future 3D nanoprinting photopolymerization reactions, for not only ITX- based systems but for more exotic systems as well, by providing insights into the critical properties of a photoinitiator molecule that leads to a desired photopolymerization performance and how to tailor a photoinitiating molecule to achieve those properties.

1.6 References

1 S. Maruo, O. Nakamura, S. Kawata. *Opt. Lett.* **1997**, *22*, 132-134.

2 S. Kawata, H.-B. Sun, T. Tanaka, K. Takada. *Nature* **2001**, *412*, 697.

3 M. Deubel, G. von Freymann, M. Wegener, S. Pereira, K. Busch, C. M. Soukoulis. *Nature Materials* **2004**, *3*, 444.

4 G. von Freymann, A. Ledermann, M. Thiel, I. Staude, S. Essig, K. Busch, M. Wegener. *Advanced Functional Materials* **2010**, *20*, 1038-1052.

5 F. Klein, B. Richter, T. Striebel, C. M. Franz, G. v. Freymann, M. Wegener, M. Bastmeyer. *Adv. Mater.* **2011**, *23*, 1341-1345.

6 V. Melissinaki, A. Gill, I. Ortega, M. Vamvakaki, A. Ranella, J. Haycock, C. Fotakis, M. Farsari, F. Claeyssens. *Biofabrication* **2011**, *3*, 045005.

7 S. W. Hell. *Physics Letters A* **2004**, *326*, 140-145.

8 S. W. Hell, J. Wichmann. *Opt. Lett.* **1994**, *19*, 780-782.

9 J. Fischer, G. von Freymann, M. Wegener. *Adv. Mater.* **2010**, *22*, 3578-3582.

10 J. Fischer, J. B. Mueller, A. S. Quick, J. Kaschke, C. Barner-Kowollik, M. Wegener. *Advanced Optical Materials* **2015**, *3*, 221-232.

11 L. Li, R. R. Gattass, E. Gershgoren, H. Hwang, J. T. Fourkas. *Science* **2009**, *324*, 910-913.

12 B. Harke, W. Dallari, G. Grancini, D. Fazzi, F. Brandi, A. Petrozza, A. Diaspro. *Adv. Mater.* **2013**, *25*, 904-909.

CHAPTER 2. TAILORED ITX-BASED PHOTOINITIATORS WITH ALKYNE BRIDGE

This chapter is reproduced with permission from **Chi, T.**; Somers, P.; Wilcox, D.A.; Schuman, A.J.; Iyer, V.; Le, R.; Gengler, J.; Ferdinandus, M.; Liebig, C.; Pan, L.; Xu, X.; and Boudouris, B.W. Tailored Thioxanthone-based Photoinitiators for Two-Photon-Controllable Polymerization and Nanolithographic Printing. *Journal of Polymer Science Part B:Polymer physics* **2019**, 57,1462-1475. John Wiley and Sons and copyright Clearance Center with **License number 4920570846871.** Chi, T.; Somers, P.; and Boudouris, B.W. were in charge of outlining and writing the paper and putting all the techniques together. Chi, T. was in charge of designing and synthesizing molecules, collecting all optical properties, and also contributed to DFT calculation. Somers, P. was in charge of all lithographic printings, Z-scan and pump-probe test. Wilcox, D.A. was in charge of DFT calculation. Schuman, A.J. was in charge of phosphorescence data. Iyer, V. and Le, R. were contributed to lithographic printing and pump-probe. Gengler, J.; Ferdinandus, M. and Liebig, C. were contributed to Z-scan.

2.1 Introduction: the Necessity of Improvement for ITX as Photoinitiator

Since DLW two-photon lithographic writing is developing rapidly and a commercially available molecule ITX was used to meet the requirement of both activating polymerization and efficiency in depletion , several two-photon photoinitiating species have been developed recent years, and some of the most promising materials have been investigated with nanolithographic applications in mind.[1-3] However, there is still a strong demand in both academic and industrial circles for more efficient photoinitiators in order to reduce the writing laser power requirements. Because the polymerization that the photoinitiator controls is key in the DLW process, we synthesized a series of new thioxanthone-based photoinitiators in order to achieve more efficient initiation (i.e., lower power) of the photopolymerizations at the nanoscale, and we established that the appropriate design of these materials and the modulation of their photophysical properties can significantly reduce the power required to create two-photon polymerized nanostructures.

The proposed photoinitiator builds from the fact that isopropyl thioxanthone (ITX) is an established photoinitiator in two-photon nanolithographic processes.[4] Despite the fact that ITX

demonstrates the desired photoinitiation and photoinhibition properties with respect to the writing and depletion wavelengths,[1,4] the writing laser power required for this material is still large at the common writing wavelength of 800 nm due to the weak two-photon absorption cross-section of the ITX molecule.[5] While not a particular issue for previously-reported proof-of-concept demonstrations, reducing the amount of power required for photoinitiation is of critical import for scalable nanomanufacturing (i.e., in cases where multiple lasers would be required in order to achieve high-throughput production). Also of concern is the tendency of larger laser powers to lead to parasitic polymerization due to thermal initiation events, which can impact the minimum feature sizes that are attainable.[6] Thus, there is a significant need to develop next-generation ITX derivatives that are capable of having improved light absorption profiles for the DLW wavelength (λ = 800 nm).

From nonlinear optics, the two-photon absorption coefficient is predicted to be optimal for an incident photon energy that is 0.7 times the bandgap of a wide bandgap material.[7] In terms of designing a molecule for a constant DLW wavelength of 800 nm, this indicates a necessity to redshift the absorption peak of the photoinitiators relative to ITX to improve this ratio of absorption peak wavelength to the incident light wavelength. Moreover, it has been shown that molecules following a donor-acceptor-donor type structure also demonstrate an improved two-photon absorption cross-section.[8] Following these lines of thinking, we strive to take ITX and develop derivatives with improved two-photon absorption (i.e., increasing the number of initial electrons that are promoted to the singlet state) while studying the resulting effects on the polymerization initiating and inhibiting properties of the new compounds (i.e., we will also evaluate the intersystem crossing processes and triplet state dynamics as well). We propose that the introduction of chromophores or electron donors leads to the generation of the donor-acceptor-

donor or donor-acceptor species, and this will cause a redshift the absorption spectrum. Compared to ITX, these derivatives should demonstrate improved two-photon absorption cross-sections. In order to accomplish this objective, the functional groups pendant to the thioxanthen-9-one core of ITX were tuned in a systematic manner. Specifically, phenyl, diphenyl, and naphthyl groups were attached to the ITX core with alkyne bridges, which leads to extended aromatic systems along the small molecule backbone. This extended conjugation, in turn, results in a bathochromic shift in the peak of the absorbance spectra of the molecules. Dialkylamino groups were added to terminate the ends of the molecules due to the strong electron-donating features of these substituents. In addition, mono-substituted and di-substituted derivatives were synthesized and compared in order to elucidate the influence of the numbers of pendant groups on the photophysical properties of the polymerization initiators. The absorption spectra of new initiators were predicted by density functional theory (DFT) calculations in order to provide a guide for the synthesis. Two-photon absorption cross-sections were measured for each of the synthesized photoinitiators to provide a direct indicator of the DLW polymerization performance. The existence of possible charge transfer states that could arise due to the donor-accepter molecular motif were rationalized by calculating the frontier molecular orbitals of the molecules. Ultra-fast transient absorption spectroscopy and phosphorescence spectra were utilized to determine excited state lifetimes in order to benchmark the polymerization inhibition characteristics and possible mechanism of the newly-synthesized polymerization photoinitiators in comparison to ITX. DLW polymerization was then performed using the most-promising photoinitiator based on these evaluations, and the photoinitiating molecule, 2,7-bis[(4-(dimethylamino)phenyl ethynyl)-9H-thioxanthen-9-one] (BDAPT), demonstrated a reduction in required laser power for DLW when pentaerythritol triacrylate (PETA) served as the monomer for the polymerizations associated with the engineered photoinitiators. The

writing laser power of BDAPT was reduced by 5-fold relative to the laser power required for the same monomer system using the commonly implemented ITX photoinitiator. Therefore, the archetype presented here is one that sets a path forward in designing next-generation photoinitiators for their application towards low-power, high-throughput photopolymerizations in 3D nanoprinted materials.

2.2 Experimental Procedure and Characterization

2.2.1 General Experimental Procedures

All chemicals were purchased from Sigma-Aldrich, and the chemicals were used as received. Ultraviolet–visible (UV–Vis) spectroscopy data were collected using a Cary 60 spectrometer in the wavelength range of 330 nm $\leq \lambda \leq$ 800 nm. Fluorescence and phosphorescence spectroscopy data were obtained using a Cary Eclipse fluorescence and phosphorescence spectrophotometer in the wavelength range of 400 nm $\leq \lambda \leq$ 800 nm (with an excitation wavelength of 350 nm). Phosphorescence data were collected using deoxygenated solutions of the samples in a glass-forming solvent, with an absorbance below 0.01 at the excitation wavelength. 9,10-diphenylanthracence was used as a fluorescence quantum yield standard (94%) as the quantum yield of this material in THF is well-established.[9] In order to correct for solvent effects, Equation 1 was utilized to normalize the quantum yield obtained for the 9,10-diphenylanthracence when PETA was the solvent.[10]

$$\Phi_{PETA} = \Phi_{THF}\left(\frac{S_{PETA}}{S_{THF}}\right)\left(\frac{n_{PETA}^2}{n_{THF}^2}\right) \qquad (1)$$

Here, Φ_{THF} (94%) is the fluorescence quantum yield of the standard in THF. S_{THF} ($\sim 2.64 * 10^6$ counts/a.u.) represents the slope of the integrated fluorescence signal obtained for the standard

molecule vs. absorbance for different concentrations when they are dissolved in THF, and S_{PETA} ($\sim 2.50 * 10^6$counts/a.u.) represents the same slope when the standard molecule is dissolved in PETA. The refractive index (n_{PETA} = 1.483 and n_{THF} = 1.407) is obtained from Sigma- Aldrich. From this equation, the fluorescence quantum yield of 9,10-diphenylanthracence in PETA was calculated as 98.7%. The quantum yield values of different photoinitiators were tested and referenced to the value of 9,10-diphenylanthracence.

2.2.2 Synthesis of New Photoinitiators

Synthesis of dibromo-9H-thioxanthene-9-one (DBTX).

Thioxanthen-9-one (Compound 7, 4 g, 19.2 mmol) was added to a 500 mL round bottle flask with 32 mL of acetic acid. Then, 8 mL of bromine were added in a dropwise manner while the reaction mixture was held at 0 °C. After the addition of the bromine, the flask was slowly heated to 118 °C. After 24 h, a dark red solution formed, and at this time, the solution was poured into an ice bath. A yellow precipitate appeared, and it was filtered. After washing with a saturated aqueous $NaHCO_3$ twice to quench any remaining acid, the yellow solid was dissolved into toluene and subsequently recrystallized to form yellow crystals in 51% yield. 1H NMR (400 MHz, Deuterated chloroform) δ: 8.74 (d, 4 J = 2.35 Hz, 2H), 7.76 (dd, 3 J = 8.59, 4 J = 2.30 Hz, 2H), 7.49 (d, 3 J = 8.61 Hz, 2H).

Synthesis of 6-bromo-*N*,*N*-dimethylnaphthalen-2-amine. (Compound 2)

6-bromo-2-naphthol (Compound 1, 1.5 g, 6.7 mmol), a solution of dimethyl amine in methanol (15 mL, 33 mmol), and $Na_2S_2O_5$ (2.7 g, 13.6 mmol), were added. Then, 5 mL H_2O was added to the reaction flask in order to increase the solubility of $Na_2S_2O_5$, and the tube was then sealed. The reaction was slowly heated to 140 °C. After 40 h, the crude mixture was obtained by filtering the inorganic solid; the organic solution was washed with brine and DI-water three times and extracted with ethyl acetate. The mixture was purified by column chromatography (Hexane:ethyl acetate = 9:1 v/v) to yield a solid with 60% yield. 1H NMR (400 MHz, Deuterated chloroform) δ 7.84 – 7.80 (m, 1H), 7.63 – 7.57 (m, 1H), 7.51 (dq, J = 8.8, 0.6 Hz, 1H), 7.41 (dd, J = 8.8, 2.0 Hz, 1H), 7.16 (dd, J = 9.1, 2.6 Hz, 1H), 6.86 (d, J = 2.6 Hz, 1H), 3.05 (s, 6H).

Synthesis of *N*,*N*-dimethyl-6-((trimethylsilyl)ethynyl) naphthalen-2-amine. (Compound 3)

$Pd(PPh_3)_2Cl_2$ (0.05 mmol), CuI (0.05 mmol), and 6-bromo-N, N-dimethylnaphthalen-2-amine (125 mg, 0.5 mmol) were added in a round bottle flask under a nitrogen blanket. Subsequently, freshly distilled diethyl amine (3 mL) with (trimethylsilyl) acetylene (0.14 mL, 1 mmol) were added to the flask. The reaction was slowly heated to 50 °C in the dark. After 24 h, the reaction mixture was diluted with ethyl acetate before being washed with brine and DI-water three times. After the organic fraction was dried by Na_2SO_4, the mixture was pushed through a silica gel flash column without further purification.

Synthesis of 4'-bromo-*N*,*N*-dimethyl-[1,1'-biphenyl]-4-amine. (Compound 5)

4-(Dimethyl amino) phenylboronic acid pinacol ester (Compound 4, 494 mg, 2 mmol) and 1-bromo-4-iodobenzene (676 mg, 2.4 mmol) were added to a 20 mL sealed tube. Then, 0.1 equivalents of Pd $(PPh_3)_4$ (0.2 mmol) and Na_2CO_3 (6 mmol) were mixed and poured into the tube;

15 mL THF and 2 mL water were then injected to the tube. The tube was sealed and slowly heated to 80 °C overnight under a nitrogen atmosphere. The dark mixture that formed was washed with brine and then deionized (DI) water three times and extracted with ethyl acetate. After drying over Na_2SO_4, the crude mixture was purified by silica gel column chromatography (hexane:ethyl acetate = 10:1 v/v) to give a solid with 40 % yield. 1H NMR (400 MHz, Deuterated chloroform) δ 7.52 – 7.48 (m, 2H), 7.48 – 7.43 (m, 2H), 7.44 – 7.38 (m, 2H), 6.79 (d, J = 8.3 Hz, 2H), 2.99 (s, 6H).

Synthesis of *N,N*-dimethyl-4'-((trimethylsilyl)-ethynyl)-[1,1'-biphenyl]-4-amine. (Compound 6)

$Pd(PPh_3)_2Cl_2$ (0.05 mmol), CuI (0.05 mmol), and 4'-bromo-N,N-dimethyl-[1,1'-biphenyl]-4-amine (Compound 5, 130 mg, 0.5 mmol,) were added in a round bottle flask under a nitrogen blanket. Subsequently, freshly distilled diethyl amine (3 mL) and (trimethylsilyl) acetylene (0.14 mL, 1 mmol) were added to the flask. The reaction was slowly heated to 50 °C in the dark. After 24 h, the reaction mixture was diluted with ethyl acetate before being washed with brine and DI-water three times. After the organic fraction was dried with Na_2SO_4, the mixture was pushed through a silica gel flash column without further purification.

Synthesis of 2,7-bis[(4-(dimethylamino)phenyl ethynyl)-9H-thioxanthen-9-one] (BDAPT).

4-ethynyl-N,N-dimethylaniline (Compound 8, 362 mg, 2.5 mmol), $Pd(PPh_3)_2Cl_2$ (42 mg, 0.06 mmol), CuI (19 mg, 0.1 mmol), and DBTX (115 mg, 0.32 mmol) were added in a round bottle flask under nitrogen protection. Then freshly distilled diethyl amine (4 mL) was injected. The reaction was stirred for 30 h at 53 °C in the dark. The reaction mixture was diluted with ethyl acetate before being washed with brine and DI-water three times. After the organic layer was dried using Na_2SO_4, the mixture was purified by column chromatography (Hexane:ethyl acetate = 6:1

v/v) to give a solid with 10% yield. It was mixed with PETA immediately for use during nanoprinting because of its fast decomposition in air or exposure to light. 1H NMR (400 MHz, Deuterated chloroform) δ 7.89 (d, J = 8.9 Hz, 2H), 7.70 (d, J = 8.0 Hz, 2H), 7.49 – 7.41 (m, 4H), 7.39 (d, J = 8.9 Hz, 2H), 6.70 – 6.64 (m, 4H), 3.00 (s, 12H).

Synthesis of 2-bromo-7-[(4-(dimethylamino) phenyl)ethynyl]-9H-thioxanthen-9-one (DAPT).

4-ethynyl-N,N-dimethylaniline (Compound 8, 50 mg, 0.32 mmol), $Pd(PPh_3)_2Cl_2$ (14 mg, 0.02 mmol), CuI (10 mg, 0.05 mmol), and DBTX (115 mg, 0.32 mmol) were added to a round bottle flask under nitrogen protection. Freshly distilled diethyl amine (2 mL) was injected and the reaction was stirred for 24 hours at 50 °C in the dark. The reaction mixture was diluted with ethyl acetate before being washed with brine and DI-water three times. After the organic layer was dried with Na_2SO_4, the mixture was purified by column chromatography (hexane:ethyl acetate = 20:1 v/v) to produce a solid with 11% yield. 1H NMR (400 MHz, Deuterated chloroform) δ 8.74 (ddd, J = 19.3, 2.1, 0.5 Hz, 2H), 7.72 (ddd, J = 8.4, 2.1, 1.5 Hz, 2H), 7.56 – 7.47 (m, 2H), 7.47 – 7.41 (m, 2H), 6.68 (d, J = 9.0 Hz, 2H), 3.01 (s, 6H).

Synthesis of 2-bromo-7-[(6-(dimethylamino) naphthalen-2-yl)ethynyl]-9H-thioxanthen-9-one (DANT).

N,N-dimethyl-6-((trimethylsilyl)-ethynyl)naphthalen-2-amine (Compound 3, 200 mg, 0.75 mmol), $Pd(PPh_3)_2Cl_2$ (28 mg, 0.04 mmol), CuI (19 mg, 0.1 mmol), and DBTX (115 mg, 0.32 mmol) were added in a round bottle flask under nitrogen protection. Freshly distilled diethyl amine (2 mL) was injected and the reaction was stirred for 30 hours at 53 °C in the dark. The reaction mixture was diluted with ethyl acetate before being washed with brine and DI-water three times. After the organic layer was dried with Na_2SO_4, the mixture was purified by column

chromatography (hexane:ethyl acetate = 20:1 v/v) to give a solid with 8% yield. It was mixed with PETA immediately for use during nanoprinting because of its fast decomposition in air or exposure to light. 1H NMR (400 MHz, Deuterated chloroform) δ 8.77 (d, J = 2.2 Hz, 1H), 7.96 – 7.89 (m, 1H), 7.80 – 7.66 (m, 3H), 7.64 – 7.57 (m, 2H), 7.53 – 7.45 (m, 2H), 7.41 – 7.34 (m, 1H), 7.17 (ddd, J = 9.1, 4.8, 2.6 Hz, 1H), 6.88 (d, J = 2.5 Hz, 1H), 3.08 (s, 6H).

2.2.3 Computational Calculation

The theoretical ultraviolet-visible (UV-Vis) absorption spectra of the relevant molecules were calculated using Gaussian 09.[11] The optimized ground-state geometries of all of the molecules were computed using density functional theory (DFT) with the Becke 3-parameter hybrid functional with Lee-Yang-Parr correlation (B3LYP) and the 6-31G(d) basis set, as implemented in Gaussian 09. The optimized structures were verified by computing the infrared (IR) absorption spectra of the structure and verifying that no imaginary frequencies were present. After computing the optimized structures, the first 40 excited states of each molecule were computed using time-dependent DFT (TD-DFT) as implemented in Gaussian 09 at the same level of theory.

To generate the theoretical spectra, each excited state transition was used to generate a Gaussian function according to Equation 2.[12]

$$\varepsilon_i(\lambda) = a \times 10^8 \frac{f_i}{\sigma} \exp\left[-\left(\frac{(1/\lambda - 1/\lambda_i)}{\sigma}\right)^2\right] \qquad (2)$$

Here a is a constant equal to 1.3062974, ε_i is the molar absorptivity of the molecule due to transition i at the given wavelength λ in units of L mol^{-1} cm^{-1}, f_i is the oscillator strength of the transition, λ_i is the wavelength of the transition, and σ is standard deviation (representing the width of the Gaussian function). Because the available range for the standard deviation is from 0.2 eV to

0.8 eV, a default value of 3.226×10^{-4} nm^{-1} (equal to 0.4 eV) was used in this calculation, as has been used previously.[9] Summing the Gaussian functions for each transition provides the theoretical UV-Vis spectrum of the molecule. The complete tabular data for the S_n and T_n energy levels for the new photoinitiator of interest, BDAPT, are shown in Table S1 and Table S2, respectively.

2.2.4 DLW Photopolymerization

The excitation source consisted of a Ti:Sapphire oscillator (Coherent Micra-10) at 800 nm center wavelength and 80 MHz repetition rate. A continuous wave 638 nm diode laser was used as the inhibition beam, introduced via a dichroic beam splitter. Both beams were focused through a 100× objective lens (Nikon, N.A. = 1.49) to the sample located on a 100 μm × 100 μm × 200 μm travel piezostage (Mad City Labs), which is computer-controlled for translation in space. Fast mechanical shutters (Uniblitz) were used to control each beam independently. Attenuation of the laser power was achieved by variable neutral density filters. For each laser, a telescoping lens pair was used to expand the beam diameters before reaching the objective lens. The samples consisted of blends of monomer and photoinitiators sandwiched between a microscope slide and glass coverslip (thickness ~170 μm) with a single layer of Scotch tape providing a gap of ~40 μm. The concentration (by weight) of single photoinitiator in PETA monomer for each sample was 0.25% for BDAPT, 0.5% for both DANT and DAPT, and 1.5% for ITX. Coarse positioning of the sample was performed by a manual, micrometer-driven stage. The stages and objective lenses were mounted on an inverted microscope. All of the writing was performed at scan speed of 100 μm s^{-1}. Laser powers were measured at the back of the objective lens through a 6 mm diameter aperture. The heights of printed polymer lines were measured using an atomic force microscope (AIST NT) with a silicon tip in tapping mode. After these height measurements were made, the structures were

sputter-coated with an Au/Pd mixture, and the samples were imaged using a scanning electron microscope (Hitachi S-4800) with 30 kV accelerating voltage.

2.2.5 Z-scan Measurements

The nonlinear two-photon absorption cross-sections were determined using an open-aperture Z-scan.[13] All Z-scan measurements were performed using 50 fs pulses from a regeneratively amplified laser (KMLabs Wyvern-1000) with a center wavelength of 788 nm and full-width, half-maximum (FWHM) bandwidth of 28 nm. The beam was first spatially filtered before being focused to a beam waist of ~16 μm. Solutions of photoinitiators in THF were evaluated with a 1 mm path length cuvette holding the solution. During the measurement, the sample was translated along the optical (z-) axis by a motorized stage. All of the transmitted signal was collected with a photodetector while a second photodetector measured the beam before the sample to remove any laser instability issues in the final reported data.

2.2.6 Excited State Lifetime Mearsurements

Excited state lifetimes of the photoinitiators were determined by transient absorption measurements using a collinear pump-probe scheme similar to a previous work.[14] Here, the 800 nm pump beam was frequency doubled to 400 nm and the probe beam was set to 633 nm using an optical parameteric amplifier (Quantronix TOPAS-C). The concentrations of ITX and BDAPT in THF were 8.2×10^{-2} M and 1.3×10^{-3} M, respectively. The pump laser fluence was ~1.4×10^{-2} Jcm^{-2} for BDAPT and ~1.2×10^{-3} Jcm^{-2} for ITX. The probe laser fluence was ~3.9×10^{-4} J cm^{-2} for BDAPT and ~4.8×10^{-4} Jcm^{-2} for ITX.

2.2.7 Procedure for the Collection of the MS and NMR Spectra.

MS spectra were collected using a Thermo LTQ coupled with an atmospheric pressure chemical ionizer (APCI) with the following parameters. The source current was set to 5 μA; the vaporizer temperature was set to 300 °C; and the capillary temperature and voltage were set as 250 °C and 12 V, respectively. All NMR data were collected by the Bruker AV-III-400-HD NMR spectrometer and Bruker AV-III-800 NMR spectrometer from department of chemistry, Purdue University.

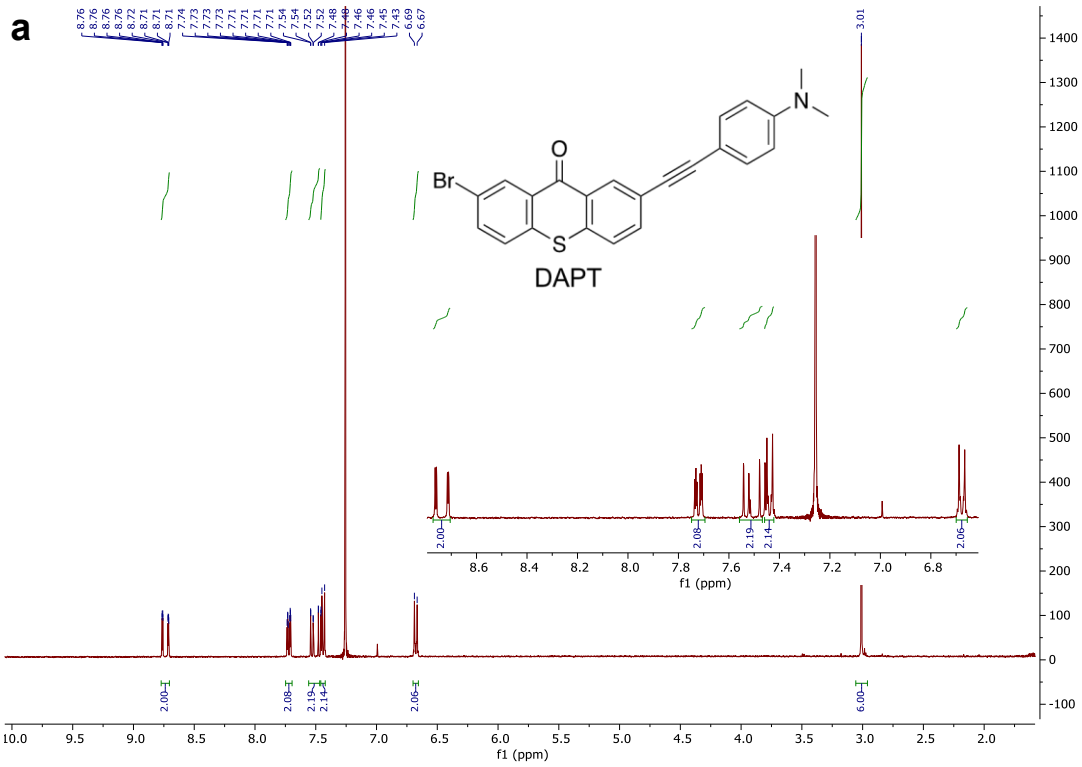

Figure 2.1. (a) ^{1}H NMR; (b) APCI mass spectrum; and (c) high resolution mass spectra of DAPT. Calculated Mass for $C_{23}H_{17}BrNOS$ $[M+H]^{+}$: 434.0214; Found 434.0236

Figure 2.1 continued

b

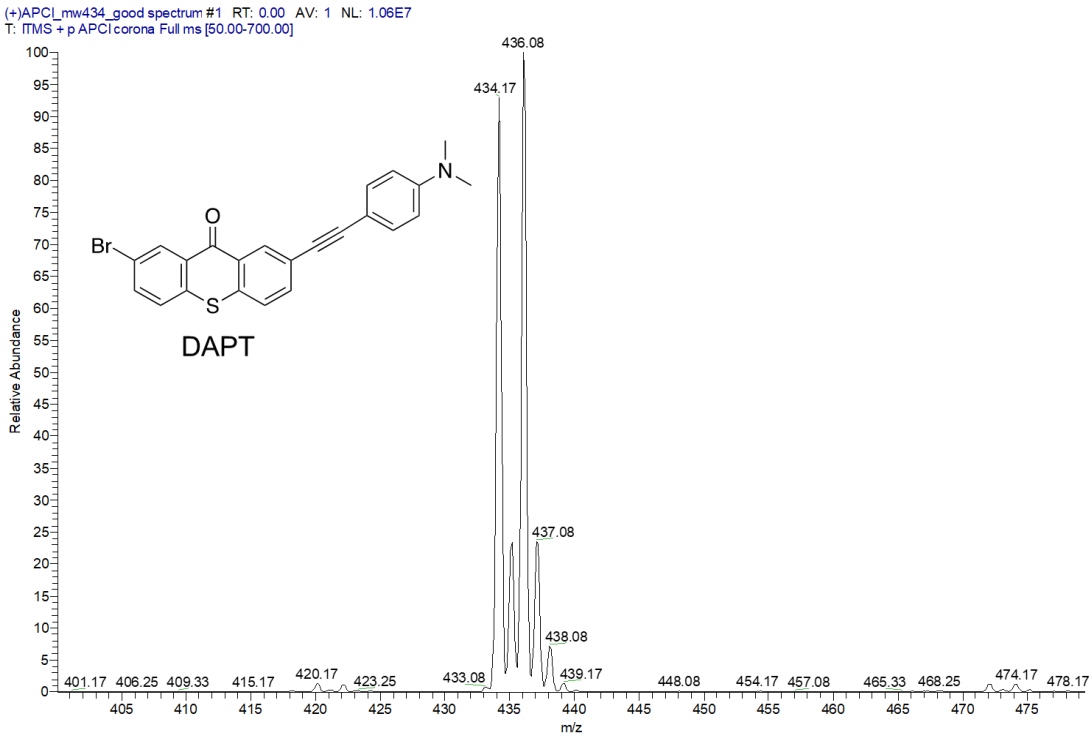

Figure 2.1 continued

c

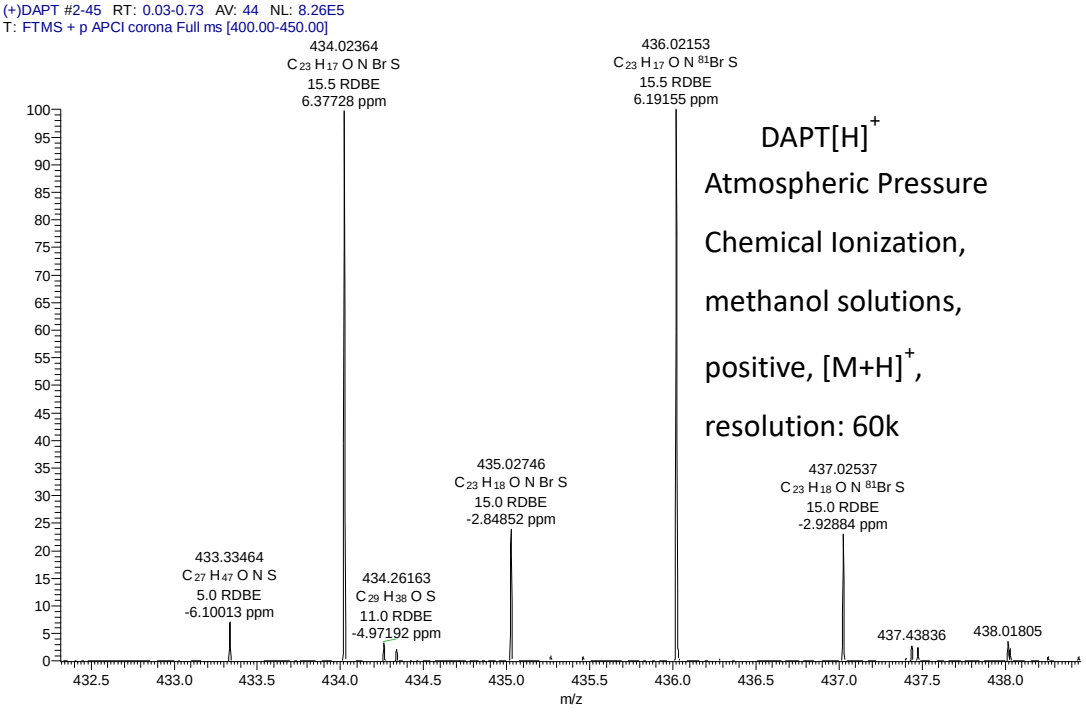

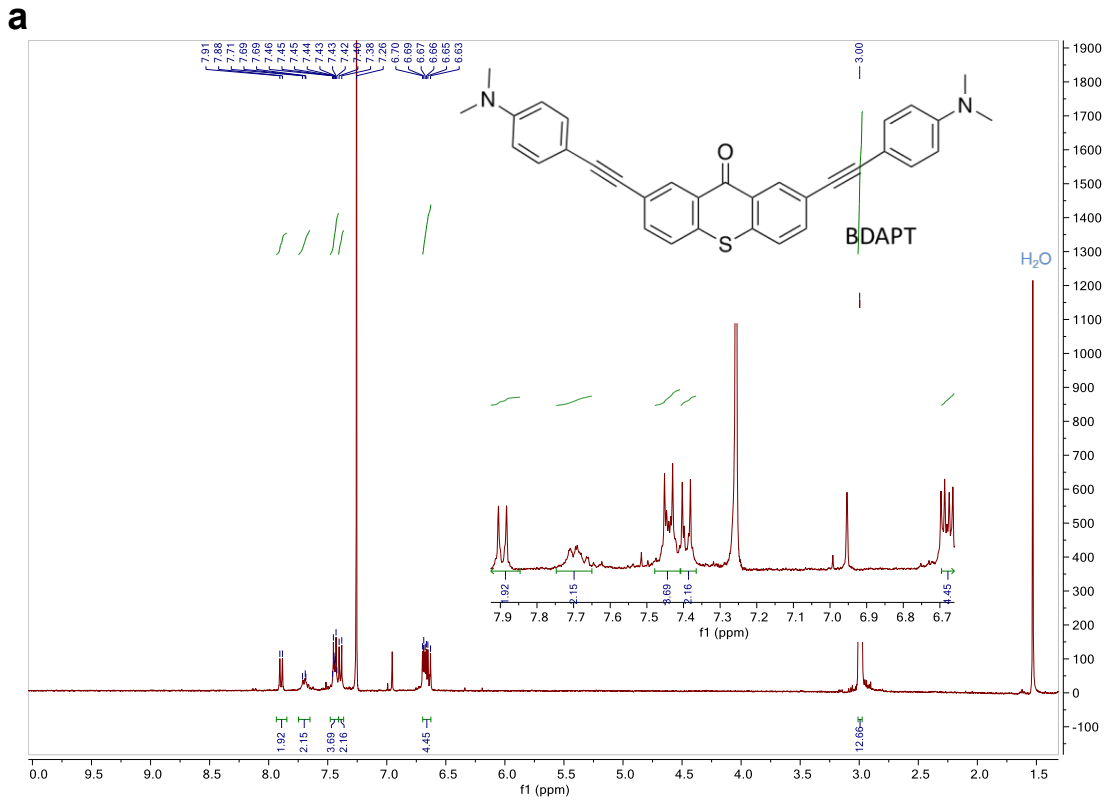

Figure 2.2. (a) ^{1}H NMR; (b) APCI mass spectrum; and (c) high resolution mass spectra of BDAPT. Calculated Mass $C_{33}H_{27}N_2OS$ $[M+H]^+$: 499.1844; Found 499.1876

Figure 2.2 continued

b

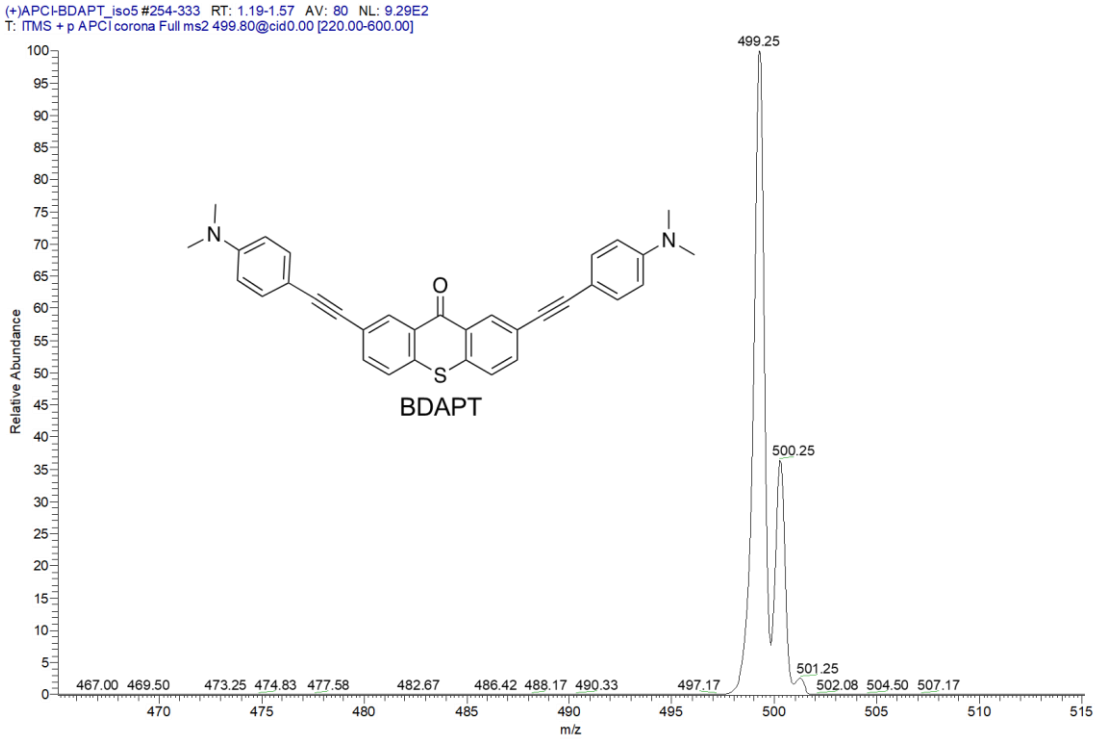

Figure 2.2 continued

c

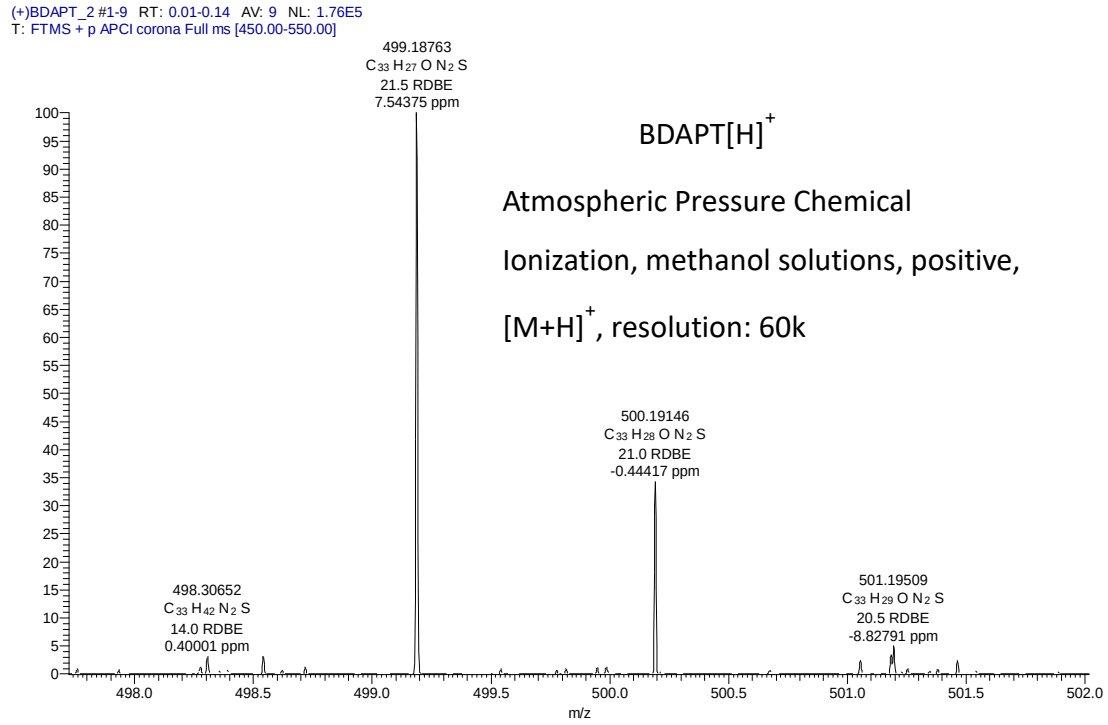

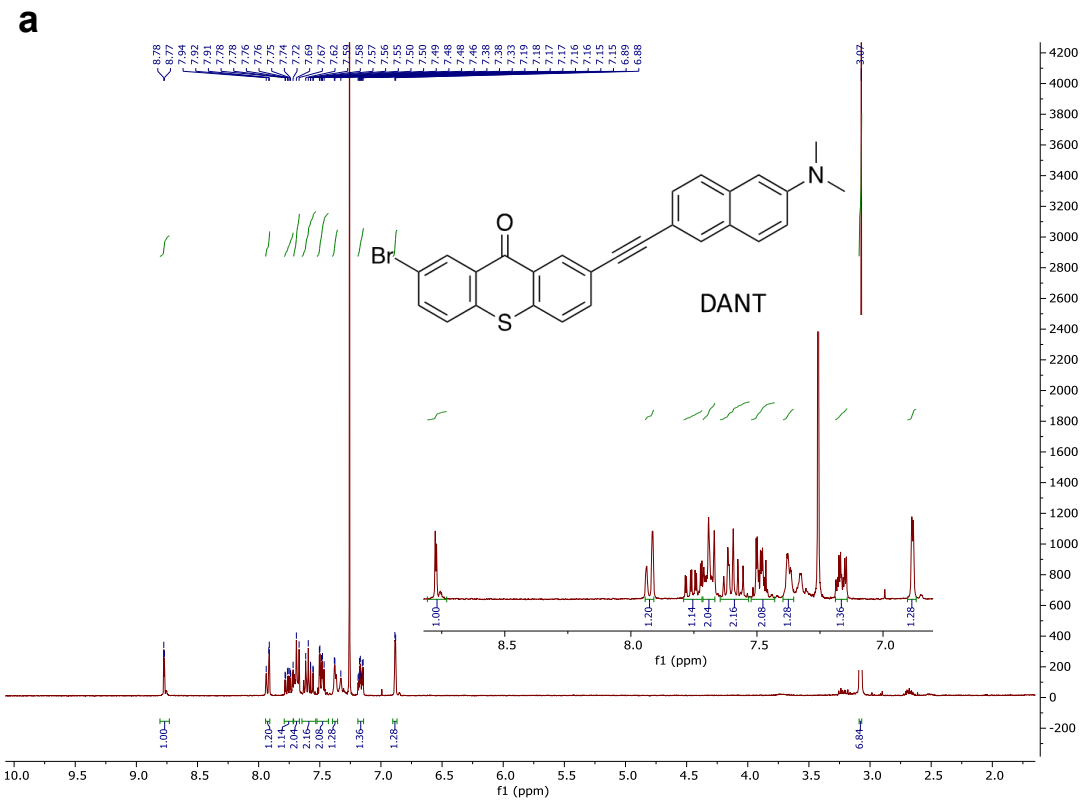

Figure 2.3. (a) ^{1}H NMR; (b) APCI mass spectrum; and (c) high resolution mass spectra of DANT. Calculated Mass $C_{27}H_{19}BrNOS$ $[M+H]^{+}$: 484.0365; Found 484.0364

Figure 2.3 continued

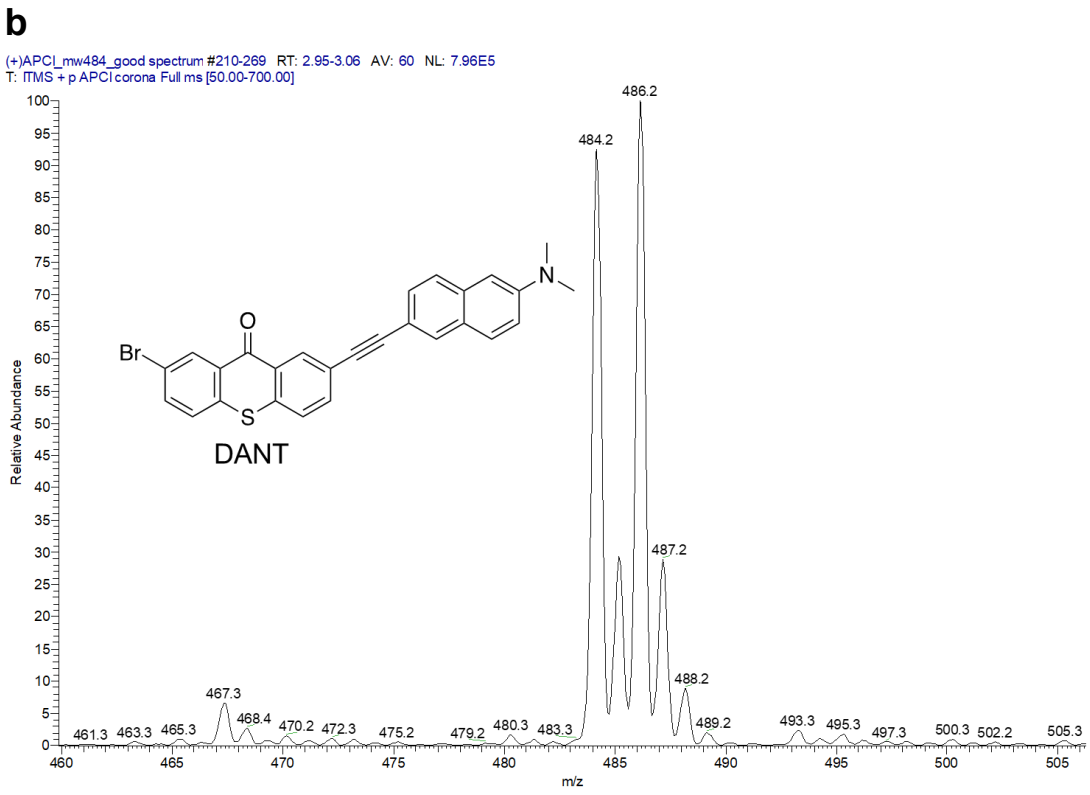

Figure 2.3 continued

c

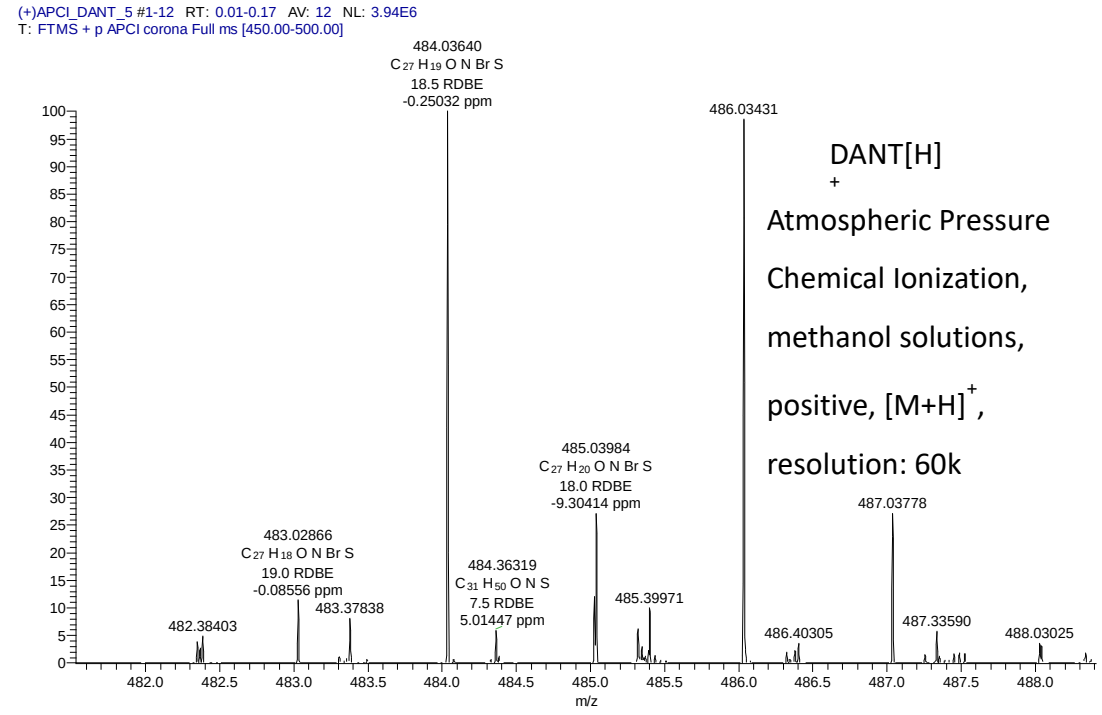

2.3 Results and Discussion

2.3.1 UV-Vis Prediction and Chemical Structure Design

As a commercially available photoinitiator, ITX has served as a model molecule that reveals the mechanism of energy transfer in two-photon DLW polymerizations, and the general picture of its operating mechanism in photopolymerizations is as follows. First, an electron in the ground state (S_0) of ITX is promoted to the first excited state (S_1) through a two-photon optical transition using an 800 nm wavelength laser.[15] Then, the excited state undergoes intersystem crossing to generate the triplet state (T_1), which initiates the polymerization when ITX is blended with the monomeric species. As revealed by previous pump-probe spectroscopy experiments,[4,15] the ITX molecule can undergo depletion of the excited state through both: (1) stimulated-emission depletion (STED) and (2) non-radiative decay by excitation of long-lived species in order to inhibit the polymerization. The latter of these two dominates in depletion DLW polymerization when ITX is the photoinitiator.[4,15]

Due to the well-understood excited state dynamics of ITX, it is useful as a starting material for the development of high-performance polymerization photoinitiators. As such, the design of our photoinitiators is based on a previous work of the Gryko group.[16] This extended conjugation,results in a bathochromic shift in the peak of the absorbance spectra of the molecules. Dialkylamino groups were added to terminate the ends of the molecules due to the strong electron-donating features of these substituents. In addition, mono-substituted and di-substituted derivatives were designed and compared in to elucidate the influence of the numbers of pendant groups on the photophysical properties of the polymerization initiators. Moreover, in order to guide the synthetic design, computational calculations were utilized to predict the absorption spectra of a set of potential photoinitiator molecules,[11] and the experimentally-synthesized materials were those that

showed the most promise from these simulations. For example, relative to ITX, the peak absorption wavelength is red-shifted for the BDAPT; 2-bromo-7-((6-(dimethylamino)naphthalen-2-yl)ethynyl)-9H-thioxanthen-9-one (DANT) and 2,7-bis((6-(dimethylamino)naphthalen-2-yl)ethynyl)-9H-thioxanthen-9-one (BDANT); 2-bromo-7-((4'-(dimethylamino)-[1,1'-biphenyl]-4-yl)ethynyl)-9H-thioxanthen-9-one (DEPT) and 2,7-bis((4'-(dimethylamino)-[1,1'-biphenyl]-4-yl)ethynyl)-9H-thioxanthen-9-one (BDEPT) compounds (Figure 2.4).

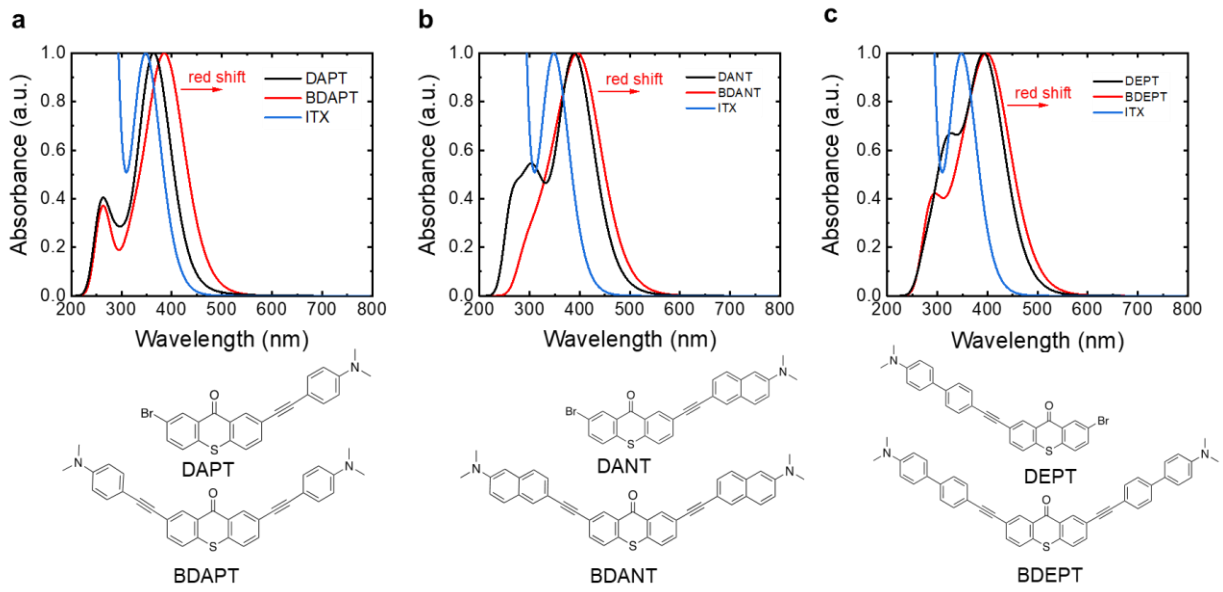

Figure 2.4. Predicted UV-Vis absorption plots for: (a) ITX, DAPT and BDAPT; (b) ITX, DANT and BDANT; and (c) ITX, DEPT and BDPET. These predictions were made using TD-DFT with a B3LYP/6-31G(d) level of theory. The structures of the simulated photoinitiating molecules (aside from ITX) are shown directly below their calculated absorption spectra.

This agrees with the concept that the extension of the π-system in photoinitiators can cause a redshift in the peak absorption of these ITX-based molecules. Moreover, there was a predicted red-shift between the mono-substituted and the di-substituted derivatives as well. For example, in the predicted UV-Vis absorption data, the maximum absorption wavelength of BDAPT was

redshifted about 25 nm relative to DAPT. This redshifted trend also was observed in the DANT-based and DEPT-based systems due to the extension of the π-system.

All the molecules have a relatively high predicted molar absorptivity coefficient at 400 nm (Table 2.1), which demonstrated their potential feasibility as efficient photoinitiators. Based upon these DFT results, the most promising compounds (i.e., DAPT, BDAPT, and DANT) were synthesized as these molecules exhibited strong absorption and were predicted to have maximum absorption wavelengths around 400 nm. Specifically, we designed a series of compounds based on an ITX core with different substituent groups. After our initial design, a straightforward series of high-throughput experiments (*vide infra*) were performed in order to down-select the most promising photoinitiating candidates. In this way, design and selection rules can be had for these types of photoinitiating systems.

In this particular effort, alkyne groups were introduced as linkers between the backbone and the branches for two major reasons. First, this functionality increases the distance between the backbone and substituent branches to avoid steric hindrance effects, which may interrupt the conjugated system due to the possibility of rotation. Second, this functionality maintains aromaticity across the molecular system. Thus, functional groups were attached through the triple bond bridge. Specifically, phenyl, diphenyl, and naphthyl groups were synthesized and bonded through the alkyne group in a systematic way (Figure 2.5). That is after a base-promoted aromatic substitution with dimethyl amine,[17] the naphthyl substituted group (compound 3) was generated by a Sonogashira coupling reaction.[18] Similarly, the diphenyl substituted group (compound 6) was generated by a Pd-catalyst Suzuki coupling[19] followed by a Sonogashira coupling reaction.[20] Finally, the 4-ethynyl-N,N-dimethylaniline (compound 8) was commercially available, and it was purchased directly from Sigma Aldrich.

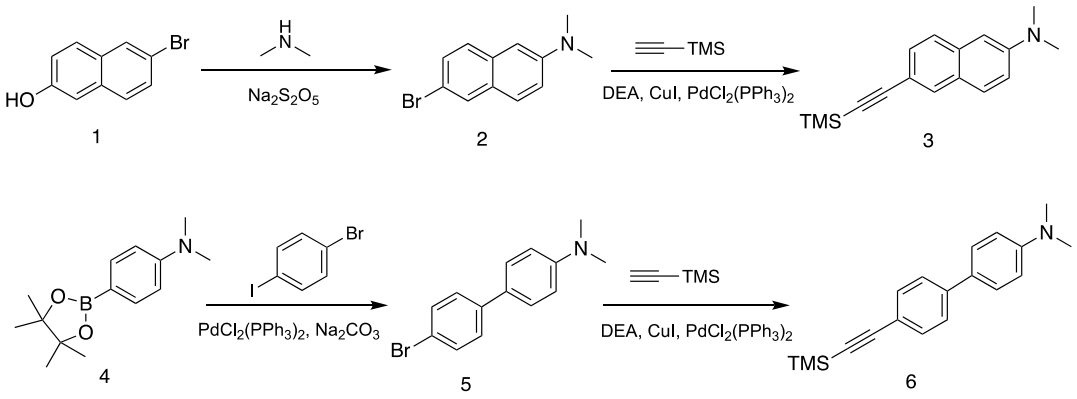

Figure 2.5. Synthetic pathway of the substituents of the photoinitiators

The synthetic pathway shown in Figure 2.6 was then utilized to create the advanced photoinitiators, and these molecules were characterized by ^{1}H NMR spectroscopy and mass spectroscopy (Figure 2.1 – Figure 2.3).[18,20] Dibromothioxanthen-9-one (DBTX) can be synthesized through a bromination reaction.[21-23] BDAPT and DAPT can be successfully formed by traditional Sonogashira coupling reactions using a single step.[18,20,24] The major product of these reactions (i.e., either the di-substituted BDAPT or mono-substituted DAPT) can be controlled by changing the ratio of two different starting materials. DANT can also be generated through the same Sonogashira coupling in similar conditions; however, due to the instability of those species, the yield of DAPT, BDAPT, and DANT were low (11%, 10%, and 8%, respectively), and BDEPT, DEPT, and BDANT were not isolated in a manner that allowed for their evaluation as photoinitiating species.[25,26]

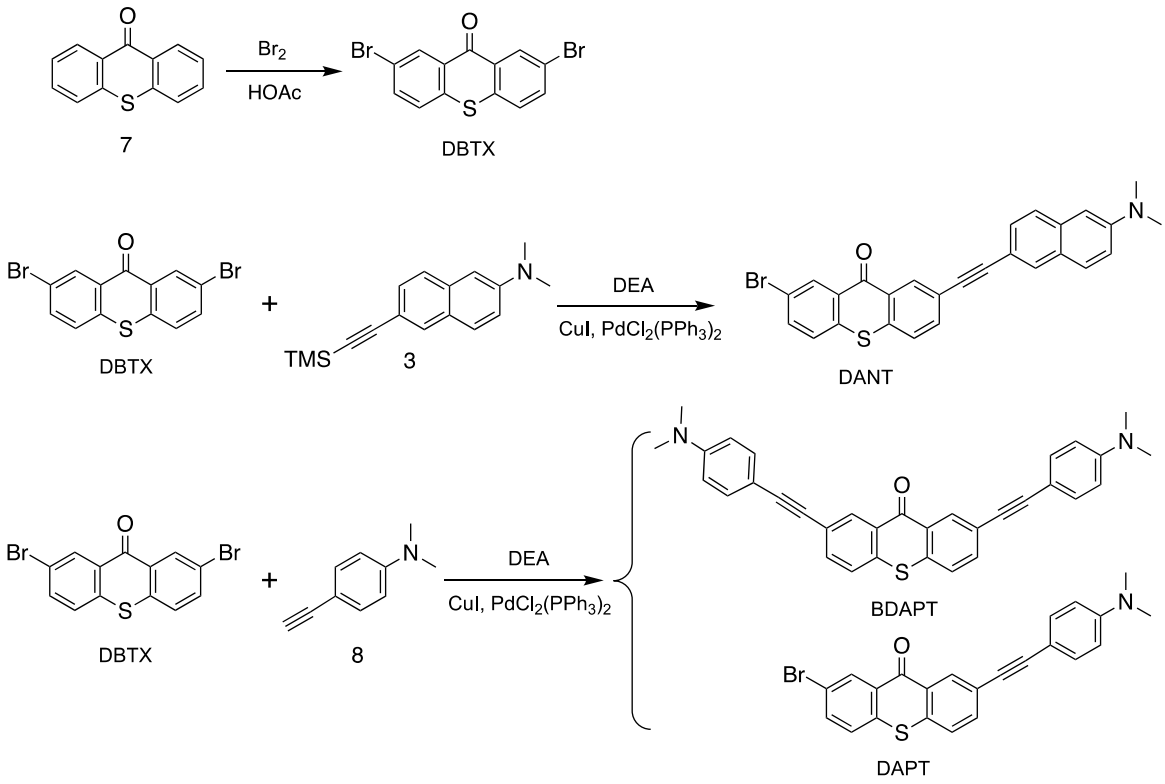

Figure 2.6. Synthetic pathway for the advanced photoinitiators.

2.3.2 TD-DFT Calculation of HOMO and LUMO

After the successful syntheses according to Figure 2.5 and 2.6, the frontier molecular orbitals were calculated and are shown in Figure 2.7. The thioxanthone core can be thought of as an acceptor and the (*N*,*N*-dimethylamino)phenyl moieties as the donors. The first two singlet excited states for BDAPT are transitions from the HOMO to the LUMO and from the HOMO–1 to the LUMO, respectively. These correspond to the intramolecular charge transfer states, as evidenced by the shift in the wavefunction density from the entire molecule to the thioxanthone center. The third calculated singlet excited state, which corresponds to the primary excitation at 400 nm, is a transition from the HOMO to the LUMO+1. This, by contrast, results in minimal change in the charge density on the molecule. Thus, the transition from S1 to the lower optically inactive singlet states could proceed by a charge transfer mechanism.

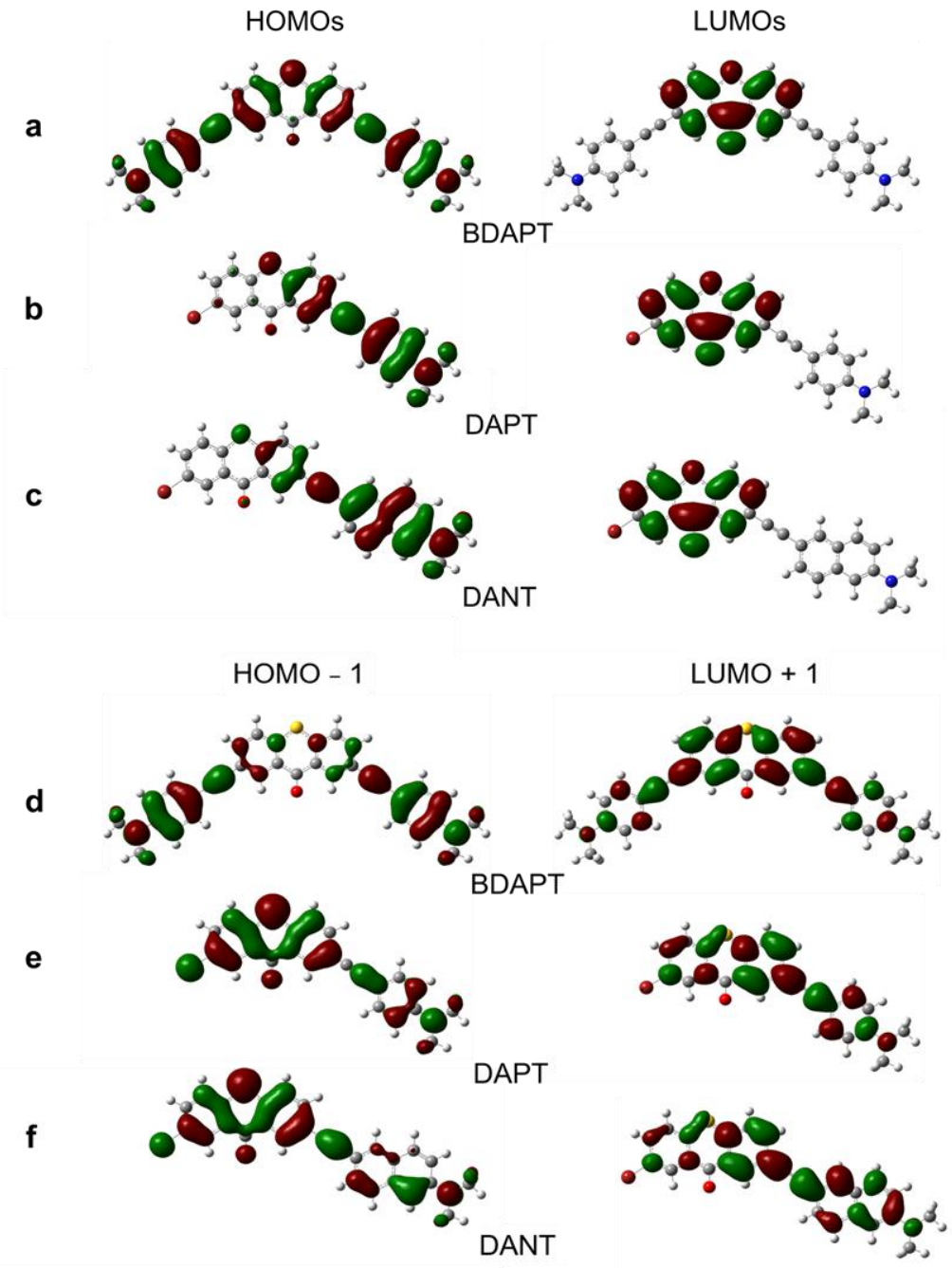

Figure 2.7. Molecular orbital diagrams calculated at an isovalue of 0.02. These plots are of the: (a) HOMO, LUMO of BDAPT; (b) HOMO and LUMO of DAPT; (c) HOMO and LUMO of DANT; (d) HOMO-1 and LUMO+1 of BDAPT; (e) HOMO-1 and LUMO+1 of DAPT; and (f) HOMO-1 and LUMO+1 of DANT. They are used to illustrate the charge transfer states in those molecules. It can be seen that the HOMO, HOMO–1, and LUMO+1 wavefunctions are either spread over the entire molecule or localized to the (N,N-dimethylamino)phenyl moieties, while the LUMO wavefunctions are localized to the thioxanthone core. Therefore, electronic transitions from the highest two occupied orbitals to the LUMO should result in a transfer of charge from the branches to the core, while transitions to the LUMO+1 should not result in a charge transfer state formation.

2.3.3 Optical Properties of New Synthesized Photoinitiators

The absorption and emission properties of the materials were characterized in order to compare their experimental properties to the predicted properties and to evaluate their potential utility in the DLW photopolymerization process. In particular, synthesizing molecules with large molar absorptivity values at half the wavelength used in the DLW process (i.e., 400 nm) is of prime interest. Moreover, these same molecules should demonstrate relatively strong emission at the common depletion laser wavelength of 532 nm in their fluorescence spectra for quenching of the polymerization via the STED process. The normalized experimental UV-Vis absorption data are shown in Figure 2.8 and 2.9. DBTX was included in the result as a comparison in order to provide a baseline material that did not include any conjugated branches, and the experimental absorption spectrum of DBTX is redshifted relative to ITX. BDAPT as well as DANT had two broad peaks[27,28] with relatively high absorbance at 400 nm, which can be attributed to the $\pi \rightarrow \pi^*$ transition at higher wavelength and $n \rightarrow \sigma^*$ jumping at lower wavelength due to the electron lone pair on the hetero atom.[29,30] DAPT was also red-shifted (Figure 2.10), likely because of the charge transfer state generated by the asymmetric structure of DAPT.[31] As a result, all the new photoinitiators were red-shifted as designed and had a relatively high absorption at 400 nm in UV-Vis spectrum (Figure 2.10), such that the excitation processes occurred readily.

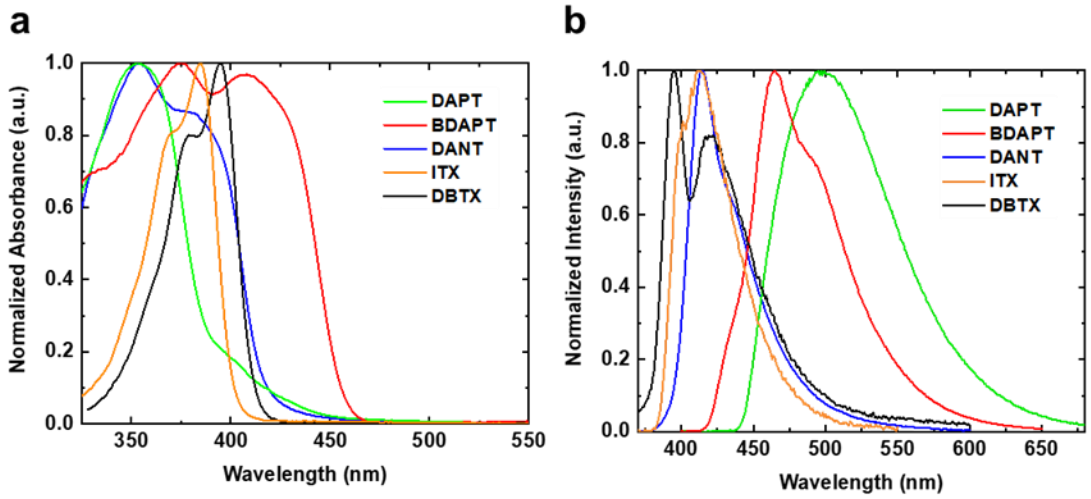

Figure 2.8. (a) The normalized UV-Vis absorbance spectra of photoinitiators in toluene. (b) The fluorescence spectra of the initiators in toluene obtained with excitation at 350 nm.

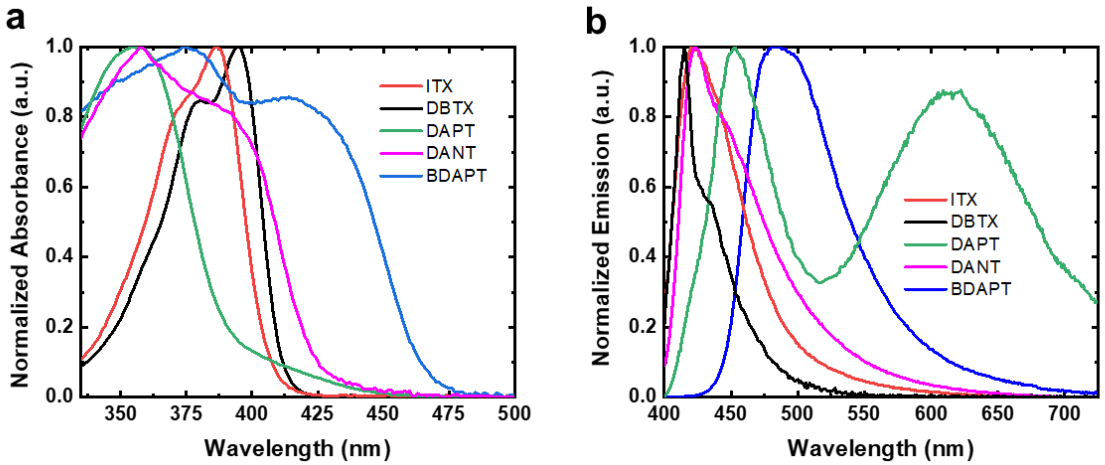

Figure 2.9. (a) The normalized UV-Vis absorbance spectra of photoinitiators in THF. (b) The fluorescence spectra of the initiators in THF obtained with excitation at 350 nm.

For light-induced inhibition of the DLW photopolymerization, ITX has been shown to predominantly follow a triplet-triplet-absorption depletion pathway for the initiating species. However, for ITX derivatives such as these, there are other potential depletion pathways that may be non-negligible, or even dominating, for inhibiting the polymerization process.[32] In order to determine the possible contribution of another popular depletion mechanism, stimulated emission

depletion, to the polymerization inhibition process, the fluorescence of each molecule was established. The peak emission wavelength trend of the different compounds is DBTX < ITX < DANT < DAPT < BDAPT (Figure 2.8b). Exposure of BDAPT at 532 nm may provide the greatest potential for STED because the peak of fluorescence emission is approaching 532 nm. Excitation spectra were collected and compared to the absorption spectra. The spectra closely matched, indicating the observed emission is not due to an instrumentation artifact (Figure 2.11). Thus, from both the UV-Vis and fluorescence spectra, BDAPT and DANT showed the potential to replace ITX as high-performing photoinitiators for DLW nanolithographic applications.

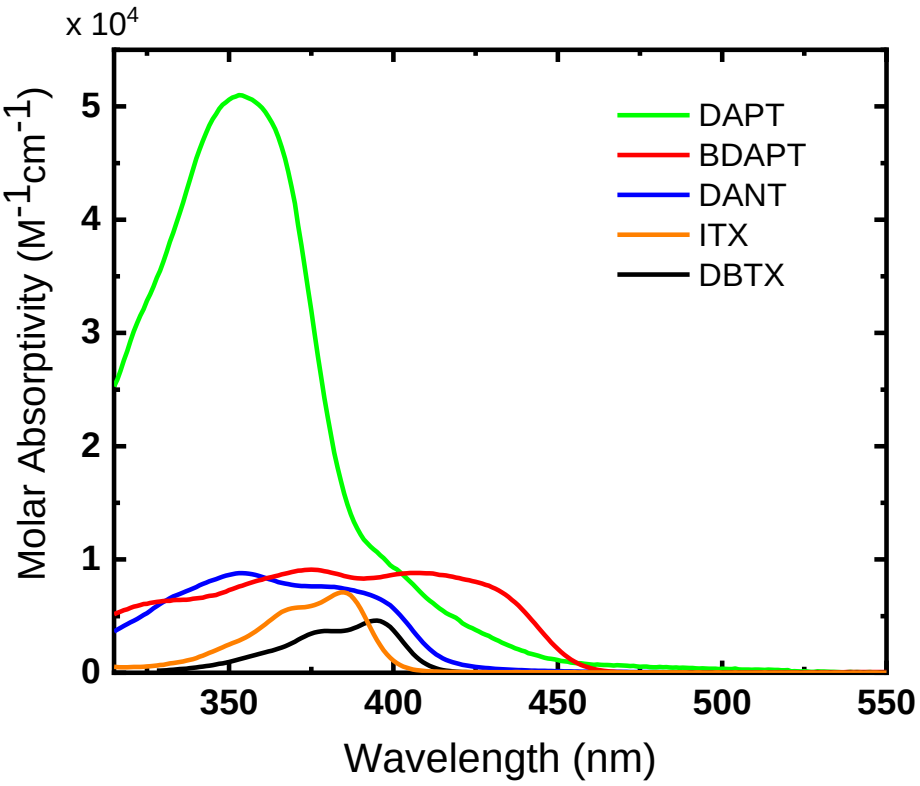

Figure 2.10. Molar absorptivity of the photoinitiators in toluene with the signals acquired at room temperature. All photoinitiators are red-shifted around 400 nm compared to ITX, with comparable molar absorptivity values.

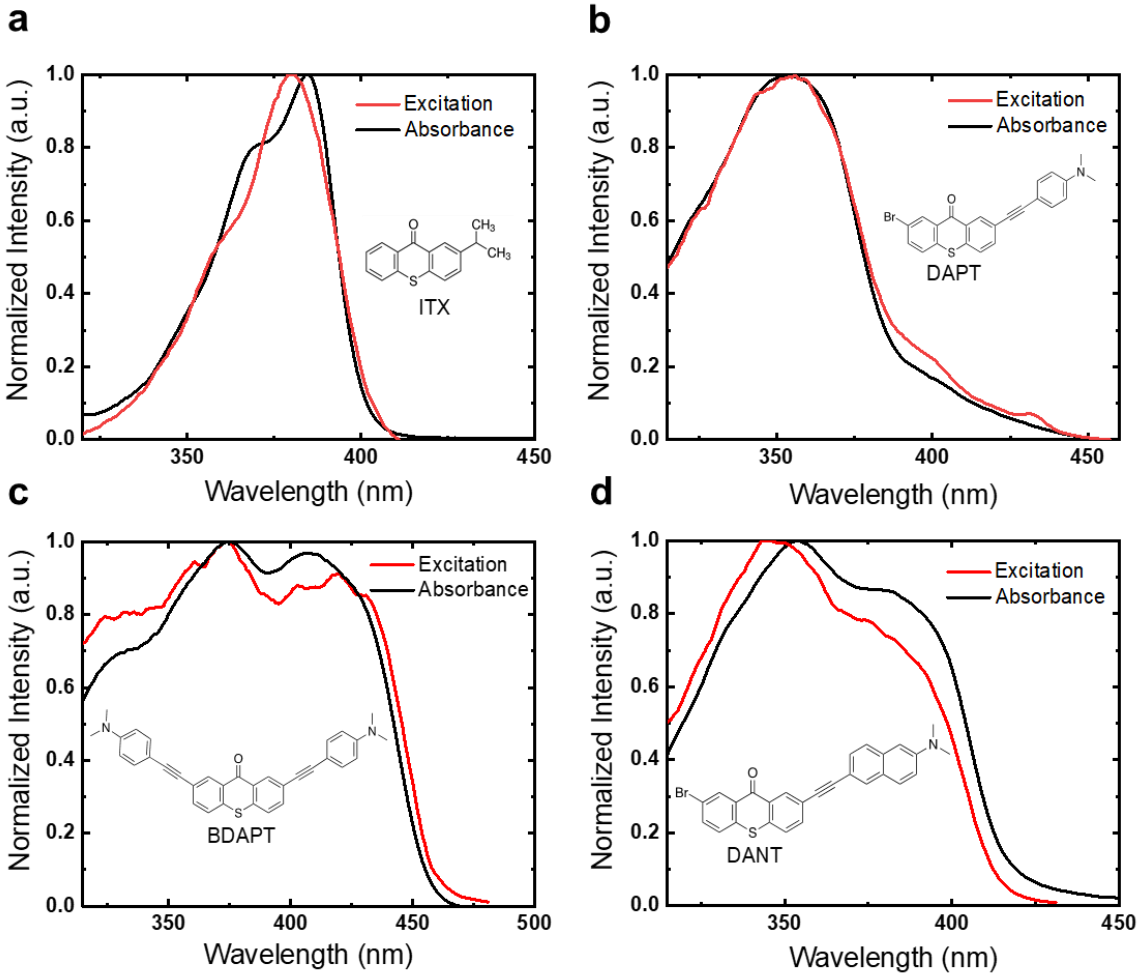

Figure 2.11. The excitation and absorbance spectra of the photoinitiators at room temperature in toluene (a) The excitation and absorbance spectrum of ITX match with each other. (b) The excitation spectrum is identical to the absorption spectrum for DAPT. The close similarity between excitation and absorbance of (c) BDAPT and (d) DANT confirms the resulting emission spectra are not due to instrumental error or sample impurity.

The coefficient of extinction and fluorescence quantum yield are listed in Table 2.1, and the raw data are presented in Figure 2.12. All of the initiators, including ITX, had a relatively low fluorescence quantum yield in PETA, which indicated that the stimulated emission depletion process likely was not a dominate pathway and non-radiative decay from the excitation of long-lived species should be the major process for depletion. Therefore, any depletion effects exhibited in DLW with new initiators can be expected to follow a similar pathway as observed with ITX.

Table 2.1. Absorption coefficients and fluorescence quantum yields of the photoinitiators

Photoinitiator	Solvent	Peak Absorption Wavelength (nm)[a]	Theoretical Peak Absorption Wavelength (nm)	ε^b (10^4 mol^{-1}Lcm^{-1})	ε^c (10^4 mol^{-1}Lcm^{-1})	Φ_{fl} %[e]
ITX	Toluene	385	348	0.71	0.57	
	PETA	387		0.23	0.21	1.6
BDAPT	Toluene	408	390	0.91	0.83	
	PETA	414		2.0	1.8	8.1
DAPT	Toluene	353	365	5.1	1.2	
	PETA	- [d]		- [d]	- [d]	- [d]
DANT	Toluene	380	389	0.88	0.71	
	PETA	390		1.6	1.4	4.4
DBTX	Toluene	395		0.46	0.42	
	PETA	- [d]		- [d]	- [d]	- [d]

[a] The peak wavelength is the maximum absorption near a wavelength of 400 nm if there are multiple peaks in the spectra. [b] The molar absorption coefficient of the species at the wavelength demonstrating the maximum absorption. [c] The molar absorption coefficient at the 390 nm wavelength. [d] Insufficient signal or difficult to dissolve in the PETA monomer. [e] Fluorescence quantum yield when the excitation wavelength was set to 390 nm.

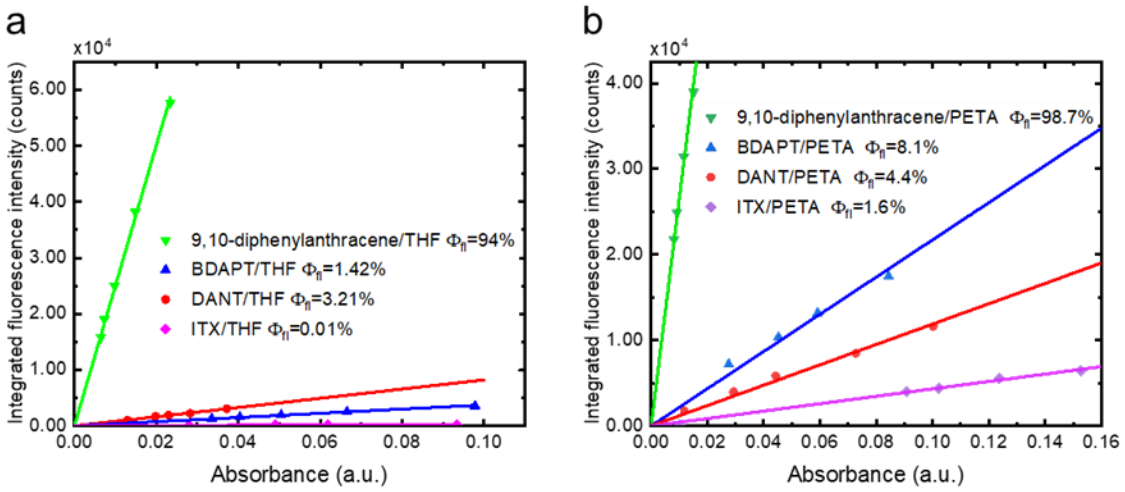

Figure 2.12. (a) The fluorescence quantum yield of BDAPT, DANT, and ITX in THF. The fluorescence quantum yield of DAPT in THF is lower than 0.01%. (b) The fluorescence quantum yield of BDAPT, DANT, and ITX in PETA. DAPT and DBTX suffered a solubility issue in PETA.

2.3.4 Practical Lithographic Printing of New Synthesized Photoinitiators

The extinction coefficient provides a clear representation of the ability of the photoinitiator to absorb light through a one-photon process; however, it was initially used here as an indicator of the absorptive properties of the new initiators through a two-photon process. To directly measure the nonlinear absorption properties, an open-aperture Z-scan was performed for each of the photoinitiators.[23] The measured two-photon absorption (TPA) cross-sections, σ_2, are presented in Table 2.2 along with the DLW polymerization writing thresholds for the initiators in PETA. The writing threshold power is the minimum laser power required to write a defined line structure that survives the development process.

For comparison purposes, the writing thresholds for each resist were calculated by dividing the photoinitiator concentration by the writing threshold power at 100 μm s^{-1}. In order to account for unknowns in the Z-scan measurement, the ITX molecule with a known σ_2[5,14] was used as a reference to calibrate the measurement and obtain the presented values.

Table 2.2. Two-photon absorption cross-section σ_2 and writing threshold of photoinitiators

Photoinitiator	σ_2 (GM)[a]	Writing threshold (10^{18} molecules mW^{-1})
BDAPT	368 (±45)	0.651
DANT	524 (± 61)	1.484
ITX	3 (± 0.4)	4.065
DAPT	122 (± 21)	- [b]
DBTX	22 (± 5)	- [b]

[a] The values in parentheses indicate one standard deviation from the average measured value. [b] Difficulty dissolving this material uniformly in the monomer.

The trend of TPA cross-sections is ITX < DBTX < DAPT < BDAPT < DANT. Although BDAPT and DANT trade spots in the TPA compared to their linear extinction coefficients determined through single-photon absorption, the simple extinction coefficient measurements provide reasonable indicators of the two-photon absorbing process. Moreover, the new initiators, especially BDAPT and DANT, were much improved relative to the ITX TPA cross-section and showed lower DLW polymerization thresholds; thus, they stood out as promising photoinitiating candidates.

Beyond improving the writing threshold for the DLW polymerization, it was necessary to investigate if the polymerization inhibition effect available in ITX was also present in the synthesized photoinitiators. To illustrate the depletion of the excited state, a 405 nm exciting laser was introduced orthogonally to a 633 nm laser beam and signal path (Figure 2.13a). In this configuration, the 633 nm laser was treated as the depletion laser. Assuming no saturation effects were occurring, if the addition of individual fluorescence signals for sample exposure by excitation (405 nm) and depletion (633 nm) lasers was equal to the signal of when both the excitation and

depletion sources were on, the photoinitiator responds to the each light independently. However, if the sum of individual signal was higher than the signal of both lasers when they were in the on state, depletion of the fluorescing state of the photoinitiator occurred. Alternatively, additional absorption was said to be detected if the sum of the individual signals was lower than that of the signals when both lasers were in the on state. For the BDAPT in THF solution shown in Figure 2.13b, three different depletion laser powers were tested, and the 405 nm wavelength excitation power was held constant. For all three depletion intensities the sum of individual signals was greater than the signal with both lasers on indicating a depletion of the BDAPT excited state by the 633 nm laser.

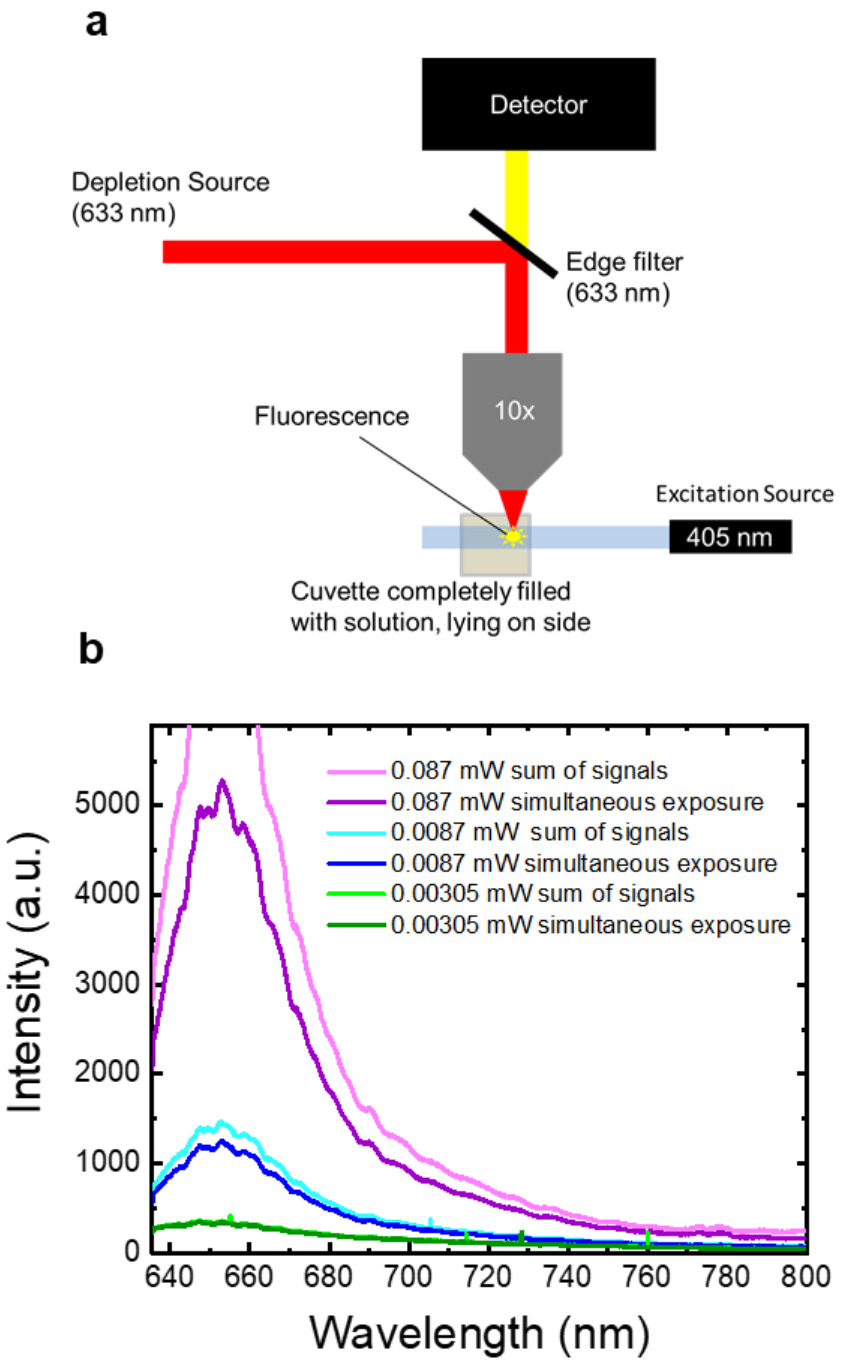

Figure 2.13. (a) A diagram of the experimental set-up for the two-laser spectroscopy system utilized to detect the depletion of select photoinitiators. (b) The fluorescence spectra with sum of individual excitation and depletion signals and the signal with both beams on simultaneously with 633nm as depleting laser. The clear evidence of depletion was a good indicator of the ability to inhibit the photopolymerization process in actual DLW polymerization processes. As such, this photoinitiator was brought forward for complete DLW photopolymerization evaluation.This effect was not observed when 633 nm laser was replaced with 532 nm laser.

Many factors contribute to a successful photoinitiator for the DLW photopolymerization process, making it difficult to accurately predict its exact performance during actual printing conditions. Specifically, the polymerization inhibition effect is not easily measured outside of a direct test inside a monomer matrix. Due to its performance in the above-mentioned experiments, BDAPT was selected for its potential ability to perform in the DLW photopolymerization process. In particular, BDAPT showed promise with respect to the two-laser system described above, due to its large TPA cross-section, and due to its relatively large solubility in the PETA monomer compared to DANT. For this evaluation, a 638 nm laser was spatially overlapped with the DLW 800 nm beam and a Gaussian profile is used for both beams; care was taken to ensure that the focused 638 nm beam diameter was at least as large as the DLW spot. The depletion laser wavelength of 638 nm was chosen as a result of the above fluorescence depletion experiments. BDAPT at a loading of 0.25% (by weight) in PETA was used as the test photoresist. Shown in Figure 2.14, a group of parallel polymer lines were printed using the DLW polymerization process. During the writing of each line, the sample was exposed to the 638 nm laser for 10 μm of the line path without turning off the DLW beam. During that time of exposure to the inhibition beam, which correlated to 10 μm in space, the polymerization was fully inhibited. It is worth noting, however, that the conditions to observe this effect required careful control of the DLW beam power slightly below the writing threshold. This led to the poor quality of printed lines observed in the figure. Beyond that, the 638 nm laser power required for inhibiting the polymerization was large compared to using ITX as photoinitiator.

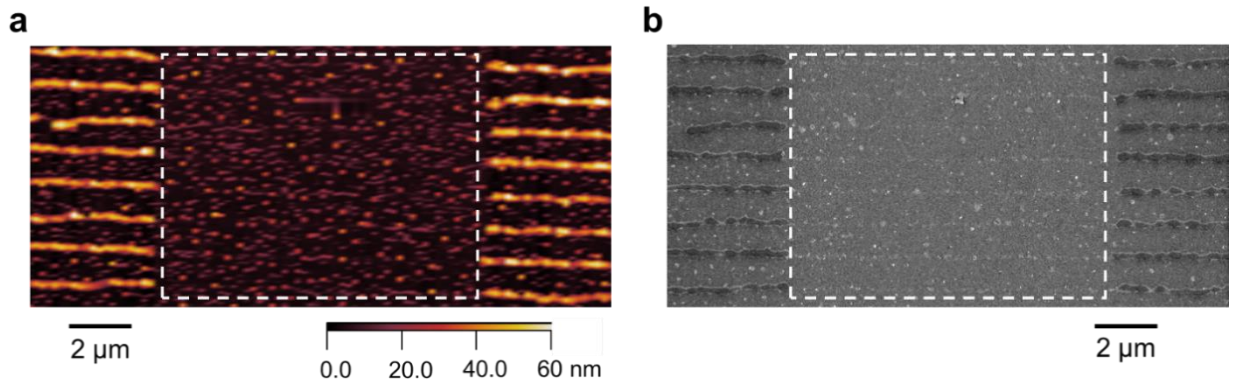

Figure 2.14. Selectively-inhibited DLW photopolymerization using BDAPT (0.25%, by weight) as a photoinitiator in the PETA monomer. Polymer lines were written at 100 µm s^{-1} with the 638 nm diode laser turned on for 10 µm, preventing polymerization in the region shown by the box highlighted by white dashed lines. Panel (a) shows the AFM image of the printed polymer nanoscale lines, and panel (b) shows the SEM image of the same polymer lines.

2.3.5 Nanowriting Mechanism Study of New Synthesized Photoinitiators

In order to elucidate the inhibition effects for BDAPT, ultra-fast transient absorption experiments were performed on BDAPT and ITX (Figure 2.15a). A wavelength of 400 nm was used as the pump in order to excite the S_1 state of the molecules, in a manner similar to other studies.[13] This wavelength matched the induced transition of the two-photon absorption occurring during the DLW polymerization process with a 800 nm laser, and it allowed for more uniform pumping of the molecules to the excited state with a lower pump laser power. The probe wavelength was chosen to be 633 nm. Two lifetimes were fit for both ITX (τ_1 = 30.2 ps, τ_2 = 4.2 ns) and BDAPT (τ_1 = 6.9 ps, τ_2 = 187 ps). In the case of ITX, because the pump energy closely matches the S_1 energy level, the fast lifetime (τ_1) is attributed to the S_1* states, and the longer lifetime is attributed to the S_1 state, which is consistent with a previous report.[13] In other words, τ_1 represents how fast S_1 is filled while τ_2 is the rate at which S_1 is depopulated, where some of the population from the S_1 state was transferred to the longer-lived triplet state which initiates polymerization. In this scenario, the probe beam is interacting with a $S_1 \rightarrow S_n$ transition.

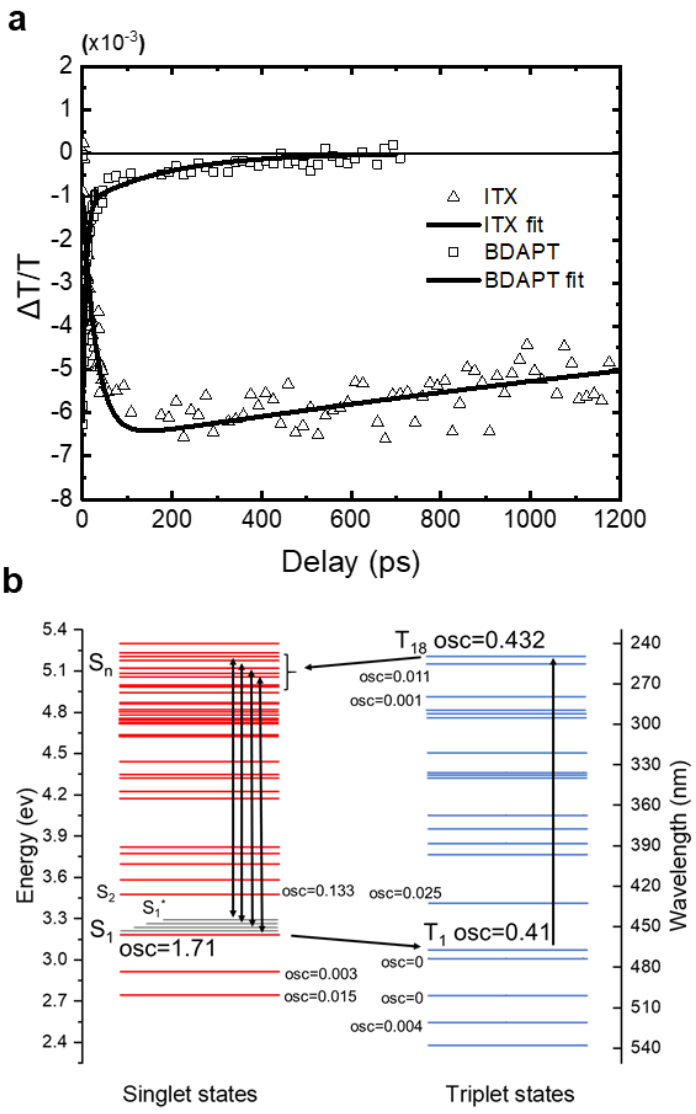

Figure 2.15. (a) Ultra-fast transient absorption measurement of ITX and BDAPT in THF. The pump and the probe wavelengths used were 400 nm and 633 nm, respectively. The solid lines represent fits to the data, which is shown as either open triangles (ITX) or open squares (BDAPT). (b) The DFT calculation of the singlet states and triplet states of BDAPT and the most likely pathway of depletion. S_1* levels are not calculated and are sketched for visualization purposes only.

In the case of BDAPT, a proposed probe interaction was with respect to both the $S_1 \rightarrow S_n$ and the $S_1^* \rightarrow S_n$ transitions. A sharp initial drop in the transmission curve occurred on a timescale comparable with the pulse duration, where S_1 and S_1* were filled by the pump beam. The $S_1^* \rightarrow$

S_1 intraband transition was then observed to have a lifetime of τ_1, which was about 4 times shorter than for ITX. A final S_1 lifetime of τ_2 (187 ps) for BDAPT was found to be about 22 times shorter than τ_2 (4.2 ns) for ITX. As shown in the calculations of Figure 2.15b, BDAPT was predicted to undergo a $T_1 \rightarrow T_n$ transition.[4] The calculated energy gap between T_1 and T_{18} was 581 nm, which is smaller than the depleting laser used during lithography because the energy gap in PETA solution is different from the energy gap with no solvent present.[34,35] This led to the inhibition of the polymerization by depopulating the T1 state before polymerization occurred, similar to the mechanism commonly-associated with depletion in ITX-based systems.[4] It is crucial to notice that the lifetime of the S_1 state (187 ps) for BDAPT is much shorter than the lifetime of S_1 state (4.2 ns) for ITX. This large difference leads to a sizeable population of BDAPT entering the T_1 state in a short period of time. T_1 is the energy state leading to polymerization during nanoprinting, which is why BDAPT can initiate writing at a 5-fold lower power than ITX.

To provide insight into the T_1 lifetimes, phosphorescence spectra at a temperature of 77 K were acquired. As shown in Figure 2.16, all the initiators possess clear phosphorescent emission, which indicates that the depletion of singlet excited state via intersystem crossing to the triplet state exists in all of the systems evaluated here. The trend of the phosphorescent lifetimes is DBTX (10 ms) < ITX (120 ms) < DAPT (219 ms) < BDAPT (287 ms) < DANT (379 ms), which represents the sequence of how long the molecules would have their T_1 states populated. When comparing DBTX, DAPT, and BDAPT, we establish that the addition of conjugated branches increases the phosphorescence lifetime, though the effect is decreased when the second branch is introduced.

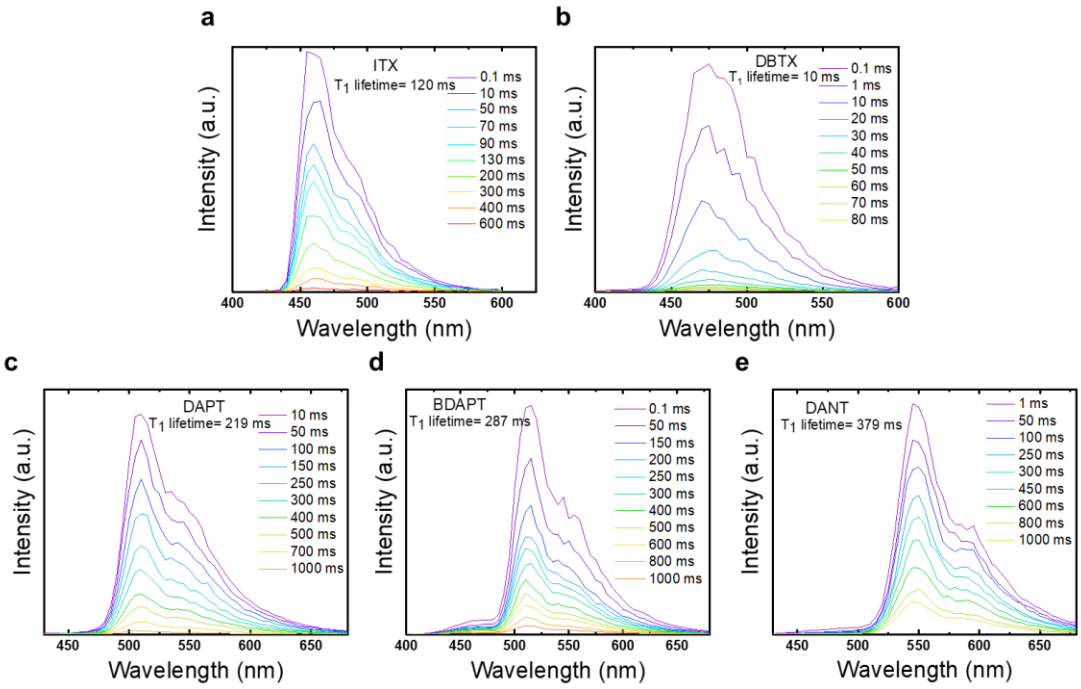

Figure 2.16. Phosphorescence spectra of the photoinitiators in toluene at T = 77 K after excitation at 350 nm. The spectra shown are: (a) ITX with a lifetime of 120 ms; (b) DBTX with a lifetime of 10 ms; (c) DAPT with a lifetime of 219 ms; (d) BDAPT with a lifetime of 287 ms; and (e) DANT with a lifetime of 379 ms.

By comparing DAPT and DANT, we see that the naphthalene substituent performs differently than phenyl substituent to increase the phosphorescence lifetime. This indicates that the structure design of branches has a significant impact on this photophysical property. Note that ITX has a moderate phosphorescence lifetime that is shorter than DAPT, BDAPT and DANT. This informs us that the triplet lifetime is not the only significant determining factor for efficient depletion. ITX seems to demonstrate an efficient $T_1 \rightarrow T_n$ transition allowing easy depletion of the printing. In the case of BDAPT, the $T_1 \rightarrow T_n$ transition was not efficient enough to fully depopulate the T_1 state, which explains why partial depletion was observed in lithography with low depleting power, but full depletion was challenging to achieve (Figure S8 and S9). To summarize, the moderate population of ITX on the T_1 state brings about moderate writing power and moderate depleting power, but the extreme population of BDAPT on the T_1 state leads to a lower writing

power and a higher depleting power. Consequently, compared to ITX, our new initiator is much more efficient in initiating the DLW photopolymerization process, but trades this advantage for a reduced polymerization inhibition capability. Therefore, this molecule could be of significant interest in applications requiring low laser power (i.e., high throughput, multiple-writing laser situations); however, additional effort could be placed in decreasing the inhibition threshold of the next-generation photoinitiators.

2.4 Summary

To summarize, the moderate population of ITX on the T_1 state brings about moderate writing power and moderate depleting power, but the extreme population of BDAPT on the T_1 state leads to a lower writing power and a higher depleting power. Consequently, compared to ITX, our new initiator is much more efficient in initiating the DLW photopolymerization process. Therefore, this molecule could be of significant interest in applications requiring low laser power (i.e., high throughput, multiple-writing laser situations); however, additional effort could be placed in decreasing the inhibition threshold of the next-generation photoinitiators.

2.5 References

1 J. Fischer, G. von Freymann, M. Wegener. *Adv. Mater.* **2010**, *22*, 3578-3582.

2 J. Fischer, J. B. Mueller, A. S. Quick, J. Kaschke, C. Barner-Kowollik, M. Wegener. *Advanced Optical Materials* **2015**, *3*, 221-232.

3 L. Li, R. R. Gattass, E. Gershgoren, H. Hwang, J. T. Fourkas. *Science* **2009**, *324*, 910-913.

4 B. Harke, W. Dallari, G. Grancini, D. Fazzi, F. Brandi, A. Petrozza, A. Diaspro. *Adv. Mater.* **2013**, *25*, 904-909.

5 K. J. Schafer, J. M. Hales, M. Balu, K. D. Belfield, E. W. Van Stryland, D. J. Hagan. *Journal of Photochemistry and Photobiology A: Chemistry* **2004**, *162*, 497-502.

6 W. Schnsbel, "*Polymers and Light*", Wiley-VCH, Weinheim **2007**, 305-329

7 M. Malinauskas, A. Žukauskas, G. Bičkauskaitė, R. Gadonas, S. Juodkazis. *Opt. Express* **2010**, *18*, 10209-10221.

8 B. H. Cumpston, S. P. Ananthavel, S. Barlow, D. L. Dyer, J. E. Ehrlich, L. L. Erskine, A. A. Heikal, S. M. Kuebler, I. Y. S. Lee, D. McCord-Maughon, J. Qin, H. Röckel, M. Rumi, X.-L. Wu, S. R. Marder, J. W. Perry. *Nature* **1999**, *398*, 51-54.

9 T. Serevičius, R. Komskis, P. Adomėnas, O. Adomėnienė, V. Jankauskas, A. Gruodis, K. Kazlauskas, S. Juršėnas. *Physical Chemistry Chemical Physics* **2014**, *16*, 7089-7101.

10 H. J. Yvon. *HORIBA, Jobin Yvon Ltd., Stanmore, Middlesex, UK* **2012**.

11 M. Frisch, G. Trucks, H. Schlegel, G. Scuseria, M. Robb, J. Cheeseman, G. Scalmani, V. Barone, G. Petersson, H. Nakatsuji. *Gaussian Inc., Wallingford CT* **2016**.

12 UV Plots from the Results of Excited States Calculations http://gaussian.com/uvvisplot/. (Accessed July 2018.)

13 M. Sheik-Bahae, A. A. Said, T. Wei, D. J. Hagan, E. W. V. Stryland. *IEEE Journal of Quantum Electronics* **1990**, *26*, 760-769.

14 C. Chen, I. Vasudevan, Z. Du, X. Xu, L. Pan. *Applied Physics Letters* **2018**, *112*, 253105.

15 T. J. A. Wolf, J. Fischer, M. Wegener, A.-N. Unterreiner. *Opt. Lett.* **2011**, *36*, 3188-3190.

16 R. Nazir, E. Balčiūnas, D. Buczyńska, F. Bourquard, D. Kowalska, D. Gray, S. Maćkowski, M. Farsari, D. T. Gryko. *Macromolecules* **2015**, *48*, 2466-2472.

17 A. S. Rao, D. Kim, T. Wang, K. H. Kim, S. Hwang, K. H. Ahn. *Organic Letters* **2012**, *14*, 2598-2601.

18 K. Sonogashira. *Journal of Organometallic Chemistry* **2002**, *653*, 46-49.

19 J. Kulhánek, F. Bureš, M. Ludwig. *Beilstein Journal of Organic Chemistry* **2009**, *5*, 11.

20 K. Sonogashira, Y. Tohda, N. Hagihara. *Tetrahedron Letters* **1975**, *16*, 4467-4470.

21 M. P. Coleman, M. K. Boyd. *The Journal of Organic Chemistry* **2002**, *67*, 7641-7648.

22 S. Dadashi-Silab, H. Bildirir, R. Dawson, A. Thomas, Y. Yagci. *Macromolecules* **2014**, *47*, 4607-4614.

23 L. Ding, Z. Zhang, X. Li, J. Su. *Chemical Communications* **2013**, *49*, 7319-7321.

24 W. Shi, Y. Luo, X. Luo, L. Chao, H. Zhang, J. Wang, A. Lei. *Journal of the American Chemical Society* **2008**, *130*, 14713-14720.

25 Y. Liu, N. Gu, P. Liu, J. Xie, X. Ma, Y. Liu, B. Dai. *Applied Organometallic Chemistry* **2015**, *29*, 736-738.

26 S. Xu, Z. Yun, Y. Feng, T. Tang, Z. Fang, T. Tang. *RSC Advances* **2016**, *6*, 69822-69827.

27 J. Yang, A. Dass, A.-M. M. Rawashdeh, C. Sotiriou-Leventis, M. J. Panzner, D. S. Tyson, J. D. Kinder, N. Leventis. *Chemistry of Materials* **2004**, *16*, 3457-3468.

28 K. D. Thériault, C. Radford, M. Parvez, B. Heyne, T. C. Sutherland. *Physical Chemistry Chemical Physics* **2015**, *17*, 20903-20911.

29 A. K. R. Junker, T. J. Sørensen. *Methods and Applications in Fluorescence* **2017**, *6*, 014002.

30 D. A. Skoog, F. J. Holler, S. R. Crouch. Principles of instrumental analysis; Cengage learning, **2017**.

31 B. Dereka, A. Rosspeintner, Z. Li, R. Liska, E. Vauthey. *Journal of the American Chemical Society* **2016**, *138*, 4643-4649.

32 T. A. Klar, S. Jakobs, M. Dyba, A. Egner, S. W. Hell. *Proceedings of the National Academy of Sciences* **2000**, *97*, 8206.

33 B. Gu, Y.-X. Fan, J. Wang, J. Chen, J. Ding, H.-T. Wang, B. Guo. *Physical Review A* **2006**, *73*, 065803.

34 M. Glukhovtsev. *Journal of Chemical Information and Computer Sciences* **1997**, *37*, 1206-1206.

35 E. Fabiano, F. D. Sala, R. Cingolani, M. Weimer, A. Görling. *The Journal of Physical Chemistry A* **2005**, *109*, 3078-308

CHAPTER 3. ITX-BASED PHOTOINITIATORS WITH ELECTRON WITHDRAWING/DONATING SUBSTRATES

3.1 Introduction: The necessity of Introducing Withdrawing and Donating Substrates to ITX Core

Direct laser writing (DLW) has developed rapidly in recent years, and it has become an essential process for 3D nanofabrication. Specifically, the two-photon polymerization (2PP) DLW process has found use in a diverse range of fields including nanophotonics,[1–3] micro-robotics,[4–6] microfluidics,[7–9] metamaterials,[10–12] micro-optics,[13] security,[14] and bioengineering.[15–17] The high spatial resolution associated with the 2PP process provides an advantage relative to other fabrication techniques. Unlike single photon absorption, two-photon absorption is confined to the focal region of a tightly focused laser, which occurs due to non-linear, multiphoton absorption. This gives rise to the submicron 3D structuring capabilities now expected of 2PP-DLW. Unfortunately, the two-photon absorption process is typically not efficient, resulting in relatively large laser power requirements. While the current power requirements are suitable for single beam 2PP-DLW processes, power becomes an issue when attempts to scale production with multiple beams or image projection. In turn, this has prompted the development of photoinitiator molecules with superior absorption abilities in the polymerization reaction medium.[18] Additionally, in many instances the current achievable spatial resolution of 2PP is not to the point where it is of utility in all operations, and this necessitates the use of resolution-enhancing strategies for 2PP-DLW.[19] By introducing a secondary laser into the DLW system, precise spatial control of the polymerization region can be achieved via a polymerization inhibition process. This leads to significantly increased DLW resolution (i.e., super resolution), with resolution limits on the order of 120 nm being achieved.[20] Inhibition of the polymerization process via a secondary laser is reliant on the properties of the photoinitiator used. Currently only a limited number of photoinitiators are known

that can achieve this polymerization inhibiting effect for controlling the 2PP-DLW process, and the library of photoinitiator candidates needs to be expanded significantly such that this promising application space can reach its full potential.

The choice of the 2PP-DLW photoinitiator can depend on the desired polymerization initiation pathway. Generally, photoinitiators are housed within two classes.[21,22] Norrish Type I initiators are molecules that generate radicals directly by photocleavage. Norrish Type II initiators absorb light to form excited states that abstract hydrogen from a co-initiator to generate radicals. In DLW, the widely-used, commercially-available photoinitiator, 2-isopropylthioxanthone (ITX), is a special Type II initiator that operates intramolecularly without the use of a co-initiator. During the design of 2PP photoinitiators, it has been observed that molecules that follow a donor-acceptor-donor structure lend themselves as stronger 2-photon initiators.[23] Holding to this idea, molecular branches attached to the ITX core have been synthesized previously, and this led to improved photoinitiating properties.[24,25] However, several of the synthesized molecules suffered from low synthesis yield, poor solubility, and poor stability.[25] Additionally, ITX is advantageous as its photoinitiation ability can be turned off through exposure to a secondary laser during the DLW polymerization process, which results in extremely high-resolution printing.[19,26,27] Thus, this is a promising molecule to derivatize to further enhance the polymerization initiation and inhibition properties that could lead to superior 2PP-DLW performance.

In this work, the above listed barriers were overcome through an improved molecular design motif. That is, the newly designed photoinitiators continue to achieve superior absorption properties compared to ITX while having high synthetic yields, good solubility in a common monomer resin, and long-term ambient stability. For these photoinitiators, the isopropyl group common to ITX was maintained, and this allowed the molecules to be readily soluble in the

monomer. To provide a guideline for synthesis, the absorption spectra of the new photoinitiators were calculated using time-dependent density functional theory (TD-DFT). The possibility of charge transfer states was predicted by measuring the frontier molecular orbitals of the photoinitiating molecules. The two-photon cross-section of each of the synthesized photoinitiators was measured using the Z-scan technique to provide an indicator of two-photon absorption efficiency in DLW. Phosphorescence spectra were used to obtain triplet excited state lifetimes as the triplet state is vital to initiating the polymerization reaction as well as the polymerization inhibition process with these photoinitiators. Finally, the polymerization initiation efficiency of the photoinitiators was determined via 2PP-DLW. In addition, the polymerization inhibition capability during 2PP-DLW was established. By establishing the properties of new photoinitiators and performing nanolithographic printing, we demonstrate a practical pathway to achieve low-power and high-resolution 3D photopolymerization through advanced photoinitiator design.

3.2 Experimental Procedure and Characterization

3.2.1 General Experimental Procedures

Phenylboronic acid pinacol ester, 4-methoxyphenylboronic acid pinacol ester, 4-cyanophenylboronic acid pinacol ester, and 4-fluorophenylboronic acid pinacol ester were purchased from Oakwood. All other chemicals were purchased from Sigma-Aldrich, and all chemicals were used as received. All ultraviolet–visible (UV–Vis) light spectroscopy data were obtained using a Cary 60 spectrometer with the wavelength range of 330 nm $\leq \lambda \leq$ 800 nm. Fluorescence and phosphorescence spectroscopy data were collected on a Cary Eclipse fluorescence and phosphorescence spectrophotometer in the wavelength range of 400 nm $\leq \lambda \leq$ 800 nm. Phosphorescence data were collected at T = 77 K using deoxygenated solutions of the

samples in a glass-forming solvent, toluene. For these measurements, the optical absorbance was below 0.01 at the excitation wavelength. Finally, the computational results were performed as described previously.[25]

3.2.2 Synthesis of New Photoinitiators with Withdrawing and Donating Substitutes

Synthesis of 2-bromo-7-isopropyl-9H-thioxanthen-9-one (ITX-Br, Compound 1)

2-isopropyl-9H-thioxanthen-9-one (6.4 g, 25 mmol) was added to a 250 mL round bottom flask with 50 mL of dichloromethane. Then, zinc chloride (0.35 g, 2.5 mmol) was poured in while the reaction mixture was held at 0 °C. After the addition of the zinc chloride, bromine (8 g, 50 mmol) in 50 mL of dichloromethane was added in a dropwise manner. Then, the temperature was gradually increased to 25 °C. After 24 h, a dark red solution formed, and the solution was quenched by $NaHSO_3$ and extracted with dichloromethane and water three times. After evaporation of the organic solvent, a light-yellow solid was dissolved into toluene and subsequently recrystallized to form white crystals in 65% yield. ^{1}H NMR (400 MHz, Chloroform-d) δ 8.75 (dd, J = 2.3, 0.4 Hz, 1H), 8.48 (d, J = 1.9 Hz, 1H), 7.70 (dd, J = 8.6, 2.3 Hz, 1H), 7.53 (dd, J = 3.5, 1.3 Hz, 2H), 7.46 (dd, J = 8.6, 0.4 Hz, 1H), 3.07 (p, J = 6.9 Hz, 1H), 1.33 (d, J = 6.9 Hz, 6H).

Synthesis of 2-isopropyl-7-(pyridin-4-yl)-9H-thioxanthen-9-one (ITX-pyridine, Compound 2)

2-bromo-7-isopropyl-9H-thioxanthen-9-one (ITX-Br, 66 mg, 0.2 mmol) was added to a 10 mL sealed tube with 1 mL of toluene. Then, 4-(4,4,5,5-tetramethyl-1,3,2-dioxaborolan-2-yl)pyridine (45 mg, 0.22 mmol) and 0.5 mL of 1 M Na_2CO_3 in water was added. Next, tetrakis(triphenylphosphine) palladium(0) (12 mg, 0.01 mmol) was added with 0.5 mL of ethanol. The reaction turned red. After three freeze-pump-thaw cycles, the sealed tube was slowly heated

to 90 °C. After 24 h, the organic mixture was washed with brine three times and DI water three times followed by an extraction with ethyl acetate. The mixture was purified by column chromatography. (Hexane:ethyl acetate = 3:1 v/v) to yield a solid with 83% yield. ^{1}H NMR (400 MHz, Chloroform-d) δ 8.93 (d, J = 2.1 Hz, 1H), 8.76 – 8.68 (m, 2H), 8.51 (s, 1H), 7.89 (dd, J = 8.4, 2.1 Hz, 1H), 7.71 (d, J = 8.4 Hz, 1H), 7.67 – 7.61 (m, 2H), 7.56 (d, J = 1.5 Hz, 2H), 3.09 (p, J = 6.9 Hz, 1H), 1.34 (d, J = 6.9 Hz, 6H).

Synthesis of 4-(7-isopropyl-9-oxo-9H-thioxanthen-2-yl)benzonitrile (ITX-phenyl-CN, Compound 3)

2-bromo-7-isopropyl-9H-thioxanthen-9-one (ITX-Br, 66 mg, 0.2 mmol) was added to a 10 mL sealed tube with 1 mL of toluene. Then, 4-(4,4,5,5-tetramethyl-1,3,2-dioxaborolan-2-yl)benzonitrile (51 mg, 0.22 mmol) was added. After this addition, 0.5 mL of 1 M Na_2CO_3 in water was added. Tetrakis(triphenylphosphine)palladium(0) (12 mg, 0.01 mmol) was added with 0.5 mL of ethanol. The reaction turned red. After three freeze-pump-thaw cycles, the sealed tube was slowly heated to 90 °C. After 24 h, the crude mixture was obtained; the organic solution was washed with brine three times and DI water three times followed by an extraction with ethyl acetate. The extracted organic layer was purified by column chromatography after evaporation of the ethyl acetate. (Hexane:ethyl acetate = 20:1 v/v) to yield a solid with 90% yield. ^{1}H NMR (800 MHz, Chloroform-d) δ 8.89 (d, J = 2.2 Hz, 1H), 8.53 (d, J = 1.9 Hz, 1H), 7.88 – 7.85 (m, 1H), 7.85 – 7.82 (m, 2H), 7.81 – 7.78 (m, 2H), 7.72 (d, J = 8.2 Hz, 1H), 7.60 – 7.57 (m, 2H), 3.11 (p, J = 7.0 Hz, 1H), 1.36 (d, J = 7.0 Hz, 6H).

Synthesis of 2-isopropyl-7-phenyl-9H-thioxanthen-9-one (ITX-phenyl, Compound 4)

2-bromo-7-isopropyl-9H-thioxanthen-9-one (ITX-Br, 66 mg, 0.2 mmol) was added to a 10 mL sealed tube with 1 mL of toluene. Then, 4,4,5,5-tetramethyl-2-phenyl-1,3,2-dioxaborolane (45 mg, 0.22 mmol) and 0.5 mL of 1 M Na_2CO_3 in water was added. After the addition of the Na_2CO_3 solution, tetrakis(triphenylphosphine) palladium(0) (12 mg, 0.01 mmol) was added with 0.5 mL of ethanol. The reaction turned an orangish-red color. After three freeze-pump-thaw cycles, the sealed tube was slowly heated to 90 °C. After 24 h, the crude mixture was obtained; the organic solution was washed with brine three times and extracted with ethyl acetate. The mixture was purified by column chromatography after evaporation of ethyl acetate. (Hexane:ethyl acetate = 16:1 v/v) to yield a solid with 80% yield. ^{1}H NMR (400 MHz, Chloroform-d) δ 8.88 (d, J = 2.2 Hz, 1H), 8.52 (s, 1H), 7.87 (dd, J = 8.4, 2.1 Hz, 1H), 7.72 (d, J = 7.2 Hz, 2H), 7.65 (d, J = 8.3 Hz, 1H), 7.54 (d, J = 1.4 Hz, 2H), 7.49 (t, J = 7.7 Hz, 2H), 7.41 (d, J = 7.4 Hz, 1H), 3.08 (p, J = 6.9 Hz, 1H), 1.34 (d, J = 6.9 Hz, 7H).

Synthesis of 2-(4-fluorophenyl)-7-isopropyl-9H-thioxanthen-9-one (ITX-phenyl-F, Compound 5)

2-bromo-7-isopropyl-9H-thioxanthen-9-one (ITX-Br, 66 mg, 0.2 mmol) was added to a 10 mL sealed tube with 1 mL of toluene. Then, 2-(4-fluorophenyl)-4,4,5,5-tetramethyl-1,3,2-dioxaborolane (49 mg, 0.22 mmol) and 0.5 mL of 1 M Na_2CO_3 in water solution were added. Tetrakis (triphenylphosphine) palladium(0) (12 mg, 0.01 mmol) and 0.5 mL of ethanol were added sequentially, and the reaction turned orange. After three freeze-pump-thaw cycles, the sealed tube was slowly heated to 90 °C. After 24 h, the crude mixture was obtained; the organic solution was washed with brine three times and DI water three times followed by an extraction with ethyl acetate. The mixture was purified by column chromatography after evaporation of the ethyl acetate.

(Hexane:ethyl acetate = 20:1 v/v) to yield a solid with 76% yield. ^{1}H NMR (800 MHz, Chloroform-d) δ 8.82 (d, J = 2.2 Hz, 1H), 8.53 (s, 1H), 7.82 (dd, J = 8.3, 2.1 Hz, 1H), 7.68 (dd, J = 8.5, 5.5 Hz, 2H), 7.65 (d, J = 8.3 Hz, 1H), 7.55 (d, J = 1.5 Hz, 2H), 7.19 (t, J = 8.6 Hz, 2H), 3.10 (p, J = 7.1 Hz, 1H), 1.36 (d, J = 7.0 Hz, 6H).

Synthesis of 2-isopropyl-7-(4-methoxyphenyl)-9H-thioxanthen-9-one (ITX-phenyl-OCH_3, Compound 6).

2-bromo-7-isopropyl-9H-thioxanthen-9-one (ITX-Br, 66 mg, 0.2 mmol) was added to a 10 mL sealed tube with 1 mL of toluene. Then, 2-(4-methoxyphenyl)-4,4,5,5-tetramethyl-1,3,2-dioxaborolane (52 mg, 0.22 mmol) and 0.5 mL of 1 M Na_2CO_3 in water was added. After the addition of the Na_2CO_3 solution, tetrakis(triphenylphosphine) palladium(0) (12 mg, 0.01 mmol) was added with 0.5 mL of ethanol. After three freeze-pump-thaw cycles, the sealed tube was slowly heated to 90 °C. After 24 h, the crude mixture was obtained; the organic solution was washed with brine three times and DI water three times followed by an extraction with ethyl acetate. The mixture was purified by column chromatography. (Hexane:ethyl acetate = 15:1 v/v) to yield a solid with 81% yield. ^{1}H NMR (400 MHz, Chloroform-d) δ 8.82 (s, 1H), 8.52 (d, J = 0.6 Hz, 1H), 7.80 (dd, J = 8.4, 2.2 Hz, 1H), 7.78 – 7.68 (m, 1H), 7.66 – 7.62 (m, 2H), 7.59 (dd, J = 8.4, 0.5 Hz, 1H), 7.50 – 7.40 (m, 1H), 7.01 (d, J = 8.8 Hz, 2H), 3.86 (s, 3H), 3.07 (pd, J = 6.9, 0.7 Hz, 1H), 1.34 (d, J = 6.9 Hz, 6H).

Synthesis of 2-isopropyl-7-(thiophen-2-yl)-9H-thioxanthen-9-one (ITX-thiophene, Compound 7).

2-bromo-7-isopropyl-9H-thioxanthen-9-one (ITX-Br, 66 mg, 0.2 mmol) was added to a 10 mL sealed tube with 1 mL of toluene. Then, 4,4,5,5-tetramethyl-2-(thiophen-2-yl)-1,3,2-dioxaborolane (46 mg, 0.22 mmol) and 0.5 mL of 1 M Na_2CO_3 in water was added. After the

addition of Na_2CO_3 solution, tetrakis(triphenylphosphine)palladium(0) (12 mg, 0.01 mmol) was added with 0.5 mL of ethanol. The reaction turned red. After three Freeze-pump-circles, the sealed tube was slowly heated to 90 °C. After 24 h, the mixture was washed with brine three times and DI water three times followed by an extraction with ethyl acetate. The mixture was purified by column chromatography. (Hexane:ethyl acetate = 10:1 v/v) to yield a solid with 77% yield. 1H NMR (400 MHz, CDCl3) δ 8.88 (d, J = 2.1 Hz, 1H), 8.53 (s, 1H), 7.88 (dd, J = 8.4, 2.2 Hz, 1H), 7.61 (d, J = 8.4 Hz, 1H), 7.56 (d, J = 1.2 Hz, 2H), 7.50 (dd, J = 3.6, 1.1 Hz, 1H), 7.37 (dd, J = 5.1, 1.1 Hz, 1H), 7.15 (dd, J = 5.1, 3.6 Hz, 1H), 3.10 (dd, J = 13.8, 6.9 Hz, 1H), 1.36 (d, J = 6.9 Hz, 6H).

3.2.3 Procedure for the Collection of ^{1}H NMR and ^{13}C NMR.

All NMR data were collected by the Bruker AV-III-400-HD NMR spectrometer and Bruker AV-III-800 NMR spectrometer from department of chemistry, Purdue University.

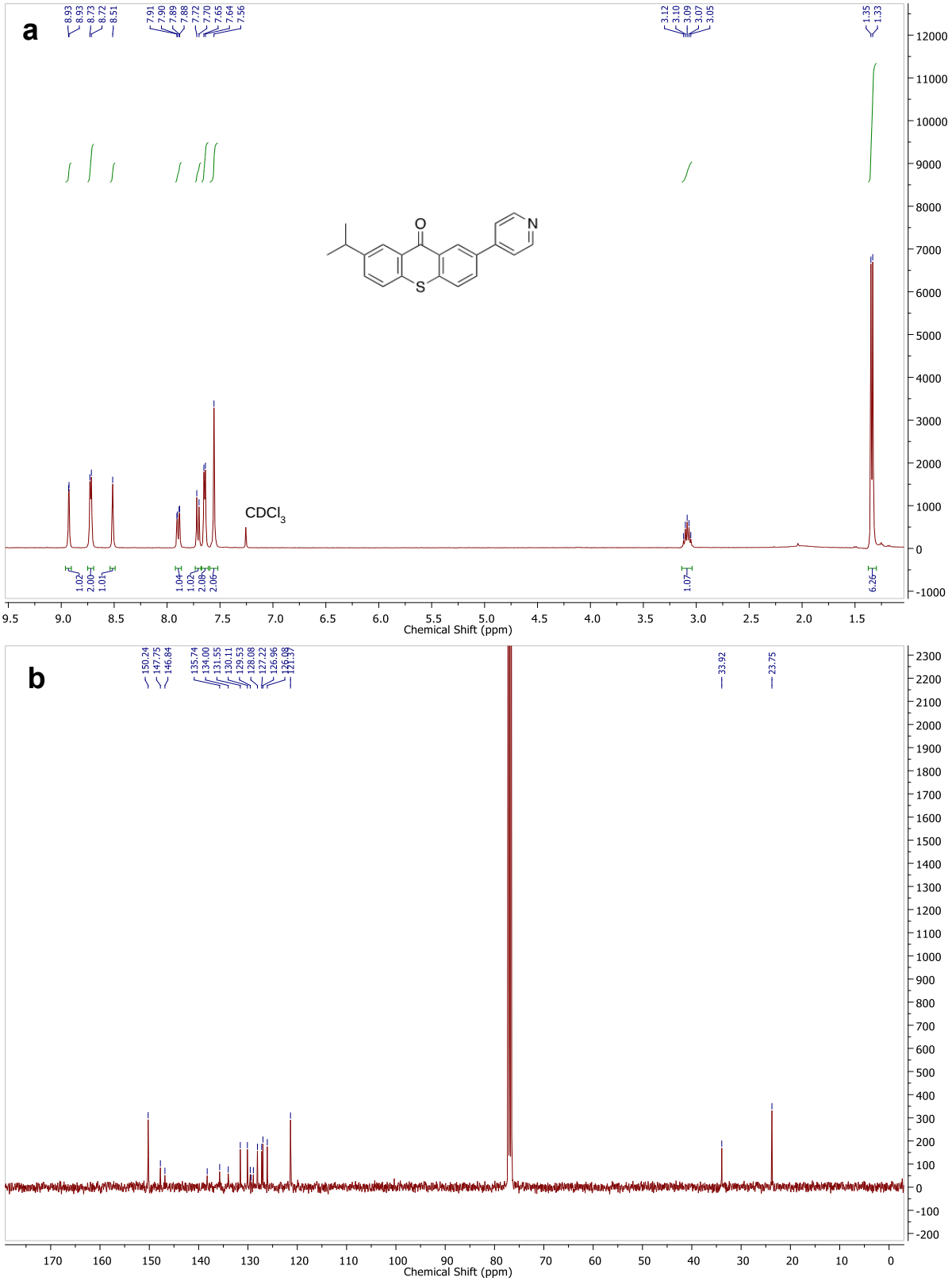

Figure 3.1. (a) ^{1}H NMR and (b) ^{13}C NMR spectra of 2-isopropyl-7-(pyridin-4-yl)-9H-thioxanthen-9-one (ITX-pyridine, Compound 2).

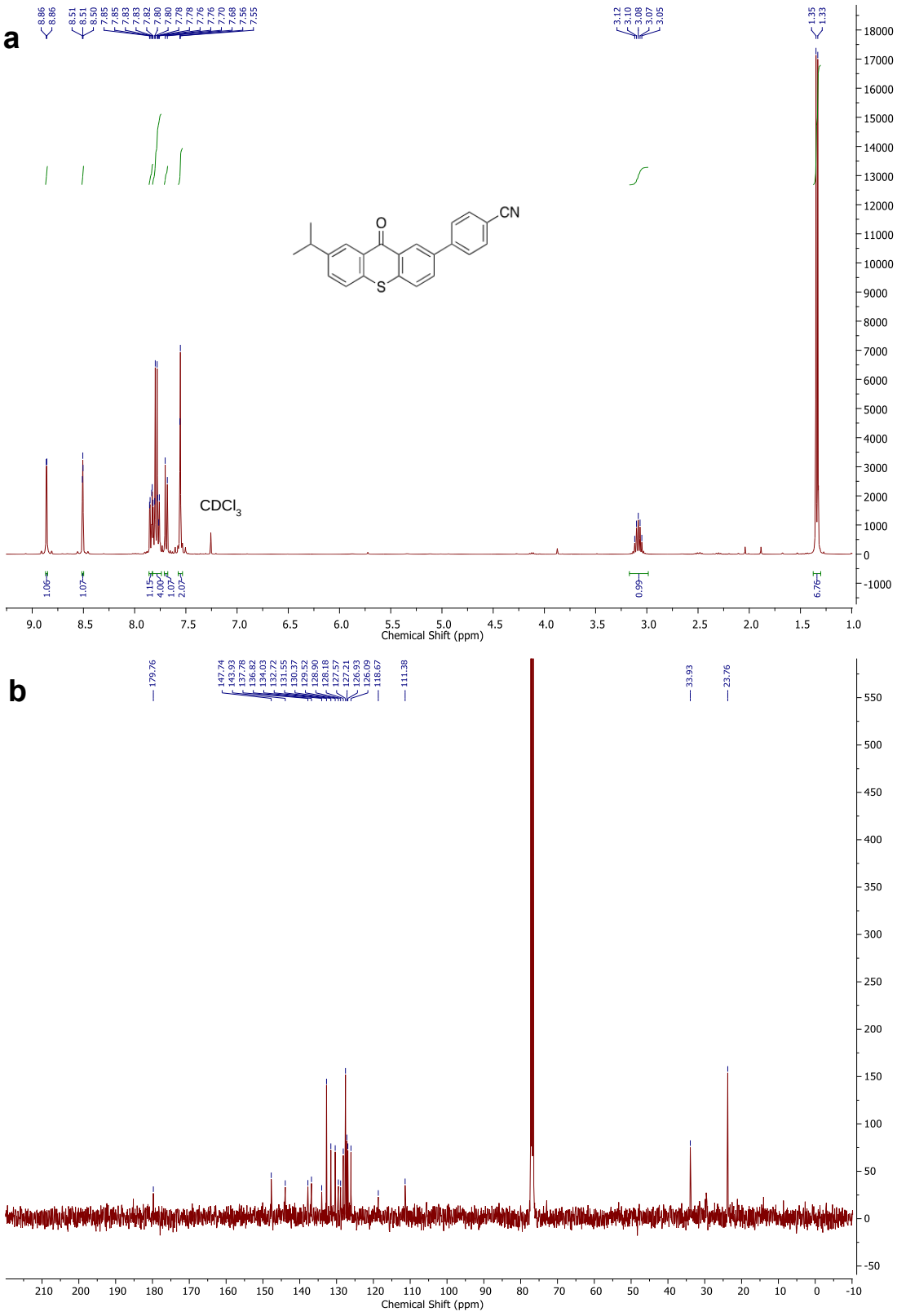

Figure 3.2. (a) ^{1}H NMR and (b) ^{13}C NMR spectra of 4-(7-isopropyl-9-oxo-9H-thioxanthen-2-yl)benzonitrile (ITX-phenyl-CN, Compound 3)

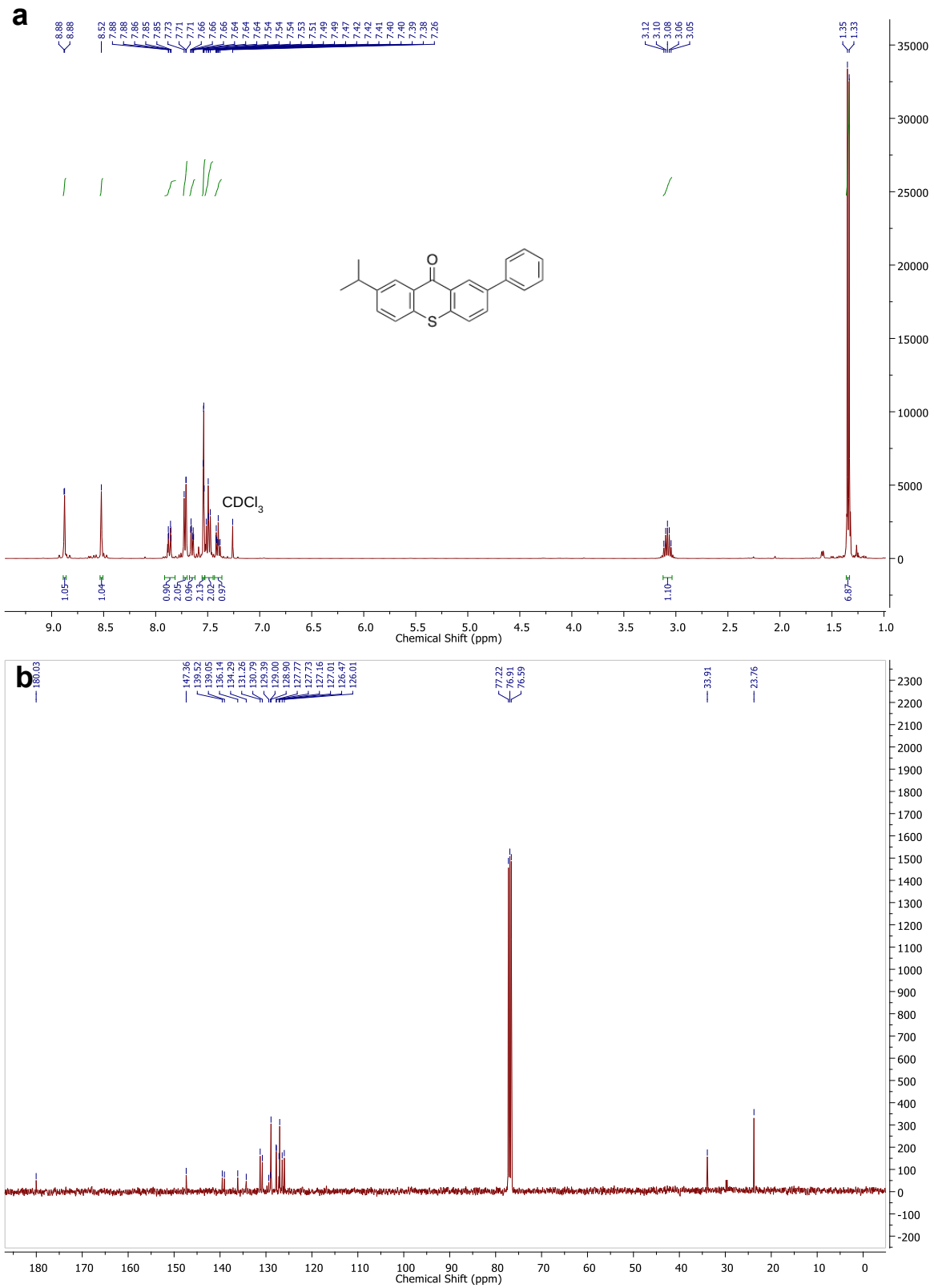

Figure 3.3. (a) ^{1}H NMR and (b) ^{13}C NMR spectra of 2-isopropyl-7-phenyl-9H-thioxanthen-9-one (ITX-phenyl, Compound 4)

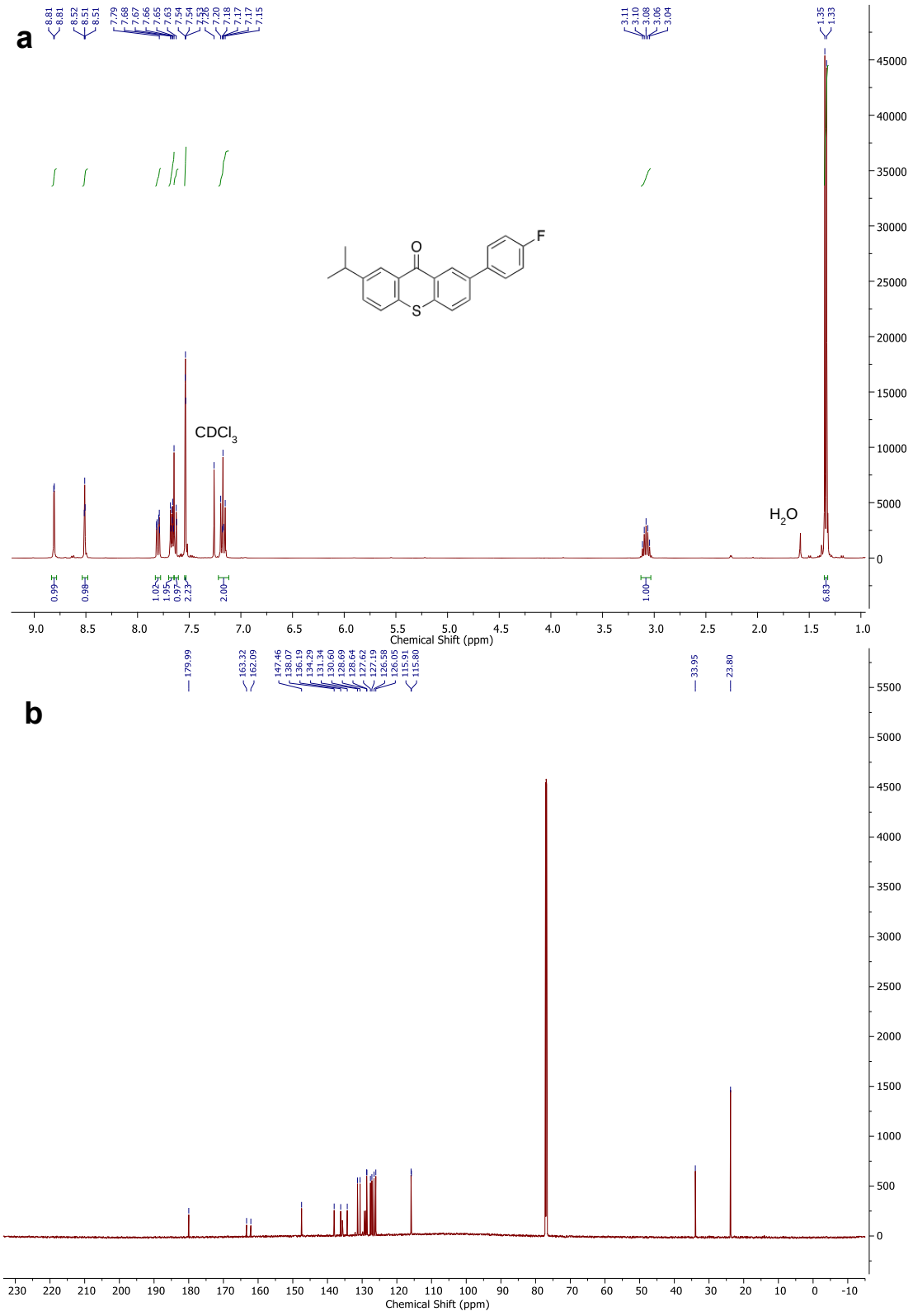

Figure 3.4. (a) ^{1}H NMR and (b) ^{13}C NMR spectra of 2-(4-fluorophenyl)-7-isopropyl-9H-thioxanthen-9-one (ITX-phenyl-F, Compound 5)

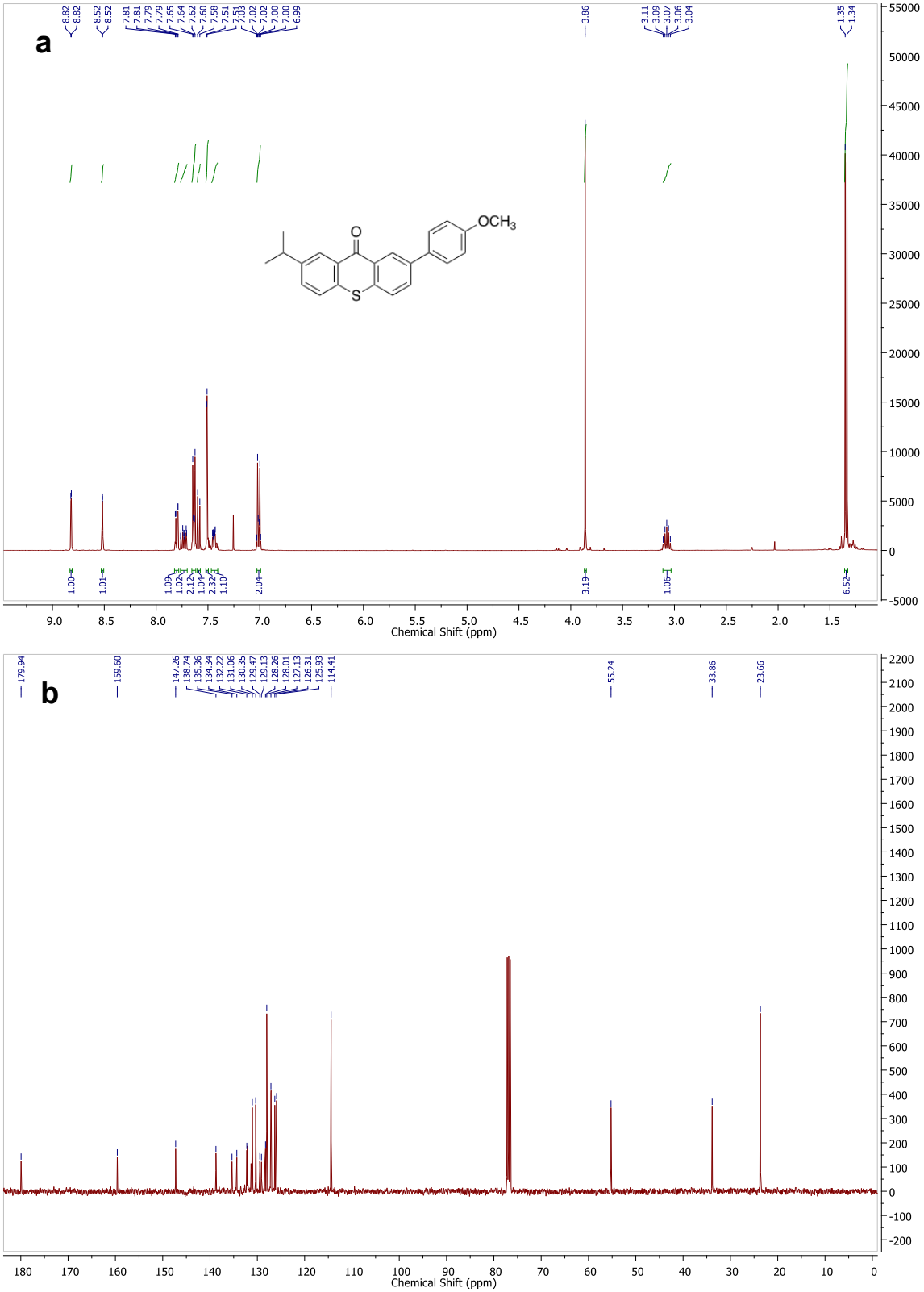

Figure 3.5. (a) ^{1}H NMR and (b) ^{13}C NMR spectra of 2-isopropyl-7-(4-methoxyphenyl)-9H-thioxanthen-9-one (ITX-phenyl-OCH_3, Compound 6).

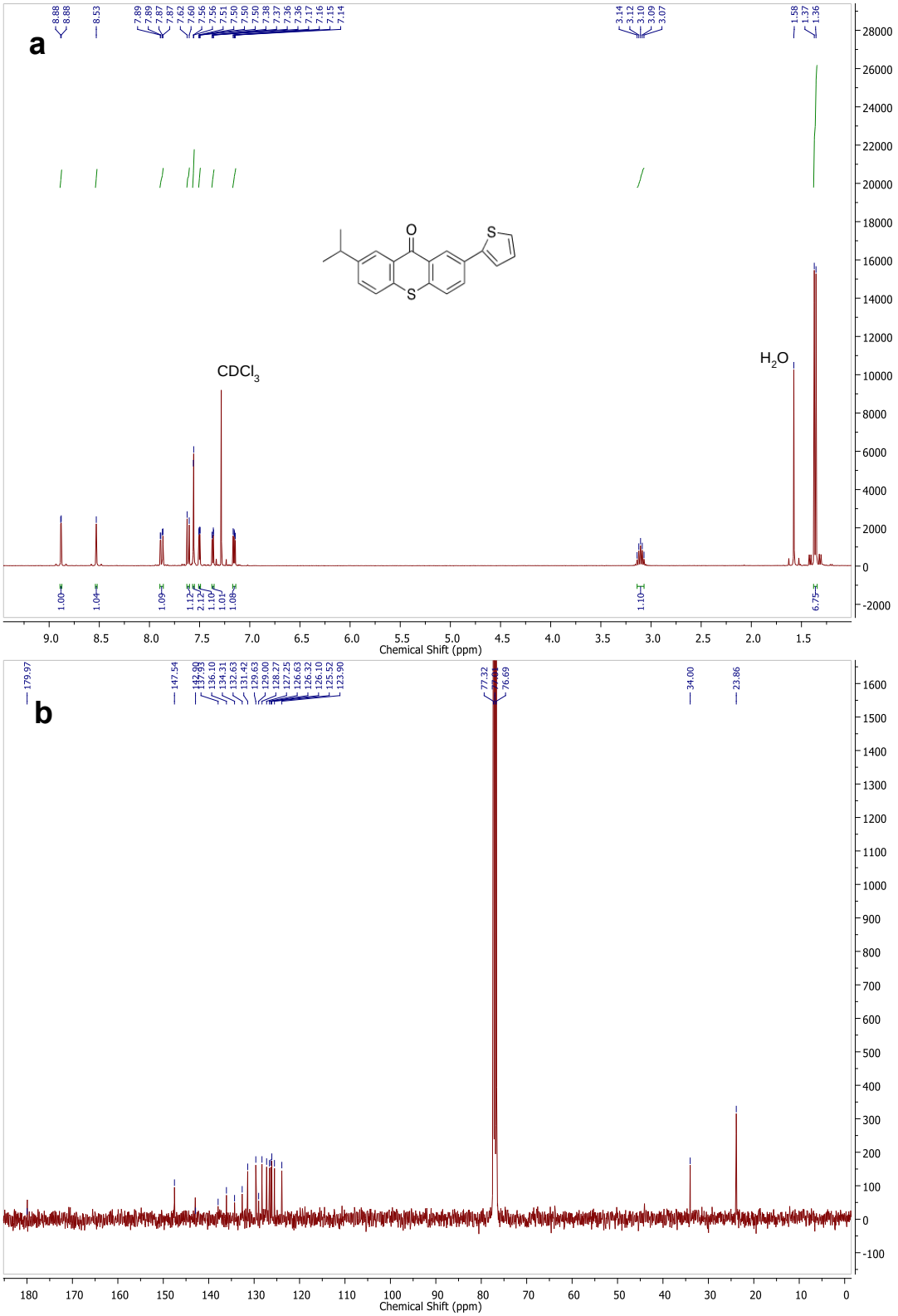

Figure 3.6. (a) ^{1}H NMR and (b) ^{13}C NMR spectra of 2-isopropyl-7-(thiophen-2-yl)-9H-thioxanthen-9-one (ITX-thiophene, Compound 7).

3.2.4 DLW Photopolymerization

DLW was performed using a custom-built fabrication system, and the details of the experimental setup have been reported previously.[25] The printing laser consisted of an 800 nm femtosecond oscillator (Coherent Micra) at 80 MHz repetition rate. A 100× oil-immersion objective lens (Nikon, N.A. = 1.49) was used to focus the laser into the photoresist to induce polymerization. Fabrication was achieved by motion of the sample via a nanopositioner (Mad City Labs) and laser control by fast mechanical shutter (Uniblitz) that was controlled with a custom LabVIEW code. The laser power was adjusted through combined use of a half-waveplate and a polarizer. Photoresists samples were sandwiched between a microscope slide and a coverslip, and tape was used to provide a ~170 μm gap between the two pieces of glass. All printing was performed at a rate of 100 μm s^{-1} writing speed. For polymerization inhibition experiments, a 638 nm continuous wave laser was introduced to the beam path by dichroic beam splitter and controlled independently by variable neutral density filter and fast shutter (Uniblitz). The 638 nm beam was passed through a telescoping lens pair to achieve a focus spot size significantly larger than that of the 800 nm laser at the sample. The laser powers for both beams were measured at the back of the objective lens through a 6 mm diameter aperture. Fabricated structures were developed in an isopropanol bath for 10 minutes, rinsed with isopropanol and dried with nitrogen. Fabricated structures were observed under optical microscope in transmission mode. Select samples were sputter coated with ~13 nm of a Au/Pd mixture before imaging with scanning electron microscope (SEM, Hitachi S-4800) to prevent charging. Atomic force microscopy (AIST NT) was performed using a silicon tip in tapping mode on samples after sputter coating.

3.2.5 Z-scan Measurements

Two-photon absorption cross-sections were measured using an open aperture Z-scan.[28] Z-scan measurements were performed using 60 fs pulses at 800 nm center wavelength from a 5 kHz regeneratively amplified laser (Spectra-Physics Spitfire). Solutions of each photoinitiator in tetrahydrofuran (THF) were prepared in a 1 mm pathlength cuvette for measurement, and these concentrations are listed in Table S1. Each sample was translated along the optical (z-) axis by motorized stage, and the transmitted beam was collected with a balanced photodetector (New Focus 2307). The signal from the photodetector was passed through a lock-in amplifier referencing the laser repetition rate. A Rayleigh range for the laser of 3 mm was fit from the measured data. Transmission values of the samples were fit using Equation 1.

$$T(z) = \sum_{m=0}^{\infty} \frac{[-q_0(z,0)]^m}{(m+1)^{3/2}} \quad (1)$$

where

$$q_0(z,t) = \frac{\beta I_0(t) L_{eff}}{\left(1+\frac{z^2}{z_0^2}\right)}. \quad (2)$$

Here, β is the two-photon absorption coefficient, $I_0(t)$ is the peak intensity at the focus of the beam, L_{eff} is the effective thickness of the sample (taken to be the cuvette path length), and z_0 is the Rayleigh length of the beam. The sample position (z) is measured relative to the minimum beam waist location. The two-photon cross-section was determined according to Equation 3.

$$\sigma_2 = \frac{\beta E_{photon}}{\rho_{mol}} \quad (3)$$

Here, E_{photon} is the photon energy of 800 nm photon and ρ_{mol} is the density of the photoinitiator molecules in the solution. A calibration factor of 19.3 was found to match ITX value with literature.

3.3 Results and Discussion

3.3.1 UV-Vis Prediction, Chemical Analyzation and Synthesis Design

According to previous efforts,[29] ITX and its derivatives have the potential to be high-performance photoinitiators in the 2PP-DLW processes. Here, we build from this previous work to modify the photoinitiator molecular design in a strategic manner. Specifically, new branches to the ITX core were introduced and classified into 3 groups based upon their chemical construct. Specifically, these were substituents that were: (1) electron-withdrawing groups, including 7-isopropyl-2-(pyridin-4-yl)-4aH-thioxanthen-9(9aH)-one (ITX-pyridine) and 4-(7-isopropyl-9-oxo-9,9a-dihydro-4aH-thioxanthen-2-yl)benzonitrile (ITX-phenyl-CN); (2) electron-donating groups, including 7-isopropyl-2-(4-methoxyphenyl)-4aH-thioxanthen-9(9aH)-one (ITX-phenyl-OCH_3) and 7-isopropyl-2-(thiophen-2-yl)-4aH-thioxanthen-9(9aH)-one (ITX-thiophene); and (3) groups that were neither strongly electron-accepting nor electron-donating, namely 7-isopropyl-2-phenyl-4aH-thioxanthen-9(9aH)-one (ITX-phenyl) and 2-(4-fluorophenyl)-7-isopropyl-4aH-thioxanthen-9(9aH)-one (ITX-phenyl-F). In all cases, the additional chemical functionality is added in a manner that makes the substituents conjugated with the core ITX structure.

To guide this molecular design, TD-DFT calculations were utilized to predict the absorption spectra of these proposed initiators (Figure 3.7).[30] The computational predictions indicated that the proposed molecules should have an absorption peak that is red-shifted relative to ITX. This is expected to increase the laser writing efficiency of the 800 nm 2PP-DLW as increasing absorption at a wavelength of 400 nm is key to an efficient photoinitiation process. Moreover, these three groups reveal a trend with respect to the optical absorption characteristics and how this design motif can be utilized to tune the absorption profile. Specifically, the ITX-based molecules with electron-donating groups showed the greatest redshift while ITX-based

molecules with electron-withdrawing groups present in the structure showed the least amount of absorption shift. Inspired by the TD-DFT calculation results, this set of molecules based on an ITX core with different substituent groups were synthesized to experimentally-verify their potential as photoinitiating candidates and to support or refute this predicted trend.

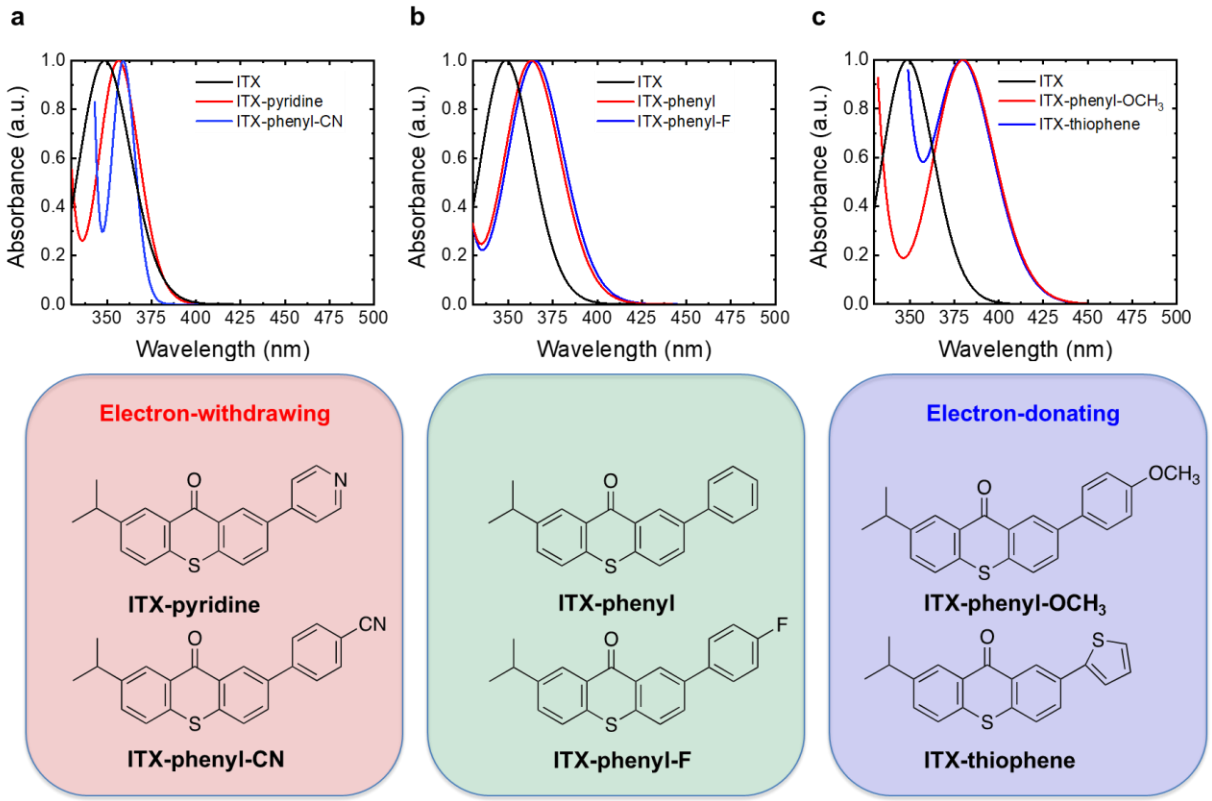

Figure 3.7. Predicted UV-Vis absorption plots for: (a) ITX, ITX-pyridine, and ITX-phenyl-CN; (b) ITX, ITX-phenyl and ITX-phenyl-F; and (c) ITX, ITX-phenyl-OCH_3 and ITX-thiophene. Those predictions were made using TD-DFT with a B3LYP/6-31G(d) level of theory. All the structures of the calculated initiating molecules (aside from ITX) are listed directly below their simulated absorption spectra.

Six different substituents were altered in a systematic way as functionalization of the conjugated branch afforded a means by which to evaluate multiple distinct chemical functionalities while maintaining a common chemical core for the photoinitiators. These added functionalities extend aromaticity across the molecular systems, which changes the optical properties

dramatically. A straightforward synthetic pathway was utilized to create the new photoinitiators (Figure 3.8), and these compounds were characterized by ^{1}H NMR spectroscopy and ^{13}C NMR spectroscopy (Figure 3.1 – Figure 3.6). Specifically, 2-bromo-7-isopropyl-9H-thioxanthen-9-one (ITX-Br) was synthesized from ITX using a bromination reaction catalyzed by zinc chloride.[31–34] Then, the six different substituents were introduced through Suzuki coupling reactions.[35–40] The final molecular targets are air-stable and insensitive to ambient conditions.

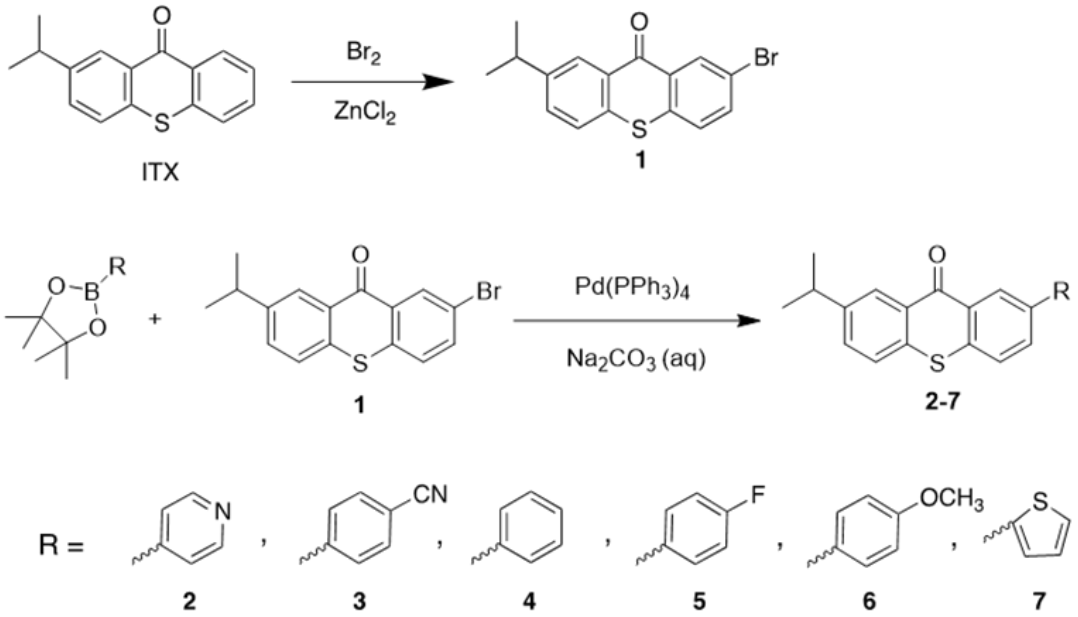

Figure 3.8. Synthetic pathway for the new photoinitiators.

3.3.2 TD-DFT Calculation of HOMO and LUMO

An improved excited state lifetime is predicted for the modified ITX molecules as the result of a direct highest occupied molecular orbital (HOMO) to lowest unoccupied molecular orbital (LUMO) transition. The frontier molecular orbitals were calculated and are shown in Figure 3.9 and 3.10. The thioxanthone core can be regarded as an acceptor and the introduced branch as the donor. The lowest-energy singlet excited state for each of the initiator candidates is a transition from the HOMO to the LUMO. This is a significant contrast from the photoinitiators we described

previously.[25] That is, while the lowest-energy singlet excited state was a HOMO to LUMO transition in this previous effort, it was an optically-inactive charge-transfer state, with the first optically active state involving both a HOMO-1 to LUMO and HOMO to LUMO+1 transition. Importantly, this means that the excited states associated with the molecules of the current effort should have fewer alternative pathways beyond that required for polymerization due to no lower singlet excited states by which to decay being available.

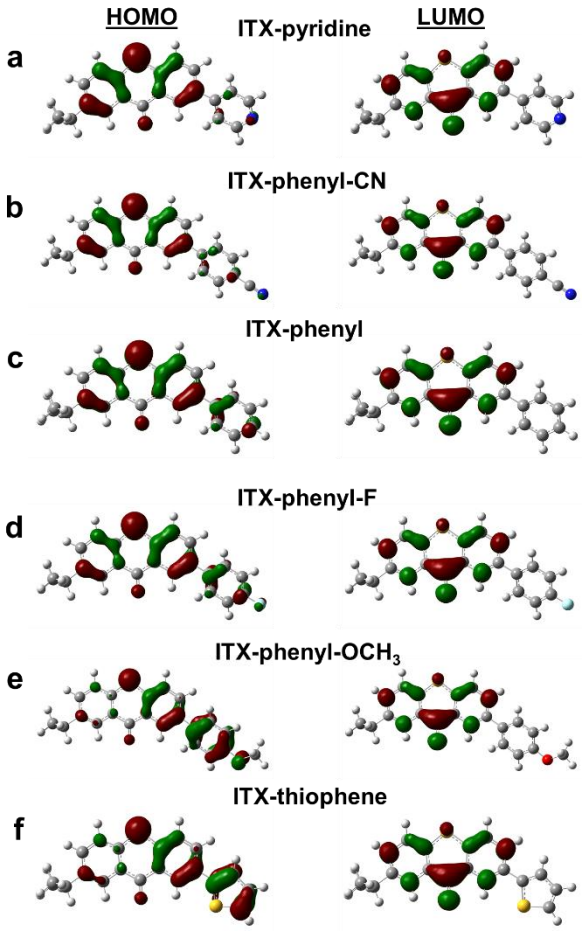

Figure 3.9. Molecular orbital diagrams calculated at an isovalue of 0.04. These plots are of the HOMO and LUMO energy levels of: (a) ITX-pyridine; (b) ITX-phenyl-CN; (c) ITX-phenyl; (d) ITX-phenyl-F; (e) ITX-phenyl-OCH_3; and (f) ITX-thiophene. They are used to show the proposed charge transfer states in these compounds. The HOMO wavefunctions are either spread through the whole compound or localized to the new attached branch, while the LUMO wavefunctions are localized to the thioxanthone core. Therefore, electronic transitions from the highest two occupied orbitals to the LUMO should bring about a transfer of charge from the pendant chemistry to the ITX core.

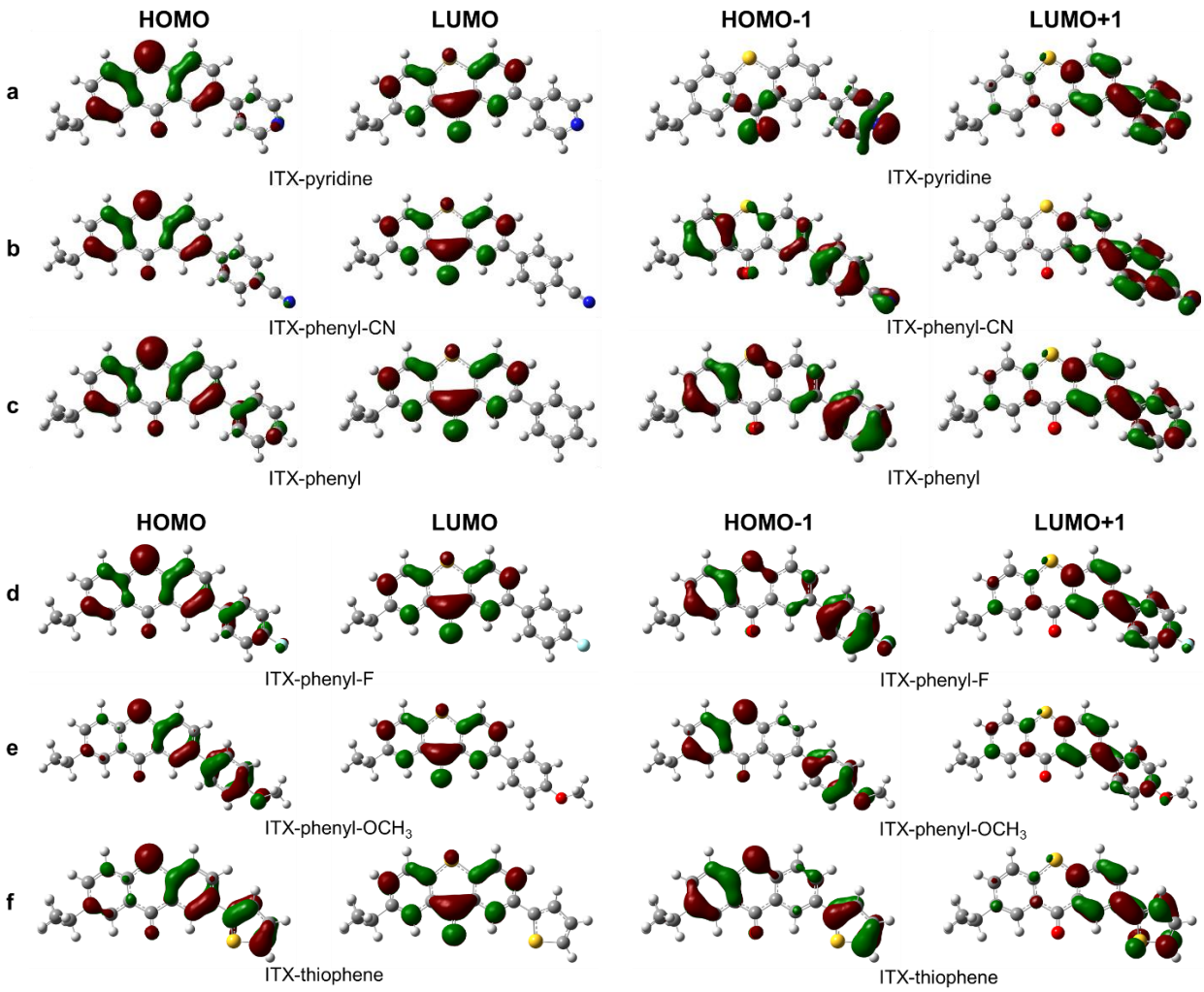

Figure 3.10. Molecular orbital diagrams calculated at an isovalue of 0.02. These plots are of the: (a) HOMO, LUMO, HOMO-1 and LUMO+1 of ITX-pyridine; (b) HOMO, LUMO, HOMO-1 and LUMO+1 of ITX-phenyl-CN; (c) HOMO, LUMO, HOMO-1 and LUMO+1 of ITX-phenyl; (d) HOMO, LUMO, HOMO-1 and LUMO+1 of ITX-phenyl-F; (e) HOMO, LUMO, HOMO-1 and LUMO+1 of ITX-phenyl-OCH_3; and (f) HOMO, LUMO, HOMO-1 and LUMO+1 of ITX-thiophene. They are used to show the proposed charge transfer states in these compounds. It can be revealed that the HOMO, HOMO–1, and LUMO+1 wavefunctions are either spread through the whole compound or localized to the new attached branch, while the LUMO wavefunctions are localized to the thioxanthone core. Therefore, electronic transitions from the highest two occupied orbitals to the LUMO should bring about a transfer of charge from the side to the core, but transitions to the LUMO+1 should not lead to a formation of charge transfer state.

3.3.3 Optical Properties of New Synthesized Photoinitiators

To evaluate these computational predictions, the optical properties of the new initiators were compared to those obtained by TD-DFT calculation. First, the molar absorption coefficients of the photoinitiators at half the wavelength (400 nm) of 2PP-DLW (800 nm) were measured (Table 3.1), and the normalized UV-Vis absorption spectra were plotted (Figure 3.11). Although there is a difference between the one-photon absorption process in this test and the two-photon absorption process that occurs in the DLW process,[41,42] the molar absorption coefficients are larger, which indicates the potential possibility of lowering the practical laser power requirements. As predicted by the computations (Figure 3.7), the introduction of new branches to the thiophene core indeed red-shifted the UV-Vis light absorption profiles of the photoinitiators. Moreover, the trend of the experimental shift in the absorption profile with respect to chemical functionality peak-shifting ability matches the computational results, indicating that the simple TD-DFT calculations shown are a useful predictive tool for photoinitiator design.

Table 3.1. Single-photon absorption coefficients and phosphorescent lifetimes of the initiators

Photoinitiator	λ_{max} (nm)[a]	ε^b (10^3 $mol^{-1}Lcm^{-1}$)	ε^c (10^3 $mol^{-1}Lcm^{-1}$)	λ_{ex} (nm)[d]	λ_{em} (nm)[e]	τ (ms)[f]
ITX	385	7.0	1.6	350	420	120
ITX-pyridine	391	4.6	2.8	365	414	125
ITX-phenyl-CN	393	1.8	1.2	365	414	256
ITX-phenyl	394	4.5	3.7	370	418	148
ITX-phenyl-F	396	5.7	4.8	365	417	144
ITX-phenyl-OCH_3	398	4.2	4.0	365	428	153
ITX-thiophene	402	0.3	0.3	365	431	87

[a] λ_{max} is the peak absorption wavelength near 400 nm if there are multiple peaks or shoulders in the spectra. [b] The molar absorption coefficient of the molecules at the wavelength of the peak. [c] The molar absorption coefficient at the 400 nm wavelength. [d] The exciting wavelength (λ_{ex}) for each molecule is the wavelength used to obtain clear fluorescence and phosphorescence data. [e] λ_{em} is the peak fluorescence wavelength of the emission spectrum at room temperature. [f] τ represents the phosphorescence lifetime of the molecules at 77 K in toluene.

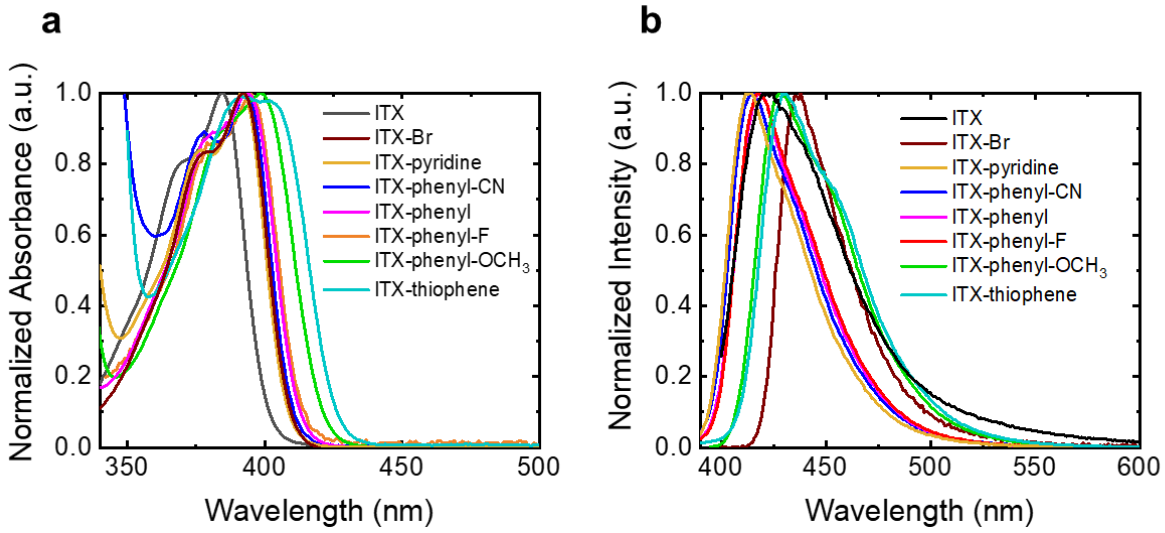

Figure 3.11. (a) The normalized UV-Vis absorption spectra of initiators in toluene at room temperature. (b) The normalized fluorescence spectra of the initiators in toluene at room temperature.

In the two most extreme examples (i.e., on the low end and high end of shifts towards the red), the maximum in the absorption peaks for ITX-pyridine and ITX-thiophene are red-shifted relative to ITX by 6 nm and 17 nm, respectively, and all of the peak absorption values are approaching the target wavelength of 400 nm. Although the extinction coefficients of new photoinitiators are smaller than that of ITX at their respective peaks, most of the extinction coefficients of the new photoinitiators are larger than ITX at 400 nm, highlighting the importance of the design strategy implemented here. The polymerization inhibition process for ITX is controlled by triplet-triplet absorption instead of stimulated emission depletion (STED),[43] which can be represented by fluorescence quantum yield. The photoinitiators synthesized here emit in a range from λ = 414 nm to λ = 431 nm (Figure S8b); however, they have weak fluorescence emission signals, which are similar to those observed for ITX. This indicates that any potential polymerization inhibition is likely to be predominantly from triplet-triplet absorption in this case as well.

Besides the first singlet state, the first triplet states (T_1) are essential to understanding the excited state mechanisms as well. Towards this end, phosphorescence spectra at 77 K were obtained.[44] Improved photoinitiator candidates for the 2PP-DLW process were found among the new molecules, which demonstrate lengthier triplet state lifetimes. As shown in Figure 3.12 and Figure 3.13, all the initiators possess clear phosphorescent signals, which illustrates that the transition from the singlet excited state to the triplet state through intersystem crossing exists in all the molecular systems evaluated here. The trend of the phosphorescent lifetimes is listed in Table 3.1, which represents the sequence of how long each molecule would have their T_1 states populated. As a reference, ITX-Br was also tested, and it had a relatively short phosphorescence lifetime of 38 ms. For most of the new initiator candidates, the phosphorescence lifetimes were moderately

increased compared to ITX. The synthesized photoinitiators provide a broad T_1 lifetime range through the varied functional groups attached to the ITX core. The existence of the lengthy triplet states makes the possibility of undergoing the proposed triplet-triplet absorption inhibition mechanism more likely.

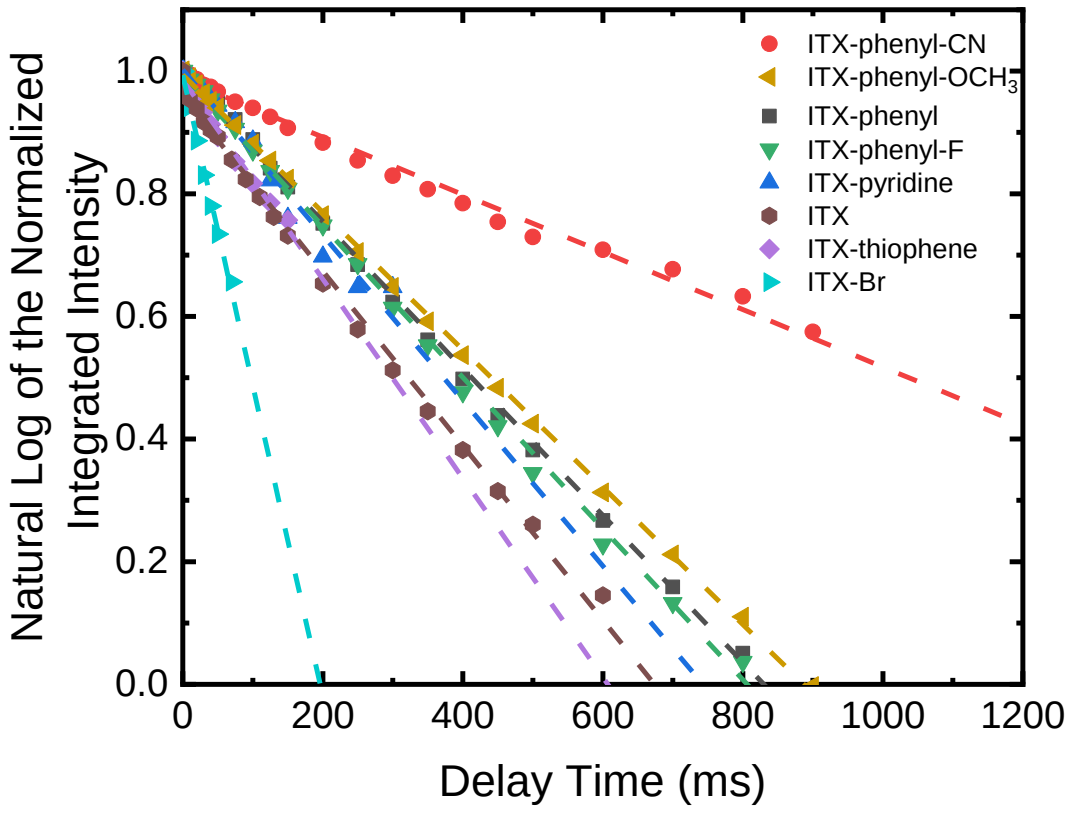

Figure 3.12. Natural log of the normalized integrated intensity vs delay time spectra of the photoinitiators in toluene at T = 77 K. The slope of each line represent the phosphorescence lifetime and the spectra shown are: (●) ITX-phenyl-CN with a lifetime of 256 ms; (◀) ITX-phenyl-OCH_3 with a lifetime of 153 ms; (■) ITX-phenyl with a lifetime of 148 ms; (▼) ITX-phenyl-F with a lifetime of 144 ms; (▲) ITX-pyridine with a lifetime of 125 ms; (●) ITX with a lifetime of 120 ms; (◆) ITX-thiophene with a lifetime of 87 ms; and (▶) ITX-Br with a lifetime of 38 ms.

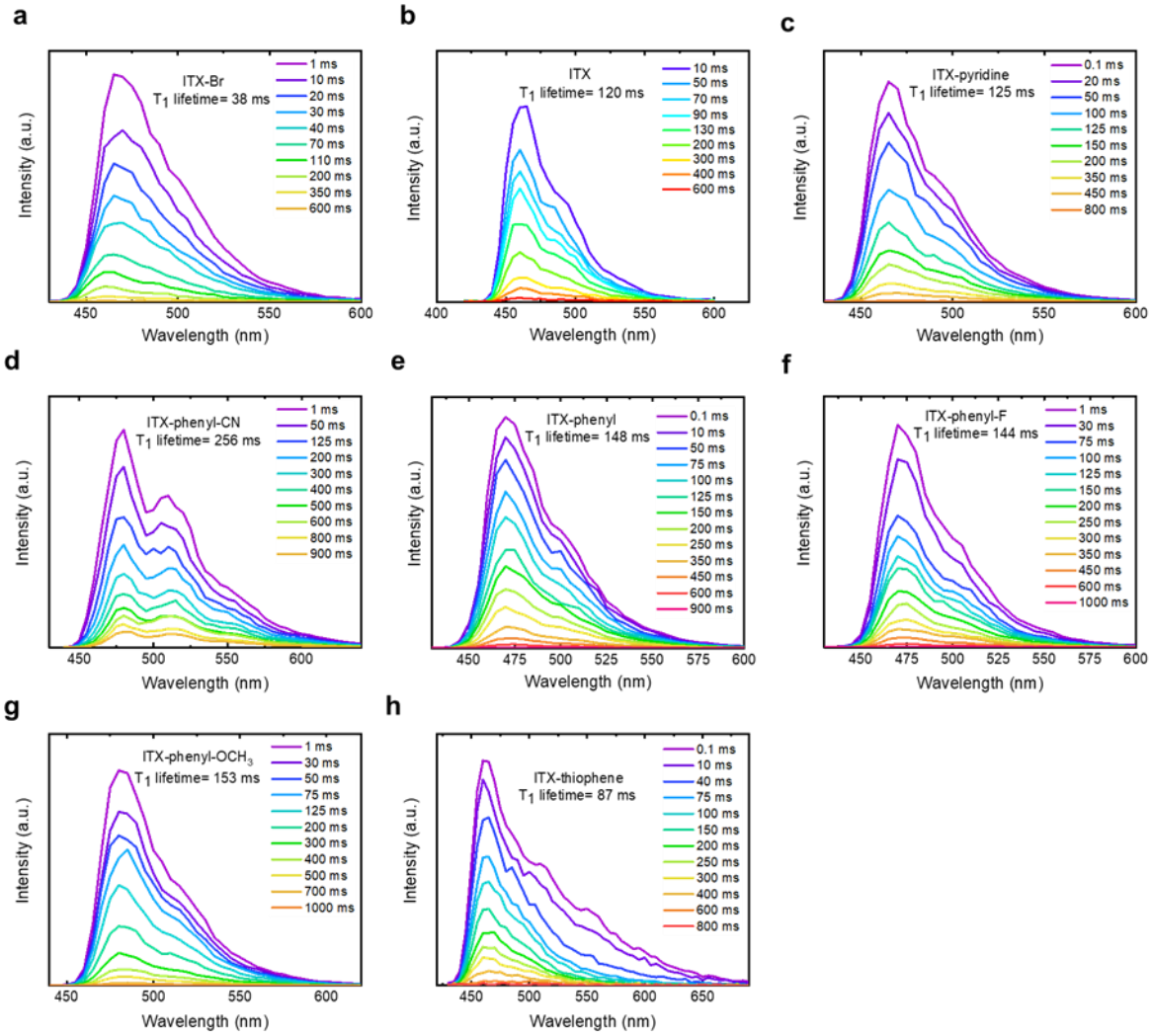

Figure 3.13. Phosphorescence spectra of the photoinitiators in toluene at T = 77 K.

3.3.4 Z-scan Measurements and Lithographic Printing

The two-photon cross-sections, σ_2, were determined for each molecule by open aperture Z-scan measurements with all the synthesized photoinitiators possessing larger σ_2 values than ITX, which is expected.[45] The two-photon cross-section value is a more promising indicator of improved two-photon absorption during 2PP-DLW compared with one-photon molar absorption. For instance, ITX-thiophene performed notably poorer in terms of molar absorption, but its σ_2 is as strong as other candidates. The measured σ_2 values are presented in Figure 3.14a. To account for unknown experimental setup variables in the Z-scan measurement (e.g., the beam quality) the data were scaled by a constant factor[46] using ITX as a calibration from previous literature.[47] This provides a more accurate representation of the two-photon cross-sections for the new photoinitiators relative to one another and ITX. Clearly, ITX-thiophene and ITX-OCH_3, both having electron donating groups, show the largest two-photon cross-section. This agrees with the previous observation of molecules that follow a donor-acceptor structure.[23] The molecules with electron-withdrawing groups had smaller cross-sections. ITX-pyridine was the least improved. Although all the two-photon cross-sections indicate improved absorption by the newly-synthsized photoinitiators, efficient two-photon absorption does not directly indicate the polymerization initiation performance.

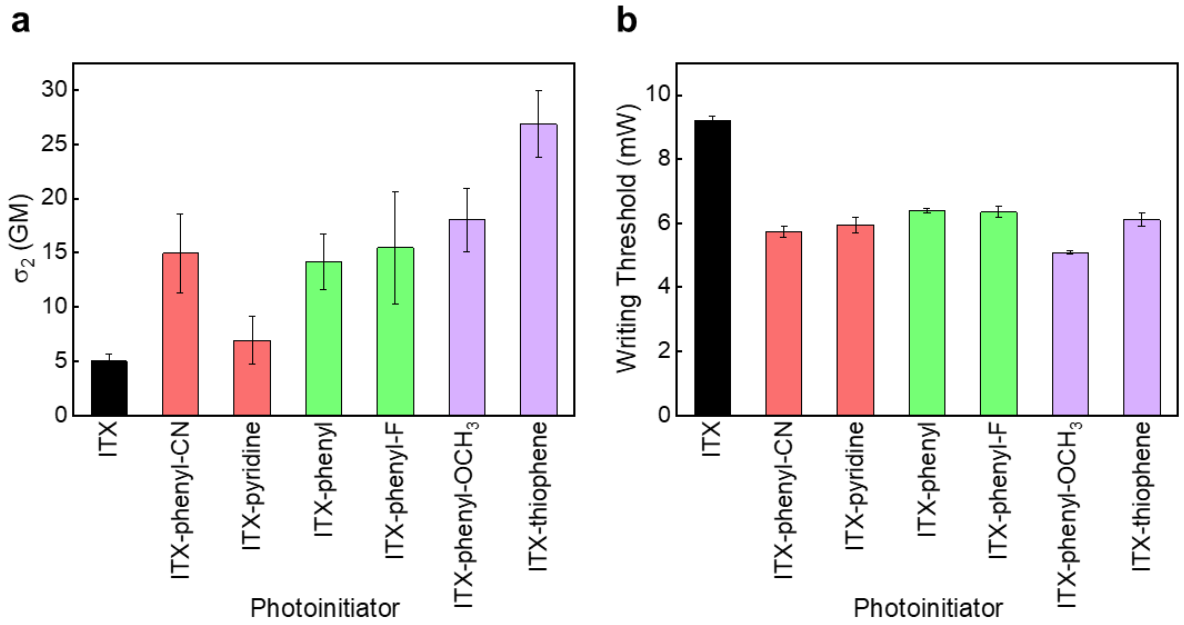

Figure 3.14. (a) Average two-photon absorption cross-section measurements for photoinitiators measured via the open-aperture Z-scan technique. Three measurements were taken for each photoinitiator. (b) Average writing thresholds for all photoinitiators determined at a 100 µm s^{-1} writing speed and concentration of 0.0025 molar ratio of the photoinitiator in the monomer. Thresholds were determined for 3 different samples of each photoinitiator. All error bars indicate one standard deviation from the average value represented by the bars in the plot.

A strong intersystem-crossing rate to the triplet state is also required. Therefore, determining the efficiency of these photoinitiators for initiating polymerization is studied by direct application in the DLW polymerization process. For the DLW polymerization testing of the photoinitiators, nanoscale lines of the polymerized materials were printed at 100 µm s^{-1} using separate photoresists containing each initiator. To provide a more direct comparison between all the initiators, each sample consisted of the photoinitiator mixed in the monomer pentaerythritol triacrylate (PETA) at a molar ratio of 0.0025:1 photoinitiator-to-PETA loading. The writing threshold of each photoresist was determined by varying the power of the printing laser. The minimum laser power required to print lines that survive the development process was considered as the writing threshold. The writing threshold determined for each photoinitiator mixture is displayed in Figure 3.14b. Clearly, the synthesized photoinitiators show improved photoinitiating

abilities compared to the standard ITX, with ITX-phenyl-OCH_3 showing the most improvement, requiring only 55% of the laser power required for printing with commercial photoinitiator ITX. The trend of the writing thresholds does not entirely follow the trend of two-photon cross-sections for the photoinitiators. This is likely due to other processes that participate in efficient photoinitiation of polymerization beyond just the photo-absorption process, such as the energy transfer efficiency between initiators and monomer.

In addition to testing the DLW ability of the photoresists, the efficiency of inhibiting the polymerization process was evaluated by exposing the resist to varying inhibition laser powers and determining the new writing threshold. In this case, a greater increase in writing threshold under the inhibition laser exposure represented a higher efficiency of the inhibition. This is significant as a photoinitiator with a high inhibition efficiency would require less inhibition laser power, thereby reducing undesired side effects such as heat accumulation. Figure 3.15 displays the results of the test, where all photoinitiators demonstrated the ability to inhibit polymerization under exposure to 638 nm laser. The 638 nm laser wavelength was chosen for its close matching to the triplet absorption peak of ITX.[43] Therefore, an efficient inhibition process was expected for ITX, and this was observed in practice. To determine a minimum 638 nm laser power required for inhibiting the polymerization, the writing laser power was set to 5% above the respective writing threshold for each photoinitiator and the inhibiting laser power was systematically varied (Figure 3.15). The ITX derivatives designed here displayed a less significant inhibition effect due to a shift in the triplet absorption peak in the modified ITX photoinitiators. Indeed, this is supported by TD-DFT calculations which predict a significant red shift of the triplet absorption peak of the novel photoinitiators compared to ITX. Those molecules following the electron-donating scheme, ITX-phenyl-OCH_3 and ITX-thiophene, exhibit the least impressive inhibition capabilities, which

follows from their expected poor triplet absorption at the 638 nm inhibition wavelength owing to the predicted absorption peaks being significantly redshifted.

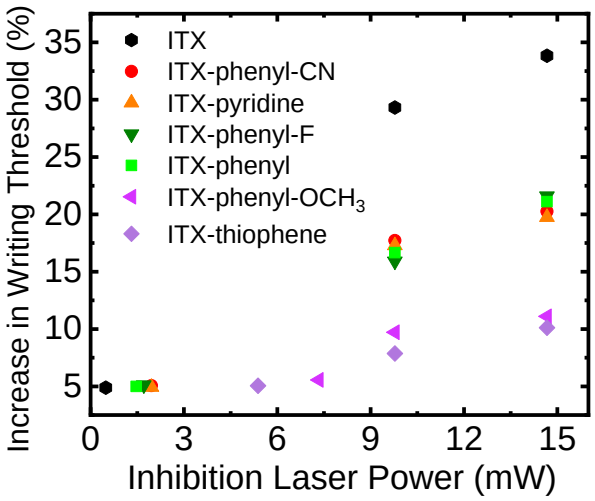

Figure 3.15. Increase in writing threshold of photoresists consisting of novel and reference photoinitiators while under exposure of 638 nm inhibition laser at varying powers.

Figure 3.16 shows a representative application of the one of the new photoinitiators, ITX-phenyl-OCH_3, at 0.0025 mol ratio in PETA used for 2PP-DLW. Figure 3.16a shows an example of the ability to fully inhibit the polymerization under 638 nm laser. Here, several polymer lines were written at 100 µm s^{-1} with a laser power 7% above the writing threshold. For a 10 µm section of the line printing, the 638 nm laser was turned on with 9.8 mW power. The foci of both beams were well-overlapped, with the 638 nm laser spot much larger than the printing laser spot. No polymerization was observed in the specified region indicating complete inhibition of the photoinitiation process. Going further, the 638 nm inhibition laser beam was modified from the previous inhibition experiment with a telescoping lens pair to achieve a near diffraction limited beam focus at the printing location.

The inhibition laser focus was partially offset laterally from the printing laser focus to inhibit polymerization in only a fraction of the printed spot. Lines were printed using printing laser power 13% above the writing threshold while the inhibition laser power was 2.8 mW. The printed lines were spaced apart by 120 nm such that they were close to the resolution of the printing system (Figure 3.16b). On the left, only the 800 nm printing laser was on, and the resultant polymerized lines are touching with little gap between them. The inhibition laser was turned on during the writing of the right side of Figure 3.16b. This region clearly demonstrates an improvement in the printing resolution as the individual lines are more clearly distinguishable with larger gap between lines. Atomic force microscopy measurements (Figure 3.16c) of the lines provide a clearer picture of the improved resolution along with a reduced height of the lines under inhibition laser exposure. These promising lithography results represent a new photoinitiator set tending towards a super-resolution capable photoresist system with reduced printing power requirements, ideal for high through-put 3D 2PP-DLW.

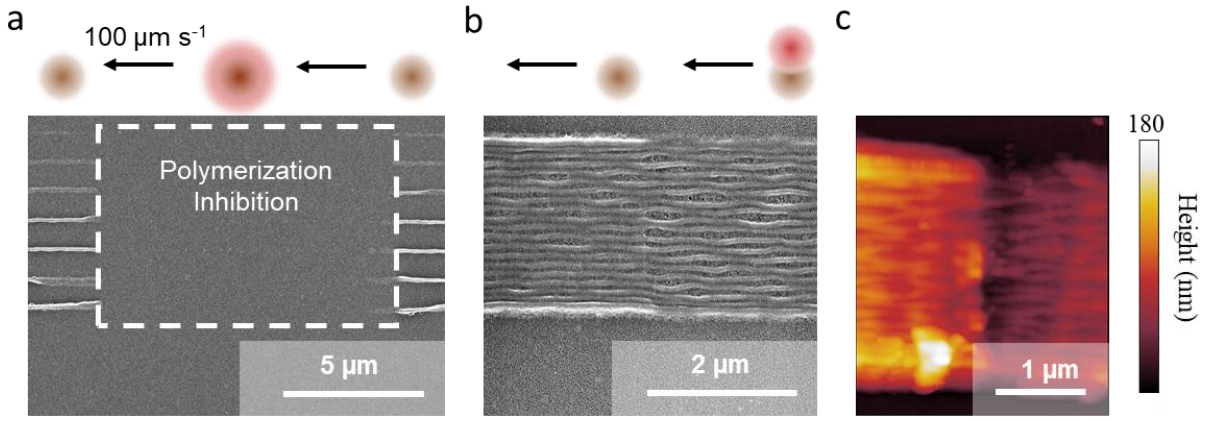

Figure 3.16. Scanning electron micrographs of polymer lines printed at 100 µm s^{-1} using ITX-phenyl-OCH_3 as photoinitiator demonstrating (a) complete inhibition of polymerization under exposure with 638 nm laser (dashed box) and (b) resolution improvement by partial overlap of 638 nm laser and printing laser. Brown spot indicates 800 nm printing laser is on and red spot indicates 638 nm laser is on. Arrows indicate direction of printing. In (a), line height is intentionally varied from top to bottom in steps of 100 nm to ensure lines are attached to the substrate. (c) AFM image of the same film that is shown in the SEM image of panel (b).

3.4 Summary

A set of six molecules based on an ITX core were designed and synthesized for the application as 2PP-DLW photoinitiators. While a desired red-shift in absorption was observed for all molecules, those molecules with electron-donating groups exhibited the largest shift towards the target 400 nm absorption wavelength for 2PP-DLW. Indeed, those molecules with electron-donating groups had the most significant absorption improvement at the 2PP-DLW wavelength of 800 nm by Z-scan measurements. Similarly, in DLW experiments the ITX-phenyl-OCH_3 molecule showed an almost 2-fold reduction in the writing threshold opposed to the base ITX photoinitiator. In fact, all the newly-synthesized photoinitiators presented had significantly improved two-photon photoinitiators compared to the ITX molecule. In addition, these molecules are stable and soluble in the photoresist monomer, in contrast to past ITX photoinitiator derivatives. An investigation into the polymerization inhibition properties of the novel photoinitiators yielded an existing

polymerization inhibition pathway similar to ITX, though not as efficient at the wavelength evaluated in this study. A further investigation into longer inhibition laser wavelengths may yield significant improvements in the polymerization inhibition efficiency, particularly for the electron-donating molecules. However, super-resolution lithography is possible with these molecules already. In summary, the ITX-derivative photoinitiators presented here are a promising option for more efficient 2PP-DLW, a necessary requirement for increasing nanoprinting throughput through parallelization or similar processes, as well as an expansion of the currently limited pool of photoinitiators for super-resolution lithography.

3.5 References

1 Von Freymann, G.; Ledermann, A.; Thiel, M.; Staude, I.; Essig, S.; Busch, K.; Wegener, M. *Adv. Funct. Mater.* **2010**, *20* (7), 1038–1052.

2 Frölich, A.; Fischer, J.; Zebrowski, T.; Busch, K.; Wegener, M. *Adv. Mater.* **2013**, *25* (26), 3588–3592.

3 Kaschke, J.; Wegener, M. *Opt. Lett.* **2015**, *40* (17), 3986.

4 Zeng, H.; Wasylczyk, P.; Parmeggiani, C.; Martella, D.; Burresi, M.; Wiersma, D. S. *Adv. Mater.* **2015**, *27* (26), 3883–3887.

5 Huang, T.-Y.; Sakar, M. S.; Mao, A.; Petruska, A. J.; Qiu, F.; Chen, X.-B.; Kennedy, S.; Mooney, D.; Nelson, B. J. *Adv. Mater.* **2015**, *27* (42), 6644–6650.

6 Martella, D.; Nocentini, S.; Nuzhdin, D.; Parmeggiani, C.; Wiersma, D. S. *Adv. Mater.* **2017**, *29* (42), 1704047.

7 Xu, B.; Du, W. Q.; Li, J. W.; Hu, Y. L.; Yang, L.; Zhang, C. C.; Li, G. Q.; Lao, Z. X.; Ni, J. C.; Chu, J. R.; et al. *Sci. Rep.* **2016**, *6* (July 2015), 1–9.

8 Maruo, S.; Inoue, H. *Appl. Phys. Lett.* **2007**, *91* (8), 1–4.

9 Alsharhan, A. T.; Acevedo, R.; Warren, R.; Sochol, R. D. *Lab Chip* **2019**, *19* (17), 2799–2810.

10 Frenzel, T.; Kadic, M.; Wegener, M. *Science (80-.).* **2017**, *358* (6366), 1072–1074.

11 Qu, J.; Kadic, M.; Naber, A.; Wegener, M. *Sci. Rep.* **2017**, *7* (1), 40643.

12 Bückmann, T.; Stenger, N.; Kadic, M.; Kaschke, J.; Frölich, A.; Kennerknecht, T.; Eberl, C.; Thiel, M.; Wegener, M. *Adv. Mater.* **2012**, *24* (20), 2710–2714.

13 Thiele, S.; Arzenbacher, K.; Gissibl, T.; Giessen, H.; Herkommer, A. M. *Sci. Adv.* **2017**, *3* (2), e1602655.

14 Mayer, F.; Richter, S.; Westhauser, J.; Blasco, E.; Barner-Kowollik, C.; Wegener, M. *Sci. Adv.* **2019**, *5* (2), 1–8.

15 Mačiulaitis, J.; Deveikytė, M.; Rekštytė, S.; Bratchikov, M.; Darinskas, A.; Šimbelytė, A.; Daunoras, G.; Laurinavičienė, A.; Laurinavičius, A.; Gudas, R.; et al. *Biofabrication* **2015**, *7* (1), 015015.

16 Zandrini, T.; Shan, O.; Parodi, V.; Cerullo, G.; Raimondi, M. T.; Osellame, R. *Sci. Rep.* **2019**, *9* (1), 11761.

17 Ovsianikov, A.; Chichkov, B.; Adunka, O.; Pillsbury, H.; Doraiswamy, A.; Narayan, R. J. *Appl. Surf. Sci.* **2007**, *253* (15), 6603–6607.

18 Kiefer, P.; Hahn, V.; Nardi, M.; Yang, L.; Blasco, E.; Barner-Kowollik, C.; Wegener, M. *Adv. Opt. Mater.* **2020**, *2000895*, 1–14.

19 Fischer, J.; Wegener, M. *Laser Photon. Rev.* **2013**, *7* (1), 22–44.

20 Wollhofen, R.; Katzmann, J.; Hrelescu, C.; Jacak, J.; Klar, T. A. *Opt. Express* **2013**, *21* (9), 10831.

21 Lauer, A.; Fast, D. E.; Kelterer, A.-M.; Frick, E.; Neshchadin, D.; Voll, D.; Gescheidt, G.; Barner-Kowollik, C. *Macromolecules* **2015**, *48* (23), 8451–8460.

22 Ding, G.; Jing, C.; Qin, X.; Gong, Y.; Zhang, X.; Zhang, S.; Luo, Z.; Li, H.; Gao, F. *Dye. Pigment.* **2017**, *137*, 456–467.

23 Cumpston, B. H.; Ananthavel, S. P.; Barlow, S.; Dyer, D. L.; Ehrlich, J. E.; Erskine, L. L.; Heikal, A. A.; Kuebler, S. M.; Lee, I.-Y. S.; McCord-Maughon, D.; et al. *Nature* **1999**, *398* (6722), 51–54.

24 Nazir, R.; Balčiunas, E.; Buczyńska, D.; Bourquard, F.; Kowalska, D.; Gray, D.; Maćkowski, S.; Farsari, M.; Gryko, D. T. *Macromolecules* **2015**, *48* (8), 2466–2472.

25 Chi, T.; Somers, P.; Wilcox, D. A.; Schuman, A. J.; Iyer, V.; Le, R.; Gengler, J.; Ferdinandus, M.; Liebig, C.; Pan, L.; et al. *J. Polym. Sci. Part B Polym. Phys.* **2019**, *57* (21), 1462–1475.

26 Harke, B.; Bianchini, P.; Brandi, F.; Diaspro, A. *ChemPhysChem* **2012**, *13* (6), 1429–1434.

27 Thiel, M.; Ott, J.; Radke, A.; Kaschke, J.; Wegener, M. *Opt. Lett.* **2013**, *38* (20), 4252.

28 Sheik-Bahae, M.; Said, A. A.; Wei, T.-H.; Hagan, D. J.; Van Stryland, E. W. *IEEE J. Quantum Electron.* **1990**, *26* (4), 760–769.

29 Fischer, J.; von Freymann, G.; Wegener, M. *Adv. Mater.* **2010**, *22* (32), 3578–3582.

30 Creating UV/Visible Plots from the Results of Excited States Calculations | Gaussian.com.

31 Wu, X.; Jin, M.; Malval, J.-P.; Wan, D.; Pu, H. *J. Polym. Sci. Part A Polym. Chem.* **2017**, *55* (24), 4037–4045.

32 Coleman, M. P.; Boyd, M. K. *J. Org. Chem.* **2002**, *67* (22), 7641–7648.

33 Dadashi-Silab, S.; Bildirir, H.; Dawson, R.; Thomas, A.; Yagci, Y. *Macromolecules* **2014**, *47* (14), 4607–4614.

34 Ding, L.; Zhang, Z.; Li, X.; Su, J. *Chem. Commun.* **2013**, *49* (66), 7319–7321.

35 Ding, L.; Zou, Q.; Qu, Y.; Su, J. *RSC Adv.* **2012**, *2* (11), 4754–4758.

36 Ding, L.; Wu, M.; Li, Y.; Chen, Y.; Su, J. *Tetrahedron Lett.* **2014**, *55* (34), 4711–4715.

37 Orazietti, M.; Kuss-Petermann, M.; Hamm, P.; Wenger, O. S. *Angew. Chemie Int. Ed.* **2016**, *55* (32), 9407–9410.

38 Miyaura, N.; Yamada, K.; Suzuki, A. *Tetrahedron Lett.* **1979**, *20* (36), 3437–3440.

39 Miyaura, N.; Suzuki, A. *J. Chem. Soc. Chem. Commun.* **1979**, No. 19, 866–867.

40 Miyaura, N.; Suzuki, A. *Chem. Rev.* **1995**, *95* (7), 2457–2483.

41 Dahlstedt, E.; Collins, H. A.; Balaz, M.; Kuimova, M. K.; Khurana, M.; Wilson, B. C.; Phillips, D.; Anderson, H. L. *Org. Biomol. Chem.* **2009**, *7* (5), 897–904.

42 Albota, M.; Beljonne, D.; Brédas, J.-L.; Ehrlich, J. E.; Fu, J.-Y.; Heikal, A. A.; Hess, S. E.; Kogej, T.; Levin, M. D.; Marder, S. R.; et al. *Science (80-.).* **1998**, *281* (5383), 1653 LP – 1656.

43 Harke, B.; Dallari, W.; Grancini, G.; Fazzi, D.; Brandi, F.; Petrozza, A.; Diaspro, A. *Adv. Mater.* **2013**, *25* (6), 904–909.

44 Kuboyama, A. *Bull. Chem. Soc. Jpn.* **1978**, *51* (10), 2771–2775.

45 Chung, S.-J.; Kim, K.-S.; Lin, T.-C.; He, G. S.; Swiatkiewicz, J.; Prasad, P. N. *J. Phys. Chem. B* **1999**, *103* (49), 10741–10745.

46 Bridges, R. E.; Fischer, G. L.; Boyd, R. W. *Opt. Lett.* **1995**, *20* (17), 1821.

47 Schafer, K. J.; Hales, J. M.; Balu, M.; Belfield, K. D.; Van Stryland, E. W.; Hagan, D. J. *J. Photochem. Photobiol. A Chem.* **2004**, *162* (2–3), 497–502.

CHAPTER 4. AN ATTEMPT TO SYNTHESIZE DETC-BASED PHOTOINITIATORS WITH MUTI-FUNCTIONALIZATION

4.1 Brief Introduction of the Difference between DETC and ITX

7-diethylamino-3-thenoylcoumarin (DETC) was another commercially available photoinitiator like ITX and studied and used in lithographic printing. As the depletion pathway was mentioned in chapter 1, unlike ITX going through the generation of triplet-triplet energy absorption, DETC's depletion mechanism is rationalized by stimulate emission for its fluorescence quantum yield is much higher compared with ITX.[1] I have modified its structure and synthesize several new molecules but unfortunately, they do not show any improvement in nanowriting relative to DETC and the further characterization was stopped.

4.2 The Synthesis Design and Experimental Results

There are three functional parts in the core structure which possess the potential to be modified in Figure 4.1. They are label in yellow, red and blue colors. The red part of the structure used to be an oxygen, nitrogen was introduced to replace it and gave the molecule the ability to connect to other chains on the side. We also introduced functional groups to the blue "R" position to extend the overall conjugated systems. The yellow area remains temporarily unchanged.

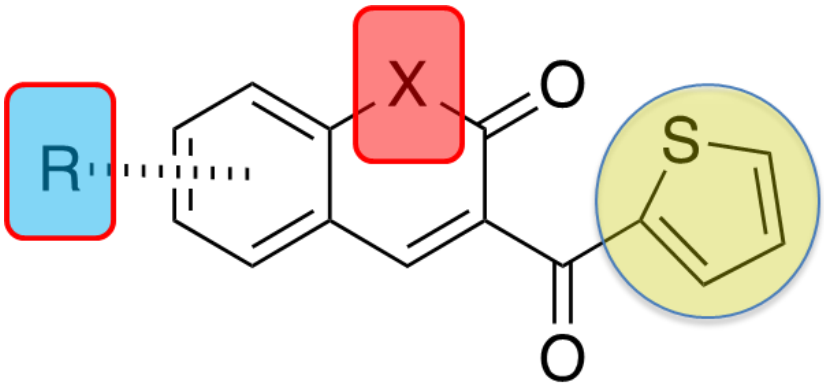

Figure 4.1. Functional points of DETC core.

The simple and practical way to construct the DETC core with new branches are listed below in Figure 4.2. By using a traditional ring closing reaction,[2] 2-aminobenzaldehyde derivatives and ethyl 3-oxo-3-(thiophen-2-yl)propanoate (bought from sigma Aldrich) can be assembled together efficiently.

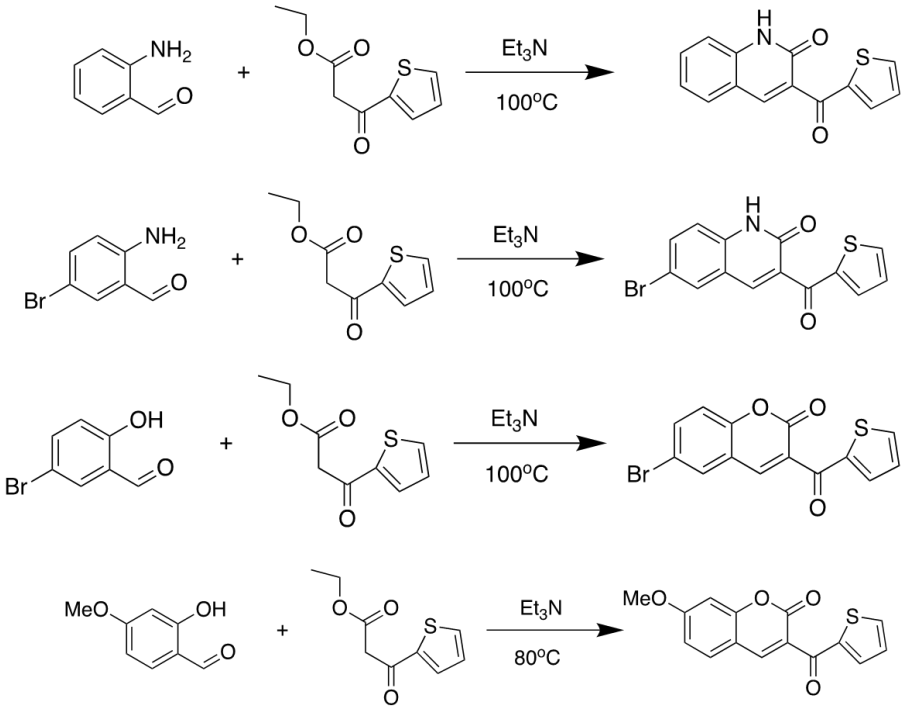

Figure 4.2. Synthetic route of new DETC derivatives.

Because of the low solubility of nitrogen replaced of detc derivatives, a side chain was introduced to increase the solubility in Figure 4.2.[3] Although the molecules can be obtained successfully and the solubility issue was fixed, the practical usage of them were unknown for their lack of efficient ability for the lithographic writing, which cause the termination of further study of them in terms of nanoprinting project.

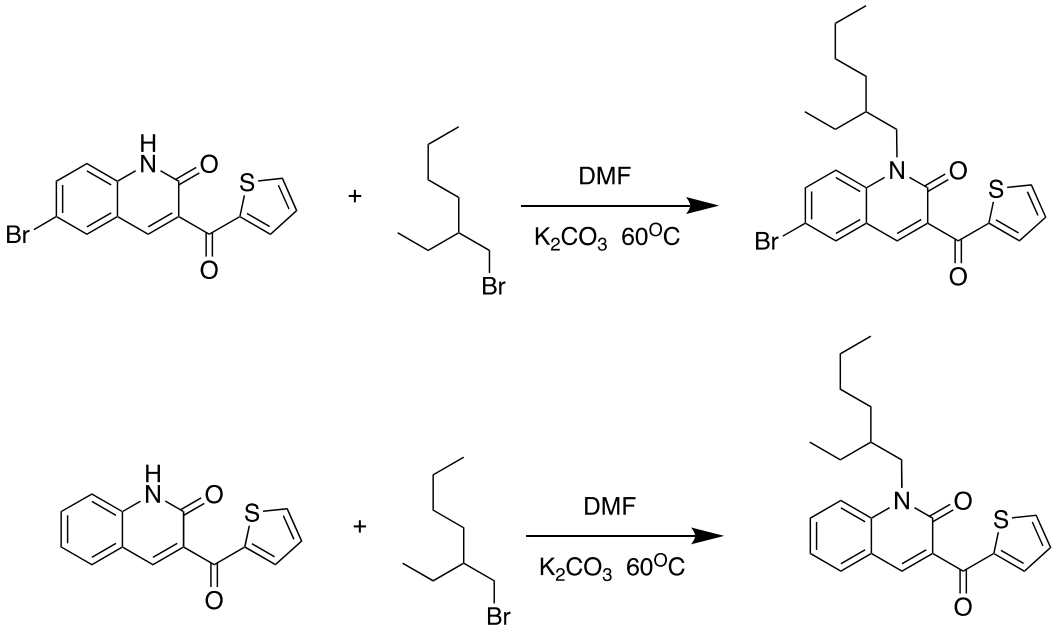

Figure 4.3. Synthetic route of introducing side chain to DETC derivatives.

4.3 The Characterization of DETC Derivatives in NMR

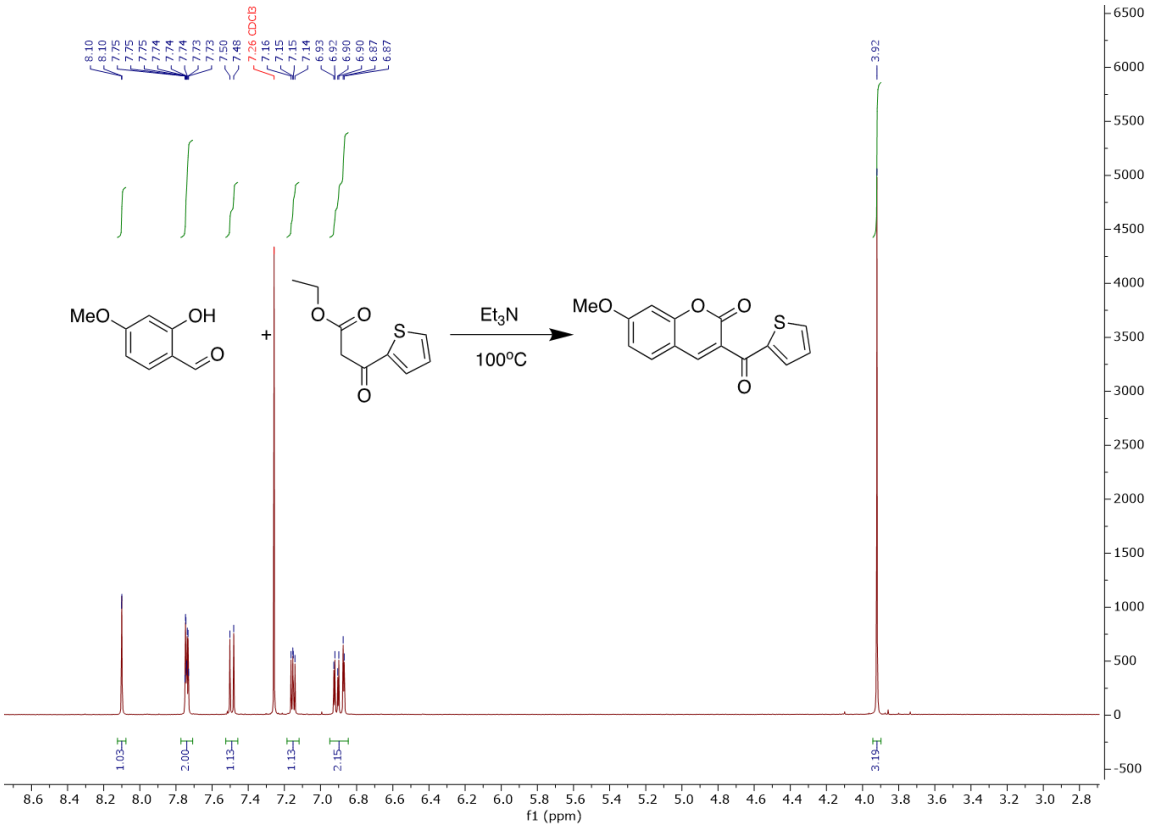

Figure 4.4. ^{1}H NMR of MeO-DETC (7-methoxy-3-(thiophene-2-carbonyl)-2H-chromen-2-one)

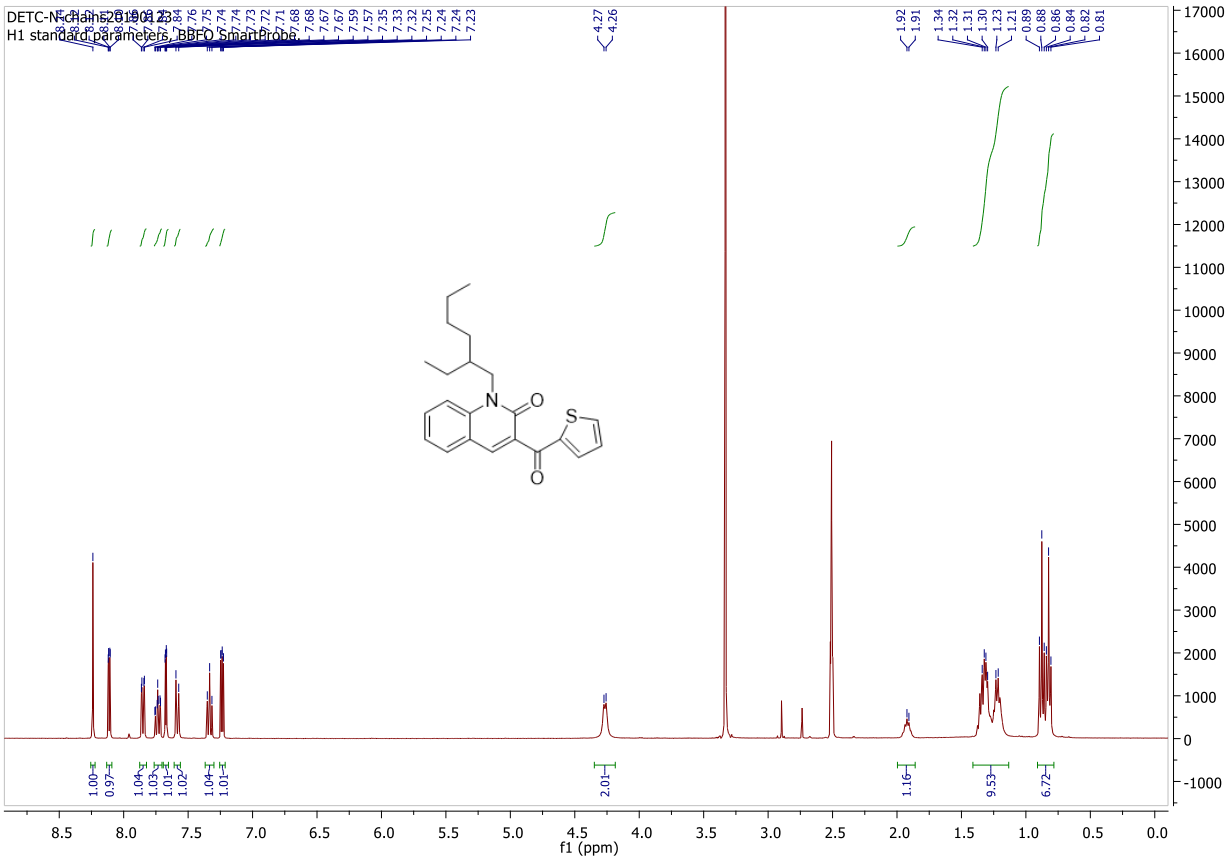

Figure 4.5. ^{1}H NMR of DETC-N-chain (1-(2-ethylhexyl)-3-(thiophene-2-carbonyl)quinolin-2(1H)-one)

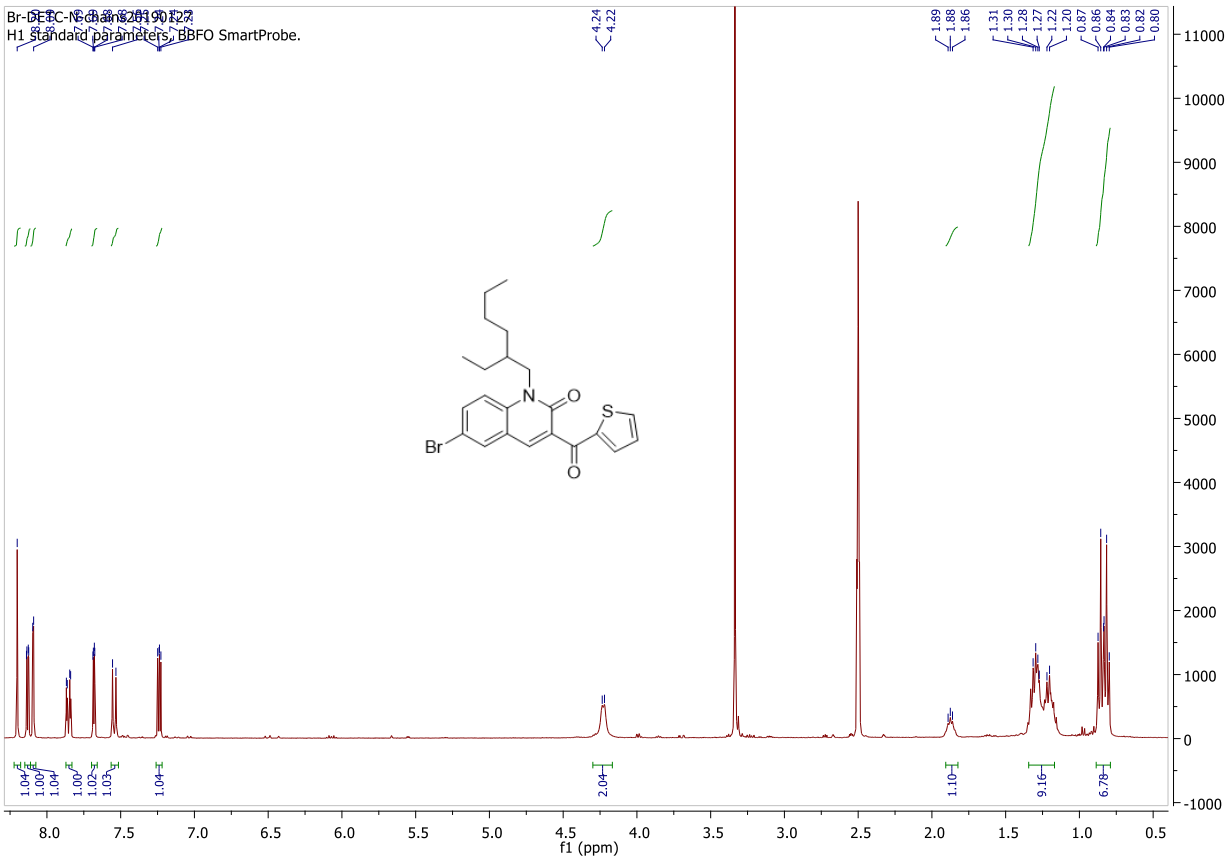

Figure 4.6. ^{1}H NMR of Br-DETC-N-chain (6-bromo-1-(2-ethylhexyl)-3-(thiophene-2-carbonyl)quinolin-2(1H)-one)

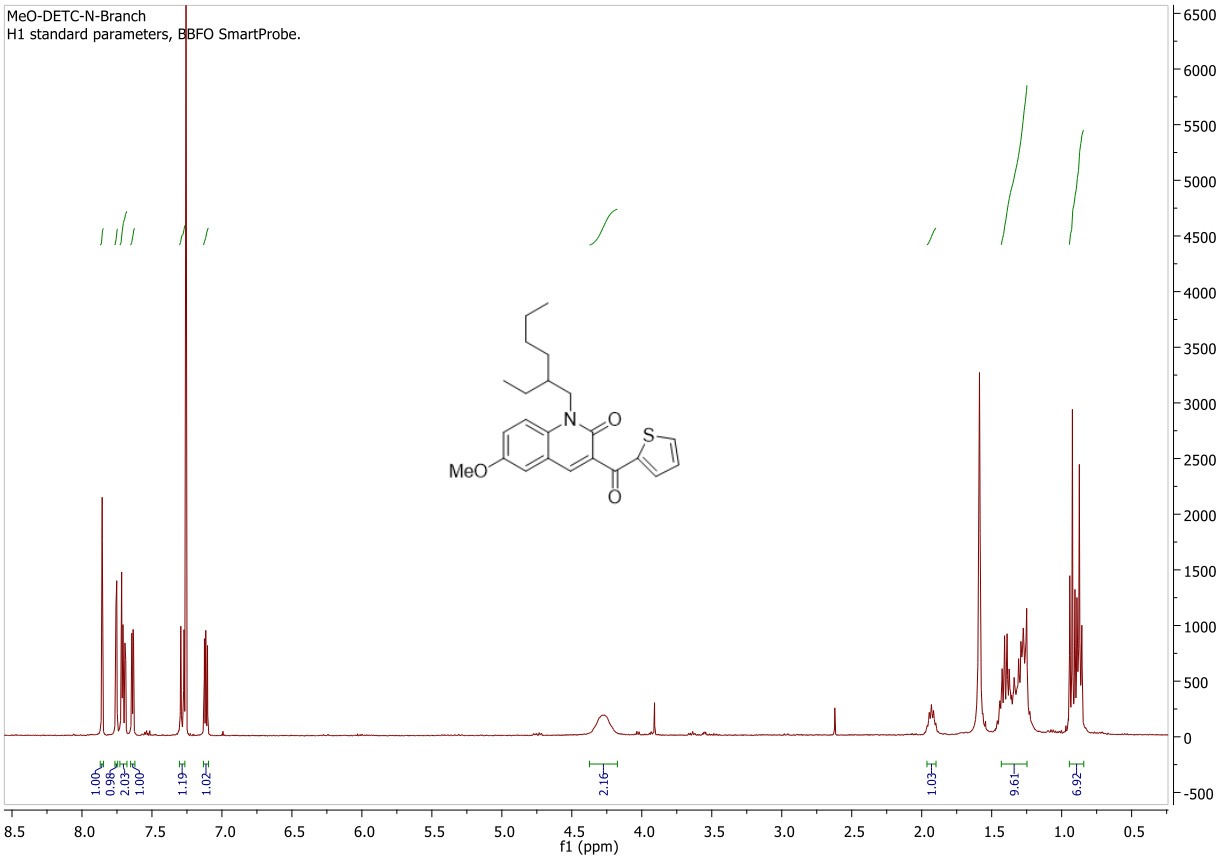

Figure 4.7. ^{1}H NMR of MeO-DETC-N-branch (1-(2-ethylhexyl)-6-methoxy-3-(thiophene-2-carbonyl)quinolin-2(1H)-one)

4.4 References

1 Harke, B., Dallari, W., Grancini, G., Fazzi, D., Brandi, F., Petrozza, A., & Diaspro, A. (2013). *Advanced materials (Deerfield Beach, Fla.)*, *25*(6), 904–909.

2 Specht, D. P., Martic, P. A., & Farid, S. (1982). Ketocoumarins: *Tetrahedron*, *38*(9), 1203-1211.

3 Huang, Y., Xu, W., Zhou, C., Zhong, W., Xie, R., Gong, X., ... & Cao, Y. (2016). *Journal of Polymer Science Part A: Polymer Chemistry*, *54*(14), 2119-2127.

VITA

Teng Chi was born in Beijing, People's Republic of China on January 4, 1993 to Jianyi Chi and Qiuhong Li. He went to Capital Normal University Middle School in 2005, High School in 2008 and graduated in 2011. In September 2011, he began his college career at Tsinghua University in Beijing and stayed there for 4 years. He majored in Chemistry and obtained his bachelor's degree in July 2015. After graduation from Tsinghua University, Teng Chi started his exciting graduate career at Purdue University in West Lafayette, Indiana, USA. In 2017, he joined the research group of Dr. Bryan Boudouris from Department of Chemistry and Forney Hall of Chemical Engineering. He studied and synthesized small organic molecules for nanolithograohic printing and radical polymers for electric conducting purpose. Teng Chi received his Doctor of Philosophy in December 2020 in Organic Chemistry.

PUBLICATION

FULL PAPER WWW.POLYMERPHYSICS.ORG JOURNAL OF POLYMER SCIENCE Polymer Physics

Tailored Thioxanthone-Based Photoinitiators for Two-Photon-Controllable Polymerization and Nanolithographic Printing

Teng Chi,[1] Paul Somers,[2] Daniel A. Wilcox,[3] Ashley J. Schuman,[1] Vasudevan Iyer,[2] Ran Le,[2] Jamie Gengler,[4,5] Manuel Ferdinandus,[4,6] Carl Liebig,[4] Liang Pan,[2] Xianfan Xu,[2] Bryan W. Boudouris[1,3]

[1]Department of Chemistry, Purdue University, 560 Oval Drive, West Lafayette, Indiana, 47907
[2]School of Mechanical Engineering and Birck Nanotechnology Center, Purdue University, West Lafayette, Indiana, 47907
[3]Charles D. Davidson School of Chemical Engineering, Purdue University, 480 W Stadium Ave, West Lafayette, Indiana, 47907
[4]Air Force Research Laboratory, 2179 12th St., Wright-Patterson Air Force Base, Ohio, 45433
[5]UES Inc., 4401 Dayton-Xenia Rd, Dayton, Ohio, 45432
[6]Air Force Institute of Technology, 2950 Hobson Way, Wright Patterseon AFB, Ohio, 45433
Correspondence to: B. W. Boudouris (E-mail: boudouris@purdue.edu)

Received 14 May 2019; revised 15 September 2019; accepted 1 October 2019; published online 20 October 2019
DOI: 10.1002/polb.24891

ABSTRACT: Printing of high-resolution three-dimensional nanostructures utilizing two-photon polymerization has gained significant attention recently. In particular, isopropyl thioxanthone (ITX) has been implemented as a photoinitiator due to its capability of initiating and depleting polymerization on demand, but new photoinitiating materials are still needed in order to reduce the power requirements for the high-throughput creation of 3D structures. To address this point, a suite of new thioxanthone-based photoinitiators were synthesized and characterized. Then two-photon polymerization was performed using the most promising photoinitiating molecule. Importantly, one of the initiators, 2,7-bis[(4-(dimethylamino) phenyl ethynyl)-9H-thioxanthen-9-one] (BDAPT), showed a fivefold improvement in the writing threshold over the commonly used ITX molecule. To elucidate the fundamental mechanism, the excitation and inhibition behavior of the BDAPT molecule were evaluated using density functional theory (DFT) calculations, low-temperature phosphorescence spectroscopy, ultra-fast transient absorption spectroscopy, and the two-photon Z-scan spectroscopic technique. The improved polymerization threshold of this new photoinitiator presents a clear pathway for the modification of photoinitiators in 3D nanoprinting. © 2019 Wiley Periodicals, Inc. J. Polym. Sci., Part B: Polym. Phys. **2019**, *57*, 1462–1475

KEYWORDS: 3D nanoprinting polymerizations; direct laser writing; thioxanthone-based photoinitiators; two-photon polymerization; ultrafast transient absorption spectroscopy

INTRODUCTION Two-photon polymerization was first reported in 1997,[1] and this has caused rapid growth in the field of nanolithography. A type of direct laser writing (DLW), this two-photon polymerization printing process takes advantage of the nonlinearity of multiphoton absorption in a polymeric photoresist to improve the spatial confinement of the printed voxel in a significant manner. In turn, this allows for the polymerization to occur inside the monomeric photoresist, and the fabrication of arbitrary 3D structures with submicron resolution is achieved.[1,2] DLW has been highlighted in recent years as a high-speed and low-cost tool for generating high-fidelity 3D nanoscale features in fields such as photonics[3,4] and tissue engineering.[5,6] While the spatial resolution of DLW is significantly improved relative to analogous single-photon polymerization systems, it remains a diffraction-limited process. This significant barrier can be overcome by introducing a polymerization-inhibiting depletion laser.[7] That is, in a concept first applied to microscopy,[8] the resolution of DLW was improved by spatially overlapping a shaped depletion laser beam such that the DLW beam is positioned in a minimum of the depletion laser beam.[9] In this configuration, the photoinitiated polymerization is inhibited anywhere outside of the depletion laser minimum. Critical to the success of this inhibition-based polymerization technique is the optical response of the photoinitiating species in the DLW process. That is, the photoinitiator must allow for efficient initiation (and subsequent propagation) of the polymerization by the excitation beam while the inhibition beam must stop the polymerization reaction in an effective manner. To this end,

Additional Supporting Information may be found in the online version of this article.

†Teng Chi and Paul Somers contributed equally to this work.

several two-photon photoinitiating species have been developed, and some of the most promising materials have been investigated with nanolithographic applications in mind.[10,11] However, there is a demand in both academic and industrial circles for more efficient photoinitiators in order to reduce the writing laser power requirements. Because the polymerization that the photoinitiator controls is key in the DLW process, we synthesized a series of new thioxanthone-based photoinitiators in order to achieve more efficient initiation (i.e., lower power) of the photopolymerizations at the nanoscale, and we established that the appropriate design of these materials and the modulation of their photophysical properties can significantly reduce the power required to create two-photon polymerized nanostructures.

The proposed photoinitiator builds from the fact that isopropyl thioxanthone (ITX) is an established photoinitiator in two-photon nanolithographic processes.[12] Despite the fact that ITX demonstrates the desired photoinitiation and photoinhibition properties with respect to the writing and depletion wavelengths,[9,12] the writing laser power required for this material is still large at the common writing wavelength of 800 nm due to the weak two-photon absorption cross section of the ITX molecule.[13] While not a particular issue for previously reported proof-of-concept demonstrations, reducing the amount of power required for photoinitiation is of critical import for scalable nanomanufacturing (i.e., in cases where multiple lasers would be required in order to achieve high-throughput production). Also of concern is the tendency of larger laser powers to lead to parasitic polymerization due to thermal initiation events, which can impact the minimum feature sizes that are attainable.[14] Thus, there is a significant need to develop next-generation ITX derivatives that are capable of having improved light absorption profiles for the DLW wavelength (λ = 800 nm).

From nonlinear optics, the two-photon absorption coefficient is predicted to be optimal for an incident photon energy that is 0.7 times the bandgap of a wide bandgap material.[15] In terms of designing a molecule for a constant DLW wavelength of 800 nm, this indicates a necessity to redshift the absorption peak of the photoinitiators relative to ITX to improve this ratio of absorption peak wavelength to the incident light wavelength. Moreover, it has been shown that molecules following a donor–acceptor–donor type structure also demonstrate an improved two-photon absorption cross section.[16] Following these lines of thinking, we strive to take ITX and develop derivatives with improved two-photon absorption (i.e., increasing the number of initial electrons that are promoted to the singlet state) while studying the resulting effects on the polymerization initiating and inhibiting properties of the new compounds (i.e., we will evaluate the intersystem crossing processes and triplet state dynamics as well). We propose that the introduction of chromophores or electron donors leads to the generation of the donor–acceptor–donor or donor–acceptor species, and this will cause a redshift in the absorption spectrum. Compared to ITX, these derivatives should demonstrate improved two-photon absorption cross sections. In order to accomplish this objective, the functional groups pendant to the thioxanthen-9-one core of ITX were tuned in a systematic manner. Specifically, phenyl, diphenyl, and naphthyl groups were attached to the ITX core with alkyne bridges, which leads to extended aromatic systems along the small molecule backbone. This extended conjugation, in turn, results in a bathochromic shift in the peak of the absorbance spectra of the molecules. Dialkylamino groups were added to terminate the ends of the molecules due to the strong electron-donating features of these substituents. In addition, mono- and di-substituted derivatives were synthesized and compared in order to elucidate the influence of the numbers of pendant groups on the photophysical properties of the polymerization initiators. The absorption spectra of the new initiators were predicted by density functional theory (DFT) calculations in order to provide a guide for the synthesis. Two-photon absorption cross sections were measured for each of the synthesized photoinitiators to provide a direct indicator of the DLW polymerization performance. The existence of possible charge transfer states that could arise due to the donor–accepter molecular motif were rationalized by calculating the frontier molecular orbitals of the molecules. Ultra-fast transient absorption spectroscopy and phosphorescence spectra were utilized to determine excited state lifetimes in order to benchmark the polymerization inhibition characteristics and possible mechanism of the newly synthesized polymerization photoinitiators in comparison to ITX. DLW polymerization was then performed using the most-promising photoinitiator based on these evaluations, and the photoinitiating molecule, 2,7-bis[(4-(dimethylamino)phenyl ethynyl)-9H-thioxanthen-9-one] (BDAPT), demonstrated a reduction in required laser power for DLW when pentaerythritol triacrylate (PETA) served as the monomer for the polymerizations associated with the engineered photoinitiators. The writing laser power of BDAPT was reduced by fivefold relative to the laser power required for the same monomer system using the commonly implemented ITX photoinitiator. Therefore, the archetype presented here is one that sets a path forward in designing next-generation photoinitiators for their application towards low-power, high-throughput photopolymerizations in 3D nanoprinted materials.

EXPERIMENTAL

General Experimental Procedures

All chemicals were purchased from Sigma-Aldrich, and the chemicals were used as received. The ^{1}H NMR spectra were measured on a Bruker DRX500 spectrometer using a ~1% polymer solution (by weight) in deuterated chloroform (Sigma-Aldrich). Ultraviolet–visible (UV–Vis) spectroscopy data were collected using a Cary 60 spectrometer in the wavelength range of 330 nm $\leq \lambda \leq$ 800 nm. Fluorescence and phosphorescence spectroscopy data were obtained using a Cary Eclipse fluorescence and phosphorescence spectrophotometer in the wavelength range of 400 nm $\leq \lambda \leq$ 800 nm (with an excitation wavelength of 350 nm). Phosphorescence data were collected using deoxygenated solutions of the samples in a glass-forming solvent, with an absorbance below 0.01 at the excitation

wavelength. 9,10-Diphenylanthracence was used as a fluorescence quantum yield standard (94%) as the quantum yield of this material in THF is well established.[17] In order to correct for solvent effects, eq 1 was utilized to normalize the quantum yield obtained for the 9,10-diphenylanthracence when PETA was the solvent.[18]

$$\Phi_{PETA} = \Phi_{THF}\left(\frac{S_{PETA}}{S_{THF}}\right)\left(\frac{n_{PETA}^2}{n_{THF}^2}\right) \quad (1)$$

Here, Φ_{THF} (94%) is the fluorescence quantum yield of the standard in THF. S_{THF} ($\sim 2.64 \times 10^6$counts/a.u.) represents the slope of the integrated fluorescence signal obtained for the standard molecule *vs.* absorbance for different concentrations when they are dissolved in THF, and S_{PETA} ($\sim 2.50 \times 10^6$counts/a.u.) represents the same slope when the standard molecule is dissolved in PETA. The refractive indeices (n_{PETA} = 1.483 and n_{THF} = 1.407) were obtained from Sigma-Aldrich. From this equation, the fluorescence quantum yield of 9,10-diphenylanthracence in PETA was calculated as 98.7%. The quantum yield values of different photoinitiators were tested and referenced to the value of 9,10-diphenylanthracence.

Synthesis of Dibromo-9H-Thioxanthene-9-One (DBTX)

Thioxanthen-9-one (Compound 7, 4 g, 19.2 mmol) was added to a 500 mL round bottle flask with 32 mL of acetic acid. Then, 8 mL of bromine were added in a dropwise manner while the reaction mixture was held at 0 °C. After the addition of the bromine, the flask was slowly heated to 118 °C. After 24 h, a dark red solution formed, and at this time, the solution was poured into an ice bath. A yellow precipitate appeared, and it was filtered. After washing with a saturated aqueous $NaHCO_3$ twice to quench any remaining acid, the yellow solid was dissolved into toluene and subsequently recrystallized to form yellow crystals in 51% yield. ^{1}H NMR (400 MHz, deuterated chloroform) δ: 8.74 (d, 4 *J* = 2.35 Hz, 2H), 7.76 (dd, 3 *J* = 8.59, 4 *J* = 2.30 Hz, 2H), 7.49 (d, 3 *J* = 8.61 Hz, 2H).

Synthesis of 6-Bromo-*N*,*N*-Dimethylnaphthalen-2-Amine. (Compound 2)

6-Bromo-2-naphthol (Compound 1, 1.5 g, 6.7 mmol), a solution of dimethyl amine in methanol (15 mL, 33 mmol), and $Na_2S_2O_5$ (2.7 g, 13.6 mmol), were added to a reaction flask. Then, 5 mL of H_2O was added to the reaction flask in order to increase the solubility of $Na_2S_2O_5$, and the tube was then sealed. The reaction was slowly heated to 140 °C. After 40 h, the crude mixture was obtained by filtering the inorganic solid; the organic solution was washed with brine and DI-water three times and extracted with ethyl acetate. The mixture was purified by column chromatography (Hexane: ethyl acetate = 9:1 v/v) to yield a solid with 60% yield. ^{1}H NMR (400 MHz, deuterated chloroform) δ 7.84–7.80 (m, 1H), 7.63–7.57 (m, 1H), 7.51 (dq, *J* = 8.8, 0.6 Hz, 1H), 7.41 (dd, *J* = 8.8, 2.0 Hz, 1H), 7.16 (dd, *J* = 9.1, 2.6 Hz, 1H), 6.86 (d, *J* = 2.6 Hz, 1H), 3.05 (s, 6H).

Synthesis of *N*,*N*-Dimethyl-6-((Trimethylsilyl)Ethynyl) Naphthalen-2-Amine (Compound 3)

$Pd(PPh_3)_2Cl_2$ (0.05 mmol), CuI (0.05 mmol), and 6-bromo-N, *N*-dimethylnaphthalen-2-amine (125 mg, 0.5 mmol) were added to a round bottle flask under a nitrogen blanket. Subsequently, freshly distilled diethyl amine (3 mL) with (trimethylsilyl) acetylene (0.14 mL, 1 mmol) were added to the flask. The reaction was slowly heated to 50 °C in the dark. After 24 h, the reaction mixture was diluted with ethyl acetate before being washed with brine and DI water three times. After the organic fraction was dried by Na_2SO_4, the mixture was pushed through a silica gel flash column without further purification.

Synthesis of 4′-Bromo-*N*,*N*-Dimethyl-[1,1′-Biphenyl]-4-Amine (Compound 5)

4-(Dimethyl amino) phenylboronic acid pinacol ester (Compound 4, 494 mg, 2 mmol) and 1-bromo-4-iodobenzene (676 mg, 2.4 mmol) were added to a 20 mL sealed tube. Then, 0.1 equivalents of Pd $(PPh_3)_4$ (0.2 mmol) and Na_2CO_3 (6 mmol) were mixed and poured into the tube; 15 mL of THF and 2 mL of water were then injected to the tube. The tube was sealed and slowly heated to 80 °C overnight under a nitrogen atmosphere. The dark mixture that formed was washed with brine and then deionized (DI) water three times and extracted with ethyl acetate. After drying over Na_2SO_4, the crude mixture was purified by silica gel column chromatography (hexane: ethyl acetate = 10:1 v/v) to give a solid with 40% yield. 1H NMR (400 MHz, deuterated chloroform) δ 7.52–7.48 (m, 2H), 7.48–7.43 (m, 2H), 7.44–7.38 (m, 2H), 6.79 (d, *J* = 8.3 Hz, 2H), 2.99 (s, 6H).

Synthesis of *N*,*N*-Dimethyl-4′-((Trimethylsilyl)-Ethynyl)-[1,1′-Biphenyl]-4-Amine (Compound 6)

$Pd(PPh_3)_2Cl_2$ (0.05 mmol), CuI (0.05 mmol), and 4′-bromo-*N*,*N*-dimethyl-[1,1′-biphenyl]-4-amine (Compound 5, 130 mg, 0.5 mmol) were added in a round bottom flask under a nitrogen blanket. Subsequently, freshly distilled diethyl amine (3 mL) and (trimethylsilyl) acetylene (0.14 mL, 1 mmol) were added to the flask. The reaction was slowly heated to 50 °C in the dark. After 24 h, the reaction mixture was diluted with ethyl acetate before being washed with brine and DI water three times. After the reaction, the organic fraction was dried with Na_2SO_4, and the mixture was pushed through a silica gel flash column without further purification.

Synthesis of 2,7-Bis[(4-(Dimethylamino)Phenyl Ethynyl)-9H-Thioxanthen-9-One]

4-Ethynyl-*N*,*N*-dimethylaniline (Compound 8, 362 mg, 2.5 mmol), $Pd(PPh_3)_2Cl_2$ (42 mg, 0.06 mmol), CuI (19 mg, 0.1 mmol), and DBTX (115 mg, 0.32 mmol) were added in a round bottle flask under nitrogen protection. Then freshly distilled diethyl amine (4 mL) was injected. The reaction was stirred for 30 h at 53 °C in the dark. The reaction mixture was diluted with ethyl acetate before being washed with brine and DI water three times. Afterwards, the organic layer was dried using Na_2SO_4, the mixture was purified by column chromatography (Hexane:ethyl acetate = 6:1 v/v) to give a solid with 10% yield. It was mixed with

PETA immediately for use during nanoprinting because of its fast decomposition in air or exposure to light. ^{1}H NMR (400 MHz, deuterated chloroform) δ 7.89 (d, J = 8.9 Hz, 2H), 7.70 (d, J = 8.0 Hz, 2H), 7.49–7.41 (m, 4H), 7.39 (d, J = 8.9 Hz, 2H), 6.70–6.64 (m, 4H), 3.00 (s, 12H).

Synthesis of 2-Bromo-7-[(4-(Dimethylamino) Phenyl) Ethynyl]-9H-Thioxanthen-9-One

4-Ethynyl-*N*,*N*-dimethylaniline (Compound 8, 50 mg, 0.32 mmol), $Pd(PPh_3)_2Cl_2$ (14 mg, 0.02 mmol), CuI (10 mg, 0.05 mmol), and DBTX (115 mg, 0.32 mmol) were added to a round bottom flask under nitrogen protection. Freshly distilled diethyl amine (2 mL) was injected and the reaction was stirred for 24 h at 50 °C in the dark. The reaction mixture was diluted with ethyl acetate before being washed with brine and DI water three times. After the organic layer was dried with Na_2SO_4, the mixture was purified by column chromatography (hexane:ethyl acetate = 20:1 v/v) to produce a solid with 11% yield. ^{1}H NMR (400 MHz, deuterated chloroform) δ 8.74 (ddd, J = 19.3, 2.1, 0.5 Hz, 2H), 7.72 (ddd, J = 8.4, 2.1, 1.5 Hz, 2H), 7.56–7.47 (m, 2H), 7.47–7.41 (m, 2H), 6.68 (d, J = 9.0 Hz, 2H), 3.01 (s, 6H).

Synthesis of 2-Bromo-7-[(6-(Dimethylamino) Naphthalen-2-Yl)Ethynyl]-9H-Thioxanthen-9-One

N,*N*-dimethyl-6-((trimethylsilyl)-ethynyl)naphthalen-2-amine (Compound 3, 200 mg, 0.75 mmol), $Pd(PPh_3)_2Cl_2$ (28 mg, 0.04 mmol), CuI (19 mg, 0.1 mmol), and DBTX (115 mg, 0.32 mmol) were added in a round bottom flask under nitrogen protection. Freshly distilled diethyl amine (2 mL) was injected and the reaction was stirred for 30 h at 53 °C in the dark. The reaction mixture was diluted with ethyl acetate before being washed with brine and DI water three times. After the organic layer was dried with Na_2SO_4, the mixture was purified by column chromatography (hexane:ethyl acetate = 20:1 v/v) to give a solid with 8% yield. It was mixed with PETA immediately for use during nanoprinting because of its fast decomposition in air or exposure to light. ^{1}H NMR (400 MHz, deuterated chloroform) δ 8.77 (d, J = 2.2 Hz, 1H), 7.96–7.89 (m, 1H), 7.80–7.66 (m, 3H), 7.64–7.57 (m, 2H), 7.53–7.45 (m, 2H), 7.41–7.34 (m, 1H), 7.17 (ddd, J = 9.1, 4.8, 2.6 Hz, 1H), 6.88 (d, J = 2.5 Hz, 1H), 3.08 (s, 6H).

Computational Calculations Procedure

The theoretical ultraviolet–visible (UV–Vis) absorption spectra of the relevant molecules were calculated using Gaussian 09.[19] The optimized ground-state geometries of all of the molecules were computed using DFT with the Becke 3-parameter hybrid functional with Lee–Yang–Parr correlation (B3LYP) and the 6-31G(d) basis set, as implemented in Gaussian 09. The optimized structures were verified by computing the infrared (IR) absorption spectra of the structure and verifying that no imaginary frequencies were present. After computing the optimized structures, the first 40 excited states of each molecule were computed using time-dependent DFT (TD-DFT) as implemented in Gaussian 09 at the same level of theory.

To generate the theoretical spectra, each excited state transition was used to generate a Gaussian function according to eq 2.[20]

$$\varepsilon_i(\lambda) = a \times 10^8 \frac{f_i}{\sigma} \exp\left[-\left(\frac{(1/\lambda - 1/\lambda_i)}{\sigma}\right)^2\right] \quad (2)$$

Here, a is a constant equal to 1.3062974, ε_i is the molar absorptivity of the molecule due to transition i at the given wavelength λ in units of L mol^{-1} cm^{-1}, f_i is the oscillator strength of the transition, λ_i is the wavelength of the transition, and σ is standard deviation (representing the width of the Gaussian function). Because the available range for the standard deviation is from 0.2 eV to 0.8 eV, a default value of 3.226×10^{-4} nm^{-1} (equal to 0.4 eV) was used in this calculation, as has been used previously.[17] Summing the Gaussian functions for each transition provides the theoretical UV–Vis spectrum of the molecule. The complete tabular data for the S_n and T_n energy levels for the new photoinitiator of interest, BDAPT, are shown in the Supporting Information Tables S1 and S2, respectively.

DLW Photopolymerization

The excitation source consisted of a Ti:Sapphire oscillator (Coherent Micra-10) at 800 nm center wavelength and 80 MHz repetition rate. A continuous wave 638 nm diode laser was used as the inhibition beam, introduced via a dichroic beam splitter. Both beams were focused through a 100× objective lens (Nikon, N.A. = 1.49) to the sample located on a 100 μm × 100 μm × 200 μm travel piezostage (Mad City Labs), which is computer-controlled for translation in space. Fast mechanical shutters (Uniblitz) were used to control each beam independently. Attenuation of the laser power was achieved by variable neutral density filters. For each laser, a telescoping lens pair was used to expand the beam diameters before reaching the objective lens. The samples consisted of blends of monomer and photoinitiators sandwiched between a microscope slide and glass coverslip (thickness ~170 μm) with a single layer of Scotch tape providing a gap of ~40 μm. The concentration (by weight) of single photoinitiator in PETA monomer for each sample was 0.25% for BDAPT, 0.5% for both DANT and DAPT, and 1.5% for ITX. Coarse positioning of the sample was performed by a manual, micrometer-driven stage. The stages and objective lenses were mounted on an inverted microscope. All of the writing was performed at scan speed of 100 μm s^{-1}. Laser powers were measured at the back of the objective lens through a 6 mm diameter aperture. The heights of printed polymer lines were measured using an atomic force microscope (AIST NT) with a silicon tip in tapping mode. After these height measurements were made, the structures were sputter-coated with an Au/Pd mixture, and the samples were imaged using a scanning electron microscope (Hitachi S-4800) with 30 kV accelerating voltage.

Z-Scan Measurements

The nonlinear two-photon absorption cross sections were determined using an open-aperture Z-scan.[21] All Z-scan measurements were performed using 50 fs pulses from a regeneratively amplified laser (KMLabs Wyvern-1000) with a center wavelength of 788 nm and full-width, half-maximum

(FWHM) bandwidth of 28 nm. The beam was first spatially filtered before being focused to a beam waist of ~16 μm. Solutions of photoinitiators in THF were evaluated with a 1 mm path length cuvette holding the solution. During the measurement, the sample was translated along the optical (z-) axis by a motorized stage. All of the transmitted signal was collected with a photodetector while a second photodetector measured the beam before the sample to remove any laser instability issues in the final reported data.

Excited State Lifetime Measurements

Excited state lifetimes of the photoinitiators were determined by transient absorption measurements using a collinear pump-probe scheme similar to a previous work.[22] Here, the 800 nm pump beam was frequency doubled to 400 nm and the probe beam was set to 633 nm using an optical parameteric amplifier (Quantronix TOPAS-C). The concentrations of ITX and BDAPT in THF were 8.2×10^{-2} M and 1.3×10^{-3} M, respectively. The pump laser fluence was ~1.4×10^{-2} Jcm^{-2} for BDAPT and ~1.2×10^{-3} Jcm^{-2} for ITX. The probe laser fluence was ~3.9×10^{-4} J cm^{-2} for BDAPT and ~4.8×10^{-4} Jcm^{-2} for ITX.

RESULTS AND DISCUSSION

As a commercially available photoinitiator, ITX has served as a model molecule that reveals the mechanism of energy transfer in two-photon DLW polymerizations, and the general picture of its operating mechanism in photopolymerizations is as follows. First, an electron in the ground state (S_0) of ITX is promoted to the first excited state (S_1) through a two-photon optical transition using an 800 nm wavelength laser.[23] Then, the excited state undergoes intersystem crossing to generate the triplet state (T_1), which initiates the polymerization when ITX is blended with the monomeric species. As revealed by previous pump-probe spectroscopy experiments,[12,23] the ITX molecule can undergo depletion of the excited state through both: (a) stimulated-emission depletion (STED) and (b) nonradiative decay by excitation of long-lived species in order to inhibit the polymerization. The latter of these two dominates in depletion DLW polymerization when ITX is the photoinitiator.[12,23]

Due to the well-understood excited state dynamics of ITX, it is useful as a starting material for the development of high-performance polymerization photoinitiators. As such, the design of our photoinitiators is based on a previous work of the Gryko group.[24] Moreover, in order to guide the synthetic design, computational calculations were utilized to predict the absorption spectra of a set of potential photoinitiator molecules,[19] and the experimentally synthesized materials were those that showed the most promise from these simulations. For example, relative to ITX, the peak absorption wavelength is red shifted for the BDAPT; 2-bromo-7-((6-(dimethylamino)naphthalen-2-yl)ethynyl)-9H-thioxanthen-9-one (DANT) and 2,7-bis((6-(dimethylamino)naphthalen-2-yl) ethynyl)-9H-thioxanthen-9-one (BDANT); 2-bromo-7-((4′-(dimethylamino)-[1,1′-biphenyl]-4-yl)ethynyl)-9H-thioxanthen-9-one (DEPT) and 2,7-bis((4′-(dimethylamino)-[1,1′-biphenyl]-4-yl) ethynyl)-9H-thioxanthen-9-one (BDEPT) compounds (Fig. 1).

This agrees with the concept that the extension of the π-system in photoinitiators can cause a redshift in the peak absorption of these ITX-based molecules. Moreover, there was a predicted redshift between the mono-substituted and the di-substituted derivatives as well. For example, in the predicted

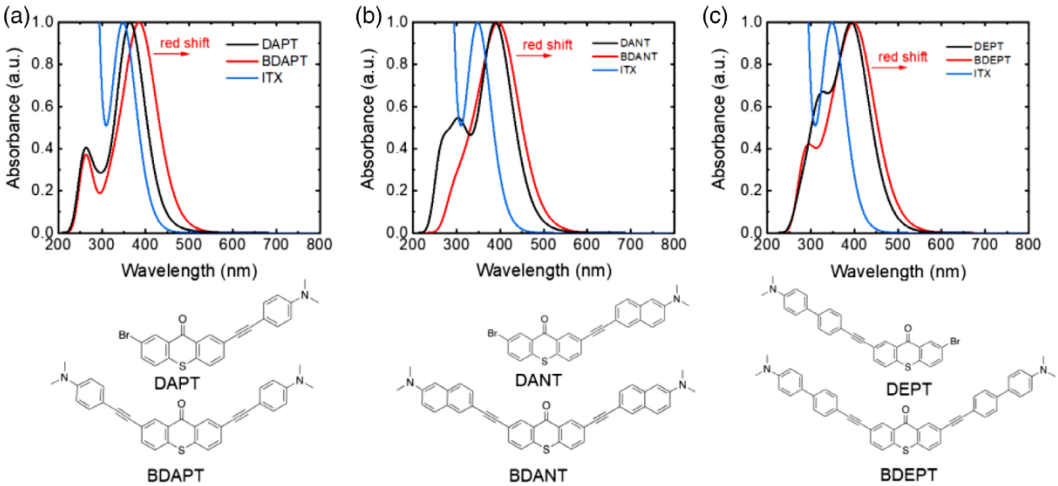

FIGURE 1 Predicted UV–Vis absorption plots for: (a) ITX, DAPT, and BDAPT; (b) ITX, DANT and BDANT; and (c) ITX, DEPT, and BDPET. These predictions were made using TD-DFT with a B3LYP/6-31G(d) level of theory. The structures of the simulated photoinitiating molecules (aside from ITX) are shown directly below their calculated absorption spectra. [Color figure can be viewed at wileyonlinelibrary.com]

TABLE 1 Absorption Coefficients and Fluorescence Quantum Yields of the Photoinitiators

Photoinitiator	Solvent	Peak absorption wavelength (nm)[a]	Theoretical peak absorption wavelength (nm)	ε^b (10^4 $mol^{-1}Lcm^{-1}$)	ε^c (10^4 $mol^{-1}Lcm^{-1}$)	Φ_{fl} (%)[e]
ITX	Toluene	385	348	0.71	0.57	
	PETA	387		0.23	0.21	1.6
BDAPT	Toluene	408	390	0.91	0.83	
	PETA	414		2.0	1.8	8.1
DAPT	Toluene	353	365	5.1	1.2	
	PETA	–[d]		–[d]	–[d]	–[d]
DANT	Toluene	380	389	0.88	0.71	
	PETA	390		1.6	1.4	4.4
DBTX	Toluene	395		0.46	0.42	
	PETA	–[d]		–[d]	–[d]	–[d]

[a] The peak wavelength is the maximum absorption near a wavelength of 400 nm if there are multiple peaks in the spectra.
[b] The molar absorption coefficient of the species at the wavelength demonstrating the maximum absorption.
[c] The molar absorption coefficient at the 390 nm wavelength.
[d] Insufficient signal or difficult to dissolve in the PETA monomer.
[e] Fluorescence quantum yield when the excitation wavelength was set to 390 nm.

UV–Vis absorption data, the maximum absorption wavelength of BDAPT was redshifted about 25 nm relative to DAPT. This redshifted trend also was observed in the DANT- and DEPT-based systems due to the extension of the π-system.

All the molecules have a relatively high predicted molar absorptivity coefficient at 400 nm (Table 1), which demonstrated their potential feasibility as efficient photoinitiators. Based upon these DFT results, the most promising compounds (i.e., DAPT, BDAPT, and DANT) were synthesized as these molecules exhibited strong absorption and were predicted to have maximum absorption wavelengths around 400 nm. Specifically, we designed a series of compounds based on an ITX core with different substituent groups. After our initial design, a straightforward series of high-throughput experiments (*vide infra*) were performed in order to down-select the most promising photoinitiating candidates. In this way, design and selection rules can be had for these types of photoinitiating systems.

In this particular effort, alkyne groups were introduced as linkers between the backbone and the branches for two major reasons. First, this functionality increases the distance between the backbone and substituent branches to avoid steric hindrance effects, which may interrupt the conjugated system due to the possibility of rotation. Second, this functionality maintains aromaticity across the molecular system. Thus, functional groups were attached through the triple bond bridge. Specifically, phenyl, diphenyl, and naphthyl groups were synthesized and bonded through the alkyne group in a systematic way (Scheme 1). That is after a base-promoted aromatic substitution with dimethyl amine,[25] the naphthyl substituted group (Compound 3) was generated by a Sonogashira coupling reaction.[26] Similarly, the diphenyl-substituted group (Compound 6) was generated by a Pd-catalyst Suzuki coupling[27] followed by a Sonogashira coupling reaction.[28] Finally, the 4-ethynyl-*N*,*N*-dimethylaniline (Compound 8) was commercially available, and it was purchased directly from Sigma-Aldrich.

The synthetic pathway shown in Scheme 2 was then utilized to create the advanced photoinitiators, and these molecules were characterized by ^{1}H NMR spectroscopy and mass spectroscopy

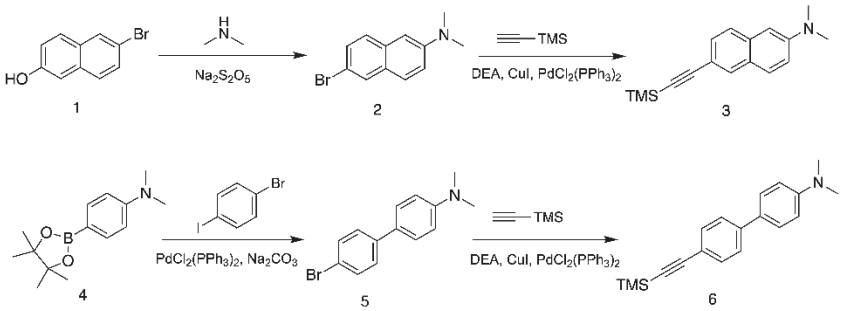

SCHEME 1 Synthetic pathway of the substituents of the photoinitiators.

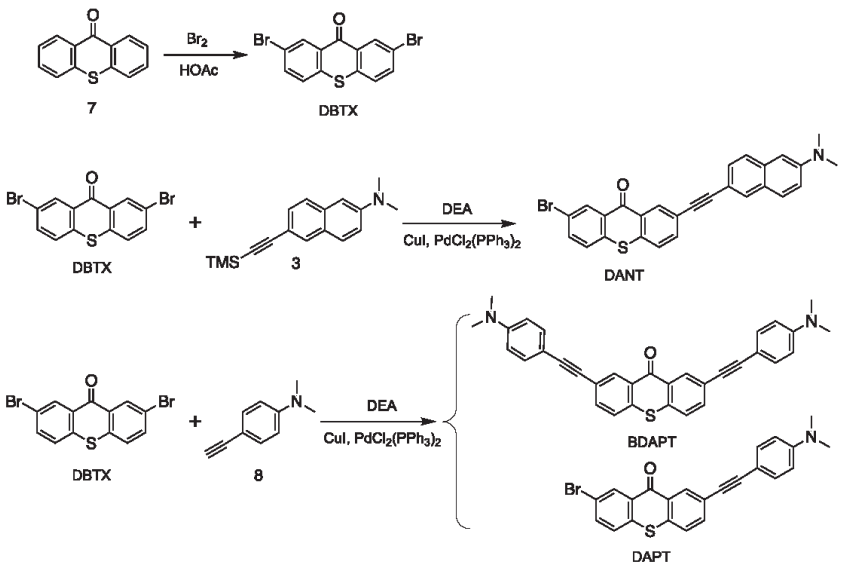

SCHEME 2 Synthetic pathway for the advanced photoinitiators.

(Supporting Information Figs. S1–S3).[26,28] Dibromothioxanthen-9-one (DBTX) can be synthesized through a bromination reaction.[29–31] BDAPT and DAPT can be successfully formed by traditional Sonogashira coupling reactions using a single step.[26,28,32] The major product of these reactions (i.e., either the di-substituted BDAPT or mono-substituted DAPT) can be controlled by changing the ratio of two different starting materials. DANT can also be generated through the same Sonogashira coupling in similar conditions; however, due to the instability of those species, the yield of DAPT, BDAPT, and DANT were low (11%, 10%, and 8%, respectively), and BDEPT, DEPT, and BDANT were not isolated in a manner that allowed for their evaluation as photoinitiating species.[33,34]

After the successful syntheses according to Schemes 1 and 2, the frontier molecular orbitals were calculated and are shown in Figure 2. The thioxanthone core can be thought of as an acceptor and the (*N*,*N*-dimethylamino)phenyl moieties as the donors. The first two singlet excited states for BDAPT are transitions from the HOMO to the LUMO and from the HOMO–1 to the LUMO, respectively. These correspond to the intramolecular charge transfer states, as evidenced by the shift in the wave function density from the entire molecule to the thioxanthone center. The third calculated singlet excited state, which corresponds to the primary excitation at 400 nm, is a transition from the HOMO to the LUMO+1. This, by contrast, results in minimal change in the charge density on the molecule. Thus, the transition from S_1 to the lower optically inactive singlet states could proceed by a charge transfer mechanism.

The absorption and emission properties of the materials were characterized in order to compare their experimental properties to the predicted properties and to evaluate their potential utility in the DLW photopolymerization process. In particular, synthesizing molecules with large molar absorptivity values at half the wavelength used in the DLW process (i.e., 400 nm) is of prime interest. Moreover, these same molecules should demonstrate relatively strong emission at the common depletion laser wavelength of 532 nm in their fluorescence spectra for quenching of the polymerization via the STED process. The normalized experimental UV–Vis absorption data are shown in Figure 3(a). DBTX was included in the result as a comparison in order to provide a baseline material that did not include any conjugated branches, and the experimental absorption spectrum of DBTX is redshifted relative to ITX. BDAPT and DANT had two broad peaks[35,36] with relatively high absorbance at 400 nm, which can be attributed to the $\pi \rightarrow \pi^*$ transition at higher wavelength and $n \rightarrow \sigma^*$ jumping at lower wavelength due to the electron lone pair on the hetero atom.[37,38] DAPT was also redshifted (Supporting Information Fig. S4), likely because of the charge transfer state generated by the asymmetric structure of DAPT.[39] As a result, all the new photoinitiators were redshifted as designed and had a relatively high absorption at 400 nm in UV–Vis spectrum (Supporting Information Fig. S4), such that the excitation processes occurred readily.

For light-induced inhibition of the DLW photopolymerization, ITX has been shown to predominantly follow a triplet–triplet absorption depletion pathway for the initiating species. However, for ITX derivatives such as these, there are other potential depletion pathways that may be non-negligible, or even dominating, for inhibiting the polymerization process.[40] In order to determine the possible contribution of another

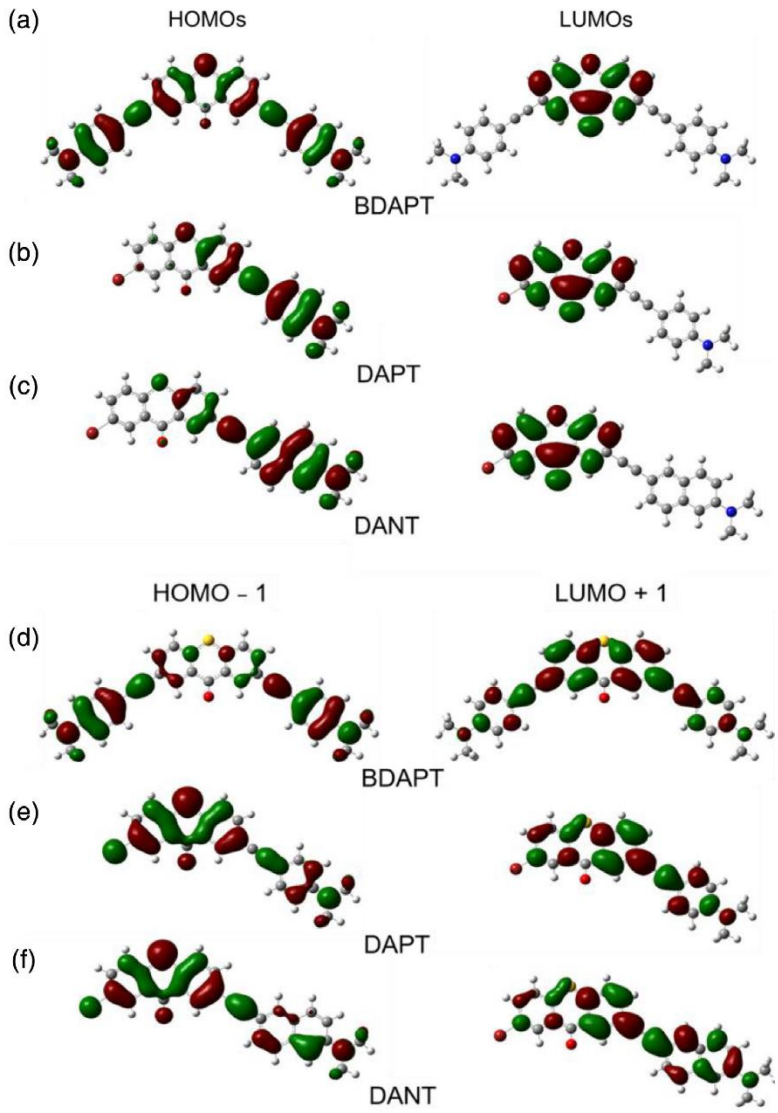

FIGURE 2 Molecular orbital diagrams calculated at an isovalue of 0.02. These plots are of the: (a) HOMO, LUMO of BDAPT; (b) HOMO and LUMO of DAPT; (c) HOMO and LUMO of DANT; (d) HOMO-1 and LUMO+1 of BDAPT; (e) HOMO-1 and LUMO+1 of DAPT; and (f) HOMO-1 and LUMO+1 of DANT. They are used to illustrate the charge transfer states in those molecules. It can be seen that the HOMO, HOMO–1, and LUMO+1 wave functions are either spread over the entire molecule or localized to the (*N*,*N*-dimethylamino) phenyl moieties, while the LUMO wave functions are localized to the thioxanthone core. Therefore, electronic transitions from the highest two occupied orbitals to the LUMO should result in a transfer of charge from the branches to the core, while transitions to the LUMO+1 should not result in a charge transfer state formation. [Color figure can be viewed at wileyonlinelibrary.com]

popular depletion mechanism, stimulated emission depletion, to the polymerization inhibition process, the fluorescence of each molecule was established. The peak emission wavelength trend of the different compounds is DBTX < ITX < DANT < DAPT < BDAPT [Fig. 3(b)]. Exposure of BDAPT at 532 nm may provide the greatest potential for STED because the peak

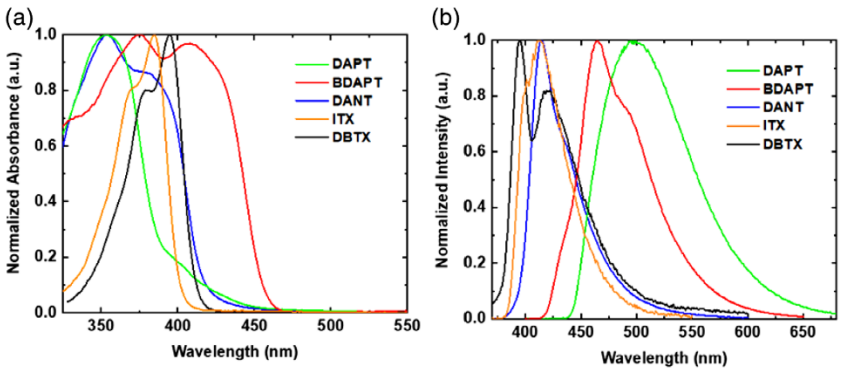

FIGURE 3 (a) The normalized UV–Vis absorbance spectra of photoinitiators in toluene. (b) The fluorescence spectra of the initiators in toluene obtained with excitation at 350 nm. [Color figure can be viewed at wileyonlinelibrary.com]

of fluorescence emission is approaching 532 nm. Excitation spectra were collected and compared to the absorption spectra. The spectra closely matched, indicating the observed emission is not due to an instrumentation artifact (Supporting Information Fig. S5). Thus, from both the UV–Vis and fluorescence spectra, BDAPT and DANT showed the potential to replace ITX as high-performing photoinitiators for DLW nanolithographic applications.

The coefficient of extinction and fluorescence quantum yield is listed in Table 1, and the raw data are presented in the Supporting Information Figure S6. All of the initiators, including ITX, had a relatively low fluorescence quantum yield in PETA, which indicated that the stimulated emission depletion process likely was not a dominate pathway and nonradiative decay from the excitation of long-lived species should be the major process for depletion. Therefore, any depletion effects exhibited in DLW with new initiators can be expected to follow a similar pathway as observed with ITX.

The extinction coefficient provides a clear representation of the ability of the photoinitiator to absorb light through a one-photon process; however, it was initially used here as an indicator of the absorptive properties of the new initiators through a two-photon process. To directly measure the nonlinear absorption properties, an open-aperture Z-scan was performed for each of the photoinitiators.[41] The measured two-photon absorption (TPA) cross sections, σ_2, are presented in Table 2 along with the DLW polymerization writing thresholds for the initiators in PETA. The writing threshold power is the minimum laser power required to write a defined line structure that survives the development process.

TABLE 2 Two-Photon Absorption Cross Section σ_2 and Writing Threshold of Photoinitiators

Photoinitiator	σ_2 (GM)[a]	Writing threshold (10^{18} molecules mW^{-1})
BDAPT	368 (±45)	0.651
DANT	524 (± 61)	1.484
ITX	3 (± 0.4)	4.065
DAPT	122 (± 21)	–[b]
DBTX	22 (± 5)	–[b]

[a] The values in parentheses indicate one standard deviation from the average measured value.
[b] Difficulty dissolving this material uniformly in the monomer.

For comparison purposes, the writing thresholds for each resist were calculated by dividing the photoinitiator concentration by the writing threshold power at 100 μm s^{-1}. In order to account for unknowns in the Z-scan measurement, the ITX molecule with a known σ_2[13,22] was used as a reference to calibrate the measurement and obtain the presented values (see the Supporting Information). The trend of TPA cross sections is ITX < DBTX < DAPT < BDAPT < DANT. Although BDAPT and DANT trade spots in the TPA compared to their linear extinction coefficients determined through single-photon absorption, the simple extinction coefficient measurements provide reasonable indicators of the two-photon absorbing process (see Supporting Information Fig. S7 for the raw data for these measurements). Moreover, the new initiators, especially BDAPT and DANT, were much improved relative to the ITX TPA cross section and showed lower DLW polymerization thresholds; thus, they stood out as promising photoinitiating candidates.

Beyond improving the writing threshold for the DLW polymerization, it was necessary to investigate if the polymerization inhibition effect available in ITX was also present in the synthesized photoinitiators. To illustrate the depletion of the excited state, a 405 nm exciting laser was introduced orthogonally to a 633 nm laser beam and signal path [Fig. 4(a)]. In this configuration, the 633 nm laser was treated as the depletion laser. Assuming no saturation effects were occurring, if the addition of individual fluorescence signals for sample exposure by excitation (405 nm) and depletion (633 nm)

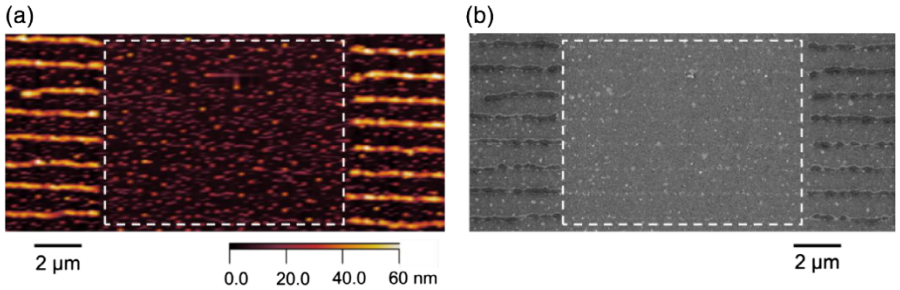

FIGURE 5 Selectively inhibited DLW photopolymerization using BDAPT (0.25 wt %) as a photoinitiator in the PETA monomer. Polymer lines were written at 100 μm s^{-1} with the 638 nm diode laser turned on for 10 μm, preventing polymerization in the region shown by the box highlighted by white dashed lines. (a) The AFM image of the printed polymer nanoscale lines. (b)The SEM image of the same polymer lines. [Color figure can be viewed at wileyonlinelibrary.com]

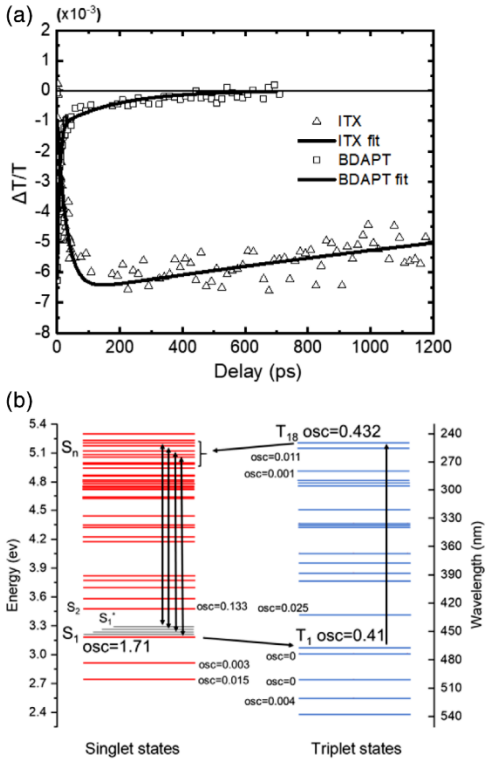

FIGURE 6 (a) Ultra-fast transient absorption measurement of ITX and BDAPT in THF. The pump and the probe wavelengths used were 400 nm and 633 nm, respectively. The solid lines represent fits to the data, which is shown as either open triangles (ITX) or open squares (BDAPT). (b) The DFT calculation of the singlet states and triplet states of BDAPT and the most likely pathway of depletion. S_1* levels are not calculated and are sketched for visualization purposes only. [Color figure can be viewed at wileyonlinelibrary.com]

initial drop in the transmission curve occurred on a timescale comparable with the pulse duration, where S_1 and S_1* were filled by the pump beam. The $S_1^* \rightarrow S_1$ intraband transition was then observed to have a lifetime of τ_1, which was about four times shorter than for ITX. A final S_1 lifetime of τ_2 (187 ps) for BDAPT was found to be about 22 times shorter than τ_2 (4.2 ns) for ITX. As shown in the calculations of Figure 6(b), BDAPT was predicted to undergo a $T_1 \rightarrow T_n$ transition.[12] The calculated energy gap between T_1 and T_{18} was 581 nm, which is smaller than the depleting laser used during lithography because the energy gap in PETA solution is different from the energy gap with no solvent present.[42,43] This led to the inhibition of the polymerization by depopulating the T_1 state before polymerization occurred, similar to the mechanism commonly associated with depletion in ITX-based systems.[12] It is crucial to notice that the lifetime of the S_1 state (187 ps) for BDAPT is much shorter than the lifetime of S_1 state (4.2 ns) for ITX. This large difference leads to a sizeable population of BDAPT entering the T_1 state in a short period of time. T_1 is the energy state leading to polymerization during nanoprinting, which is why BDAPT can initiate writing at a fivefold lower power than ITX.

To provide insights into the T_1 lifetimes, phosphorescence spectra at a temperature of 77 K were acquired. As shown in Figure 7, all the initiators possess clear phosphorescent emission, which indicates that the depletion of singlet-excited state via intersystem crossing to the triplet state exists in all of the systems evaluated here. The trend of the phosphorescent lifetimes is DBTX (10 ms) < ITX (120 ms) < DAPT (219 ms) < BDAPT (287 ms) < DANT (379 ms), which represents the sequence of how long the molecules would have their T_1 states populated. When comparing DBTX, DAPT, and BDAPT (Fig. 8), we establish that the addition of conjugated branches increases the phosphorescence lifetime, although the effect is decreased when the second branch is introduced.

By comparing DAPT and DANT, we see that the naphthalene substituent performs differently than phenyl substituent to increase the phosphorescence lifetime. This indicates that the structure design of branches has a significant impact on this

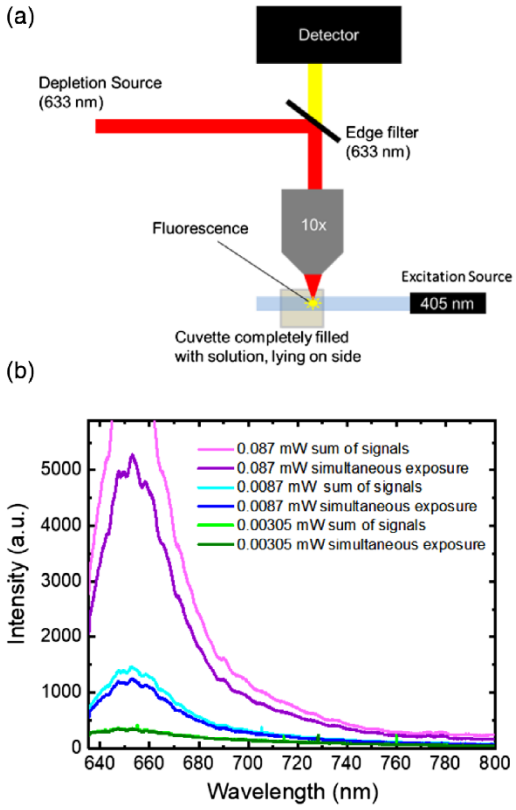

FIGURE 4 (a) A diagram of the experimental set-up for the two-laser spectroscopy system utilized to detect the depletion of select photoinitiators. (b) The fluorescence spectra with sum of individual excitation and depletion signals and the signal with both beams on simultaneously with 633 nm as depleting laser. The clear evidence of depletion was a good indicator of the ability to inhibit the photopolymerization process in actual DLW polymerization processes. As such, this photoinitiator was brought forward for complete DLW photopolymerization evaluation. [Color figure can be viewed at wileyonlinelibrary.com]

lasers was equal to the signal of when both the excitation and depletion sources were on, the photoinitiator responds to the each light independently. However, if the sum of individual signal was higher than the signal of both lasers when they were in the on state, depletion of the fluorescing state of the photoinitiator occurred. Alternatively, additional absorption was said to be detected if the sum of the individual signals was lower than that of the signals when both lasers were in the on state. For the BDAPT in THF solution shown in Figure 4(b), three different depletion laser powers were tested, and the 405 nm wavelength excitation power was held constant. For all three depletion intensities, the sum of individual signals was greater than the signal with both lasers on indicating a depletion of the BDAPT excited state by the 633 nm laser.

This effect was not observed when 633 nm laser was replaced with 532 nm laser. Many factors contribute to a successful photoinitiator for the DLW photopolymerization process, making it difficult to accurately predict its exact performance during actual printing conditions. Specifically, the polymerization inhibition effect is not easily measured outside of a direct test inside a monomer matrix. Due to its performance in the aforementioned experiments, BDAPT was selected for its potential ability to perform in the DLW photopolymerization process. In particular, BDAPT showed promise with respect to the aforementioned two-laser system, due to its large TPA cross section, and due to its relatively large solubility in the PETA monomer compared to DANT. For this evaluation, a 638 nm laser was spatially overlapped with the DLW 800 nm beam and a Gaussian profile is used for both beams; care was taken to ensure that the focused 638 nm beam diameter was at least as large as the DLW spot. The depletion laser wavelength of 638 nm was chosen as a result of the above fluorescence depletion experiments. BDAPT at a loading of 0.25 wt % in PETA was used as the test photoresist. As shown in Figure 5, a group of parallel polymer lines were printed using the DLW polymerization process. During the writing of each line, the sample was exposed to the 638 nm laser for 10 μm of the line path without turning off the DLW beam. During that time of exposure to the inhibition beam, which correlated with 10 μm in space, the polymerization was fully inhibited. It is worth noting, however, that the conditions to observe this effect required careful control of the DLW beam power slightly below the writing threshold. This led to the poor quality of printed lines observed in the figure. Beyond that, the 638 nm laser power required for inhibiting the polymerization was large compared to using ITX as photoinitiator.

In order to elucidate the inhibition effects for BDAPT, ultrafast transient absorption experiments were performed on BDAPT and ITX [Fig. 6(a)]. A wavelength of 400 nm was used as the pump in order to excite the S_1 state of the molecules, in a manner similar to other studies.[21] This wavelength matched the induced transition of the two-photon absorption occurring during the DLW polymerization process with a 800 nm laser, and it allowed for more uniform pumping of the molecules to the excited state with a lower pump laser power. The probe wavelength was chosen to be 633 nm. Two lifetimes were fit for both ITX (τ_1 = 30.2 ps, τ_2 = 4.2 ns) and BDAPT (τ_1 = 6.9 ps, τ_2 = 187 ps). In the case of ITX, because the pump energy closely matches the S_1 energy level, the fast lifetime (τ_1) is attributed to the S_1* states, and the longer lifetime is attributed to the S_1 state, which is consistent with a previous report.[21] In other words, τ_1 represents how fast S_1 is filled while τ_2 is the rate at which S_1 is depopulated, where some of the population from the S_1 state was transferred to the longer-lived triplet state, which initiates polymerization. In this scenario, the probe beam is interacting with a $S_1 \rightarrow S_n$ transition.

In the case of BDAPT, a proposed probe interaction was with respect to both the $S_1 \rightarrow S_n$ and the $S_1^* \rightarrow S_n$ transitions. A sharp

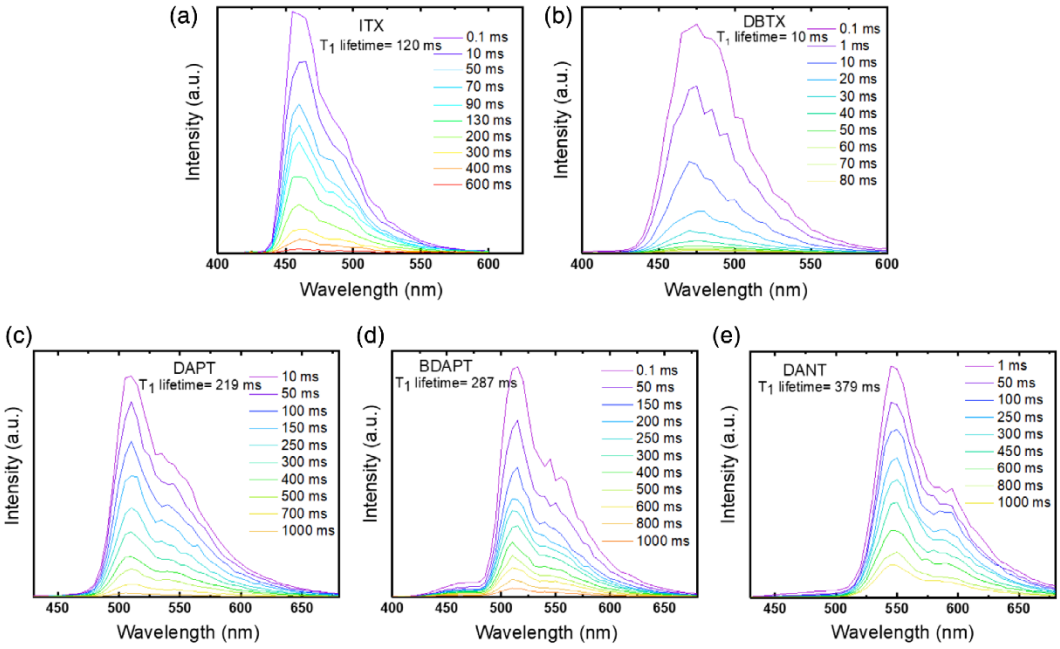

FIGURE 7 Phosphorescence spectra of the photoinitiators in toluene at $T = 77$ K after excitation at 350 nm. The spectra shown are: (a) ITX with a lifetime of 120 ms; (b) DBTX with a lifetime of 10 ms; (c) DAPT with a lifetime of 219 ms; (d) BDAPT with a lifetime of 287 ms; and (e) DANT with a lifetime of 379 ms. [Color figure can be viewed at wileyonlinelibrary.com]

photophysical property. Note that ITX has a moderate phosphorescence lifetime that is shorter than DAPT, BDAPT, and DANT. This informs us that the triplet lifetime is not the only significant determining factor for efficient depletion. ITX seems to demonstrate an efficient $T_1 \rightarrow T_n$ transition allowing easy depletion of the printing. In the case of BDAPT, the $T_1 \rightarrow T_n$ transition was not efficient enough to fully depopulate the T_1 state, which explains why partial depletion was

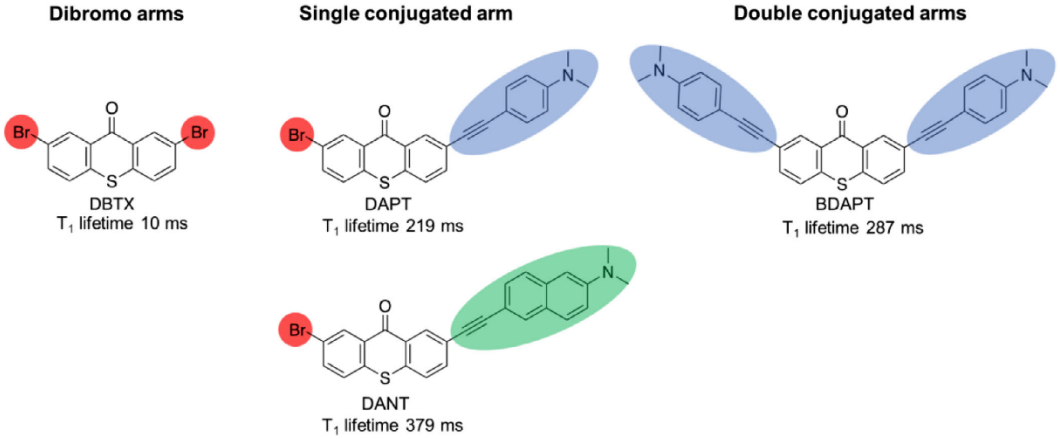

FIGURE 8 The influence of replacing the Br atom by either a single conjugated branch or two conjugated branches to the corresponding T_1 lifetime. These results indicate that both the exact chemistry and the degree of conjugation (for the same chemistry) can alter the lifetimes of the T_1 states for these ITX-based molecules. [Color figure can be viewed at wileyonlinelibrary.com]

observed in lithography with low depleting power, but full depletion was challenging to achieve (Supporting Information Figs. S8 and S9). To summarize, the moderate population of ITX on the T_1 state brings about moderate writing power and moderate depleting power, but the extreme population of BDAPT on the T_1 state leads to a lower writing power and a higher depleting power. Consequently, compared to ITX, our new initiator is much more efficient in initiating the DLW photopolymerization process but trades this advantage for a reduced polymerization inhibition capability. Therefore, this molecule could be of significant interest in applications requiring low laser power (i.e., high throughput, multiple-writing laser situations); however, additional effort could be placed in decreasing the inhibition threshold of the next-generation photoinitiators.

CONCLUSIONS

In this work, we developed and synthesized several new photoinitiating species based on a thiophene-9-one core and carried the most promising molecule forward as the photoinitiator for DLW photopolymerization. The extension of the π-system of our initiators led to a redshift of the visible light absorption toward the direction of the desired 400 nm peak (i.e., at half the wavelength of the pulsed writing laser). Moreover, this molecular feature increased the molar extinction coefficient of BDAPT relative to the ITX core. BDAPT demonstrated a fivefold decrease in threshold writing power compared to ITX for the photopolymerization of interest, which is key in minimizing energy requirements and for the potential to use these materials in high throughput photopolymerization writing. Beyond that, BDAPT had photopolymerization inhibition capabilities under DLW when an additional depletion laser was used. Ultrafast spectroscopic experiments, low-temperature phosphorescence spectroscopy and DFT calculations were used to explain the mechanism of both excitation and depletion of BDAPT. These data indicate that a short excited state lifetime leads to poor inhibition of photopolymerization due to a strongly populated triplet state with inefficient triplet–triplet absorption depletion pathway. Therefore, we have proposed a practical direction to modify and improve existing photoinitiators for two-photon DLW photopolymerization. In turn, this should allow for the ready modification of existing photoinitiators in the future 3D nanoprinting photopolymerization reactions, for not only ITX-based systems but for more exotic systems as well, by providing insights into the critical properties of a photoinitiator molecule that leads to a desired photopolymerization performance and how to tailor a photoinitiating molecule to achieve those properties.

ACKNOWLEDGMENTS

This work was supported by the National Science Foundation (NSF) through the Scalable Nanomanufacturing Program (Award Number: 1634832, Program Manager: Dr. Khershed Cooper), and we thank the NSF for their gracious support. We thank Mr. Duanchen Ding from the group of Professor Hilkka I. Kenttämaa at Purdue University for his assistance regarding mass spectrometry data. We thank Dr. Xikang Zhao for helpful discussions.

REFERENCES AND NOTES

1 S. Maruo, O. Nakamura, S. Kawata, *Opt. Lett.* **1997**, *22*, 132.

2 S. Kawata, H.-B. Sun, T. Tanaka, K. Takada, *Nature* **2001**, *412*, 697.

3 M. Deubel, G. von Freymann, M. Wegener, S. Pereira, K. Busch, C. M. Soukoulis, *Nat. Mater.* **2004**, *3*, 444.

4 G. von Freymann, A. Ledermann, M. Thiel, I. Staude, S. Essig, K. Busch, M. Wegener, *Adv. Funct. Mater.* **2010**, *20*, 1038.

5 F. Klein, B. Richter, T. Striebel, C. M. Franz, G. v. Freymann, M. Wegener, M. Bastmeyer, *Adv. Mater.* **2011**, *23*, 1341.

6 V. Melissinaki, A. Gill, I. Ortega, M. Vamvakaki, A. Ranella, J. Haycock, C. Fotakis, M. Farsari, F. Claeyssens, *Biofabrication* **2011**, *3*, 045005.

7 S. W. Hell, *Phys. Lett. A* **2004**, *326*, 140.

8 S. W. Hell, J. Wichmann, *Opt. Lett.* **1994**, *19*, 780.

9 J. Fischer, G. von Freymann, M. Wegener, *Adv. Mater.* **2010**, *22*, 3578.

10 J. Fischer, J. B. Mueller, A. S. Quick, J. Kaschke, C. Barner-Kowollik, M. Wegener, *Adv. Opt. Mater.* **2015**, *3*, 221.

11 L. Li, R. R. Gattass, E. Gershgoren, H. Hwang, J. T. Fourkas, *Science* **2009**, *324*, 910.

12 B. Harke, W. Dallari, G. Grancini, D. Fazzi, F. Brandi, A. Petrozza, A. Diaspro, *Adv. Mater.* **2013**, *25*, 904.

13 K. J. Schafer, J. M. Hales, M. Balu, K. D. Belfield, E. W. Van Stryland, D. J. Hagan, *J. Photochem. Photobiol. A Chem.* **2004**, *162*, 497.

14 W. Schnsbel, *Polymers and Light*; Wiley-VCH: Weinheim, **2007**, p. 305.

15 M. Malinauskas, A. Žukauskas, G. Bičkauskaitė, R. Gadonas, S. Juodkazis, *Opt. Express* **2010**, *18*, 10209.

16 B. H. Cumpston, S. P. Ananthavel, S. Barlow, D. L. Dyer, J. E. Ehrlich, L. L. Erskine, A. A. Heikal, S. M. Kuebler, I. Y. S. Lee, D. McCord-Maughon, J. Qin, H. Röckel, M. Rumi, X.-L. Wu, S. R. Marder, J. W. Perry, *Nature* **1999**, *398*, 51.

17 T. Serevičius, R. Komskis, P. Adomėnas, O. Adomėnienė, V. Jankauskas, A. Gruodis, K. Kazlauskas, S. Juršėnas, *Phys. Chem. Chem. Phys.* **2014**, *16*, 7089.

18 H. J. Yvon, *HORIBA*; Jobin Yvon Ltd.: Stanmore, Middlesex, UK, **2012**.

19 M. Frisch, G. Trucks, H. Schlegel, G. Scuseria, M. Robb, J. Cheeseman, G. Scalmani, V. Barone, G. Petersson, H. Nakatsuji. Gaussian Inc., Wallingford, CT **2016**.

20 UV Plots from the Results of Excited States Calculations, http://gaussian.com/uvvisplot/ (accessed July 2018)

21 M. Sheik-Bahae, A. A. Said, T. Wei, D. J. Hagan, E. W. V. Stryland, *IEEE J. Quantum Electron.* **1990**, *26*, 760.

22 C. Chen, I. Vasudevan, Z. Du, X. Xu, L. Pan, *Appl. Phys. Lett.* **2018**, *112*, 253105.

23 T. J. A. Wolf, J. Fischer, M. Wegener, A.-N. Unterreiner, *Opt. Lett.* **2011**, *36*, 3188.

24 R. Nazir, E. Balčiūnas, D. Buczyńska, F. Bourquard, D. Kowalska, D. Gray, S. Maćkowski, M. Farsari, D. T. Gryko, *Macromolecules* **2015**, *48*, 2466.

25 A. S. Rao, D. Kim, T. Wang, K. H. Kim, S. Hwang, K. H. Ahn, *Org. Lett.* **2012**, *14*, 2598.

26 K. Sonogashira, *J. Organomet. Chem.* **2002**, *653*, 46.

27 J. Kulhánek, F. Bureš, M. Ludwig, *Beilstein J. Org. Chem.* **2009**, *5*, 11.

28 K. Sonogashira, Y. Tohda, N. Hagihara, *Tetrahedron Lett.* **1975**, *16*, 4467.

29 M. P. Coleman, M. K. Boyd, *J. Org. Chem.* **2002**, *67*, 7641.

30 S. Dadashi-Silab, H. Bildirir, R. Dawson, A. Thomas, Y. Yagci, *Macromolecules* **2014**, *47*, 4607.

31 L. Ding, Z. Zhang, X. Li, J. Su, *Chem. Commun.* **2013**, *49*, 7319.

32 W. Shi, Y. Luo, X. Luo, L. Chao, H. Zhang, J. Wang, A. Lei, *J. Am. Chem. Soc.* **2008**, *130*, 14713.

33 Y. Liu, N. Gu, P. Liu, J. Xie, X. Ma, Y. Liu, B. Dai, *Appl. Organomet. Chem.* **2015**, *29*, 736.

34 S. Xu, Z. Yun, Y. Feng, T. Tang, Z. Fang, T. Tang, *RSC Adv.* **2016**, *6*, 69822.

35 J. Yang, A. Dass, A.-M. M. Rawashdeh, C. Sotiriou-Leventis, M. J. Panzner, D. S. Tyson, J. D. Kinder, N. Leventis, *Chem. Mater.* **2004**, *16*, 3457.

36 K. D. Thériault, C. Radford, M. Parvez, B. Heyne, T. C. Sutherland, *Phys. Chem. Chem. Phys.* **2015**, *17*, 20903.

37 A. K. R. Junker, T. J. Sørensen, *Methods Appl. Fluores.* **2017**, *6*, 014002.

38 D. A. Skoog, F. J. Holler, S. R. Crouch, *Principles of Instrumental Analysis*; Cengage Learning: Boston, MA, **2017**.

39 B. Dereka, A. Rosspeintner, Z. Li, R. Liska, E. Vauthey, *J. Am. Chem. Soc.* **2016**, *138*, 4643.

40 T. A. Klar, S. Jakobs, M. Dyba, A. Egner, S. W. Hell, *Proc. Natl. Acad. Sci.* **2000**, *97*, 8206.

41 B. Gu, Y.-X. Fan, J. Wang, J. Chen, J. Ding, H.-T. Wang, B. Guo, *Phys. Rev. A* **2006**, *73*, 065803.

42 M. Glukhovtsev, *J. Chem. Inf. Comput. Sci.* **1997**, *37*, 1206.

43 E. Fabiano, F. D. Sala, R. Cingolani, M. Weimer, A. Görling, *Chem. A Eur. J.* **2005**, *109*, 3078.